A REVIEW OF THE LONG-TERM PERSISTENCE OF THE PASSIVE FILM ON ALLOY 22 IN POTENTIAL YUCCA MOUNTAIN REPOSITORY ENVIRONMENTS

Prepared for

U.S. Nuclear Regulatory Commission
Contract NRC–02–02–012

Prepared by

H. Jung
T. Mintz
D.S. Dunn
O. Pensado
T. Ahn (NRC)

Center for Nuclear Waste Regulatory Analyses
San Antonio, Texas

October 2007

PREVIOUS REPORTS IN SERIES

Number	Name	Date Issued
CNWRA 91-004	A Review of Localized Corrosion of High-Level Nuclear Waste Container Materials—I	April 1991
CNWRA 91-008	Hydrogen Embrittlement of Candidate Container Materials	June 1991
CNWRA 92-021	A Review of Stress Corrosion Cracking of High-Level Nuclear Waste Container Materials—I	August 1992
CNWRA 93-003	Long-Term Stability of High-Level Nuclear Waste Container Materials: I—Thermal Stability of Alloy 825	February 1993
CNWRA 93-004	Experimental Investigations of Localized Corrosion of High-Level Nuclear Waste Container Materials	February 1993
CNWRA 93-006	Characteristics of Spent Nuclear Fuel and Cladding Relevant to High-Level Waste Source Term	May 1993
CNWRA 93-014	A Review of the Potential for Microbially Influenced Corrosion of High-Level Nuclear Waste Containers	June 1993
CNWRA 94-010	A Review of Degradation Modes of Alternate Container Designs and Materials	April 1994
CNWRA 94-028	Environmental Effects on Stress Corrosion Cracking of Type 316L Stainless Steel and Alloy 825 as High-Level Nuclear Waste Container Materials	October 1994
CNWRA 95-010	Experimental Investigations of Failure Processes of High-Level Radioactive Waste Container Materials	May 1995
CNWRA 95-020	Expert-Panel Review of the Integrated Waste Package Experiments Research Project	September 1995
CNWRA 96-004	Thermal Stability and Mechanical Properties of High-Level Radioactive Waste Container Materials: Assessment of Carbon and Low-Alloy Steels	May 1996
CNWRA 97-010	An Analysis of Galvanic Coupling Effects on the Performance of High-Level Nuclear Waste Container Materials	August 1997

PREVIOUS REPORTS IN SERIES (continued)

Number	Name	Date Issued
CNWRA 98-004	Effect of Galvanic Coupling Between Overpack Materials of High-Level Nuclear Waste Containers—Experimental and Modeling Results	March 1998
CNWRA 98-008	Effects of Environmental Factors on Container Life	July 1998
CNWRA 99-003	Assessment of Performance Issues Related to Alternate Engineered Barrier System Materials and Design Options	September 1999
CNWRA 99-004	Effects of Environmental Factors on the Aqueous Corrosion of High-Level Radioactive Waste Containers—Experimental Results and Models	September 1999
CNWRA 2000-06 Revision 1	Assessment of Methodologies to Confirm Container Performance Model Predictions	January 2001
CNWRA 2001-003	Effect of Environment on the Corrosion of Waste Package and Drip Shield Materials	September 2001
CNWRA 2002-01	Effect of In-Package Chemistry on the Degradation of Vitrified High-Level Radioactive Waste and Spent Nuclear Fuel Cladding	October 2001
CNWRA 2002-02	Evaluation of Analogs for the Performance Assessment of High-Level Waste Container Materials	March 2002
CNWRA 2003-01	Passive Dissolution of Container Materials—Modeling and Experiments	October 2002
CNWRA 2003-02	Stress Corrosion Cracking and Hydrogen Embrittlement of Container and Drip Shield Materials	October 2002
CNWRA 2003-05	Assessment of Mechanisms for Early Waste Package Failures	March 2003
CNWRA 2004-01	Effect of Fabrication Processes on Materials Stability—Characterization and Corrosion	October 2003
CNWRA 2004-02	Natural Analogs of High-Level Waste Container Materials—Experimental Evaluation of Josephinite	January 2004

PREVIOUS REPORTS IN SERIES (continued)

Number	Name	Date Issued
CNWRA 2004-03	The Effects of Fabrication Processes on the Mechanical Properties of Waste Packages—Progress Report	July 2004
CNWRA 2004-08	A Review Report on High Burnup Spent Nuclear Fuel—Disposal Issues	September 2004
CNWRA 2005-01	Microbially Influenced Corrosion Studies of Engineered Barrier System Materials	October 2004
CNWRA 2005-02 Revision 1	Passive and Localized Corrosion of Overpack Materials—Modeling and Experiments	November 2005
CNWRA 2005-03	Microstructural Analyses and Mechanical Properties of Alloy 22	March 2005
CNWRA 2006-001	Crevice Corrosion Penetration Rates of Alloy 22 in Chloride-Containing Waters—Progress Report	December 2005
CNWRA 2006-02	Corrosion of Alloy 22 in Concentrated Nitrate and Chloride Salt Environments at Elevated Temperatures—Progress Report	April 2006
CNWRA 2007-01	Stress Corrosion Cracking of Waste Package Material—Modeling and Experiments	December 2006

ABSTRACT

The focus of this report is to provide an assessment of the long-term persistence of the passive film on Alloy 22 (Ni-22Cr-13Mo-4Fe-3W) as the candidate material for the waste package outer container in the potential high-level waste repository at Yucca Mountain, Nevada. Specifically, the areas of review in this report are (i) general corrosion rate data; (ii) stability-evolution of film thickness, composition, and structure with time; and (iii) corrosion-related potential degradation processes that may affect the passive film on Alloy 22.

Alloy 22 exhibits very low general corrosion rates that tend to decrease with time. This decrease may be attributable to restructuring of the overall passive film, changes in film thickness, precipitation of corrosion products, and changes of the base metal at the metal-oxide interface. The corrosion rate follows an Arrhenius dependence on the temperature. Extrapolations to 150 °C [302 °F] in the U.S. Department of Energy performance assessment model for general corrosion appear consistent with experimental data.

Under certain environmental conditions several potential degradation processes might affect the long-term persistence of the passive film on Alloy 22. The processes considered in this report include enhanced dissolution rates by anodic sulfur segregation, effects of base metal chromium depletion at the metal-film interface, film spallation by void formation, anion-selective sorption, increased cathodic kinetics, and alteration of the passive film by dry–wet pulse process. Among these potential processes, anodic sulfur segregation process might be detrimental and requires further experimental evaluation. The other considered processes are not expected to appreciably affect the long-term stability of the passive film on Alloy 22.

CONTENTS

CONTENTS (continued)

FIGURES

FIGURES (continued)

TABLES

ACKNOWLEDGMENTS

This report describes work performed by the Center for Nuclear Waste Regulatory Analyses (CNWRA) for the U.S. Nuclear Regulatory Commission (NRC) under Contract No. NRC–02–02–012. The activities reported here were performed on behalf of the NRC Office of Nuclear Material Safety and Safeguards, Division of High-Level Waste Repository Safety. This report is an independent product of CNWRA and does not necessarily reflect the view or regulatory position of NRC.

The authors gratefully acknowledge G. Cragnolino for his technical review, K. Axler for his concurrence review, S. Mohanty for his programmatic review, L. Mulverhill for her editorial review, and J. Gonzalez and S. Odam for their administrative support. The authors also acknowledge Y.-M. Pan for his assistance throughout this project.

QUALITY OF DATA, ANALYSES, AND CODE DEVELOPMENT

DATA: All CNWRA-generated original data contained in this report meet the quality assurance requirements described in the Geosciences and Engineering Division Quality Assurance Manual. Sources for other data should be consulted for determining the level of quality for those data. Computational calculations have been recorded in CNWRA Scientific Notebook number 835.

ANALYSES AND CODES: None.

EXECUTIVE SUMMARY

The long lifetime of waste packages is an important attribute of the potential high-level waste repository at Yucca Mountain, Nevada (DOE, 2002) to isolate nuclear waste from the geosphere. The reference waste package design in the U.S. Department of Energy (DOE) site recommendation (DOE, 2002) consists of an outer cylindrical container made of a highly corrosion-resistant nickel-based alloy, Alloy 22 (Ni-22Cr-13Mo-4Fe-3W), and an inner container of Type 316 nuclear grade stainless steel (low C-high N-Fe-18Cr-12Ni-2.5Mo) for mechanical strength.

Multiple investigations indicate that Alloy 22 is highly resistant to various modes of corrosion including dry-air oxidation, general (uniform) corrosion, localized corrosion, and stress corrosion cracking. The corrosion resistance is due to the presence of a chromium-rich passive film formed on the alloy surface in a wide range of environments from oxidizing to reducing conditions at various pH and temperatures. In the absence of environments leading to localized corrosion, Alloy 22 is expected to corrode uniformly in an aqueous environment with very low corrosion rates under the potential repository conditions (Dunn, et al., 2005; Pensado, et al., 2002). Low corrosion rates are a function of the passive film on Alloy 22. If the passive film persists for an extended time, the waste package could last very long. For example, in the Total-system Performance Assessment (TPA) model developed by the Center for Nuclear Waste Regulatory Analyses (CNWRA) and the U.S. Nuclear Regulatory Commission (NRC) (Mohanty, et al., 2002), waste package failure by general corrosion is estimated to occur well beyond 10,000 years.

General corrosion rates could increase substantially, however, if the passive film becomes unstable, depending on material alteration states and exposure conditions during the disposal period. Loss of passivity (i.e., depassivation) could lead to general corrosion rates that are orders of magnitude higher than those corresponding to passive dissolution, resulting in shorter waste package lifetimes and potential release of radionuclides. Thus, the long-term persistence of the passive film on Alloy 22 is considered of high significance to waste isolation, relative to other corrosion modes (NRC, 2004).

The focus of this report is an assessment of the long-term persistence of the passive film on Alloy 22. In this report the existence of low-temperature (less than 100 °C [212 °F]) corrosion processes capable of altering the passivity of Alloy 22 is analyzed under environmental conditions commonly associated with passive dissolution. This report draws conclusions from currently available DOE, CNWRA, and published literature data.

The areas of review in this report are (i) general corrosion rate data; (ii) passive film stability-evolution of film thickness, composition, and structure with time; (iii) potential degradation processes under environmental conditions commonly associated with passive dissolution; and (iv) effect of these processes on the long-term persistence of the passive film on Alloy 22.

A number of studies have shown that Alloy 22 exhibits very low general corrosion rates (e.g., generally less than 10^{-4} mm/yr [3.9×10^{-5} in/yr]) characteristic of dissolution controlled by a passive film under environmental conditions not conducive to localized corrosion. At temperatures below 100 °C [212 °F], corrosion rates tend to decrease with time although the mechanisms causing the decrease are not well understood. Multiple studies have also

confirmed an Arrhenius dependence of the corrosion rate on the temperature. Although there is some discrepancy on the general corrosion rates at elevated temperatures, extrapolations to 150 °C [302 °F] in the DOE performance assessment model for general corrosion appear consistent with experimental data.

The passive film mostly exhibits a bilayer (two-layered) structure, consisting of an outer porous layer and an inner thin, compact layer. The inner layer, also referred to as barrier layer, is believed to play the main role in the phenomenon of passivity. According to the point defect model, the inner layer tends to maintain a steady-state (constant thickness and structure) as time elapses. This layer of constant properties would imply a constant general corrosion rate. However, DOE data from the long-term corrosion test facility gathered over 5 years under full immersion conditions indicate corrosion rates that continuously decrease with time. Therefore, potentially there are other characteristics of the passive film that control the Alloy 22 corrosion rates. Over time, the dissolution of local defects in the passive film can lead to a restructuring of the passive film. It is likely that the decrease in the corrosion rate with time may be attributable to restructuring of the passive film, changes in film thickness, precipitation of corrosion products as oxi-hydroxides, and changes of the base metal at the metal-oxide interface. From analyses of the passive film reported in the literature, it can be concluded that the main barrier against corrosion degradation is a chromium-rich oxide (e.g., Cr_2O_3 or $NiCr_2O_4$) in the inner layer. Chromium is in the +3 oxidation state, which could be Cr_2O_3 or $NiCr_2O_4$. Other metal elements (i.e., molybdenum and tungsten) promote enhanced resistance against localized forms of corrosion.

Under environmental conditions commonly associated with passive dissolution, several potential degradation processes are identified that might affect the long-term persistence of the passive film on Alloy 22. The processes considered in this report include enhanced dissolution rate by anodic sulfur segregation, detrimental effects of base metal chromium depletion at the metal-film interface, film spallation by void formation, anion-selective sorption, increased cathodic kinetics (e.g., large cathodic area development and oxidizing species generation by radiolysis), and alteration of the passive film by dry–wet cyclic process. The potential effects of these processes on the passive film on Alloy 22 are evaluated as function of the structural or compositional changes of the passive film and base metal at the metal-oxide interface. The evaluation was based on qualitative assessment of currently available literature data from Alloy 22 and industrial analogs, focusing on the passivation or repassivation capability of Alloy 22. Among these potential processes, anodic sulfur segregation process might be detrimental and requires further experimental evaluation. The other considered processes are not expected to appreciably affect the long-term stability of the passive film on Alloy 22.

To reduce existing uncertainties related to the extrapolation from the existing short-term corrosion data to the extended period (e.g., 10^6 years), further long-term confirmation testing is recommended.

References

DOE. DOE/RW–0539–1, "Yucca Mountain Science and Engineering Report: Technical Information Supporting Site Recommendation Consideration." Rev. 1. Las Vegas, Nevada: DOE, Office of Civilian Radioactive Waste Management. 2002.

Dunn, D.S., O. Pensado, Y.-M. Pan, R.T. Pabalan, L. Yang, X. He, and K.T. Chiang. "Passive and Localized Corrosion of Alloy 22-Modeling and Experiments." CNWRA 2005-02. Rev. 1. San Antonio, Texas: CNWRA. 2005.

Mohanty, S., T.J. McCartin, and D.W. Esh. "Total-system Performance Assessment (TPA) Version 4.0 Code: Module Description and User's Guide." CNWRA 2002-01. San Antonio, Texas: CNWRA. 2002.

NRC. "Risk Insights Baseline Report." ML040560162. Washington, DC: Division of High-Level Waste Repository Safety, Office of Nuclear Material Safety and Safeguards. 2004. <http://www.nrc.gov/waste/hlw-disposal/reg-initiatives/resolve-key-tech-issues.html> (June 1, 2007)

Pensado, O., D.S. Dunn, G.A. Cragnolino, and V. Jain. "Passive Dissolution of Container Materials-Modeling and Experiments." CNWRA 2003-01. San Antonio, Texas: CNWRA. 2002.

1 INTRODUCTION

The U.S. Nuclear Regulatory Commission (NRC) is currently preparing to review a potential license application by the U.S. Department of Energy (DOE) for construction and operation of a potential repository at Yucca Mountain, Nevada, for the permanent disposal of high-level waste. One of the key attributes for the overall system performance of the potential repository is the long lifetime of waste package as a barrier to radionuclide release. For undisrupted conditions, corrosion-related degradation processes such as dry-air oxidation, general (uniform) corrosion, localized corrosion, and stress corrosion cracking are considered to be important factors in the potential degradation of the waste package and the drip shield. The reference waste package design in the DOE site recommendation (DOE, 2002) consists of an outer cylindrical container made of a highly corrosion-resistant nickel-based alloy, Alloy 22 (Ni-22Cr-13Mo-4Fe-3W), and an inner container of Type 316 nuclear grade stainless steel (low C-highN-Fe-18Cr-12Ni-2.5Mo) to provide structural support.

Multiple investigations indicate that Alloy 22 is highly resistant to various modes of corrosion including dry-air oxidation, general (uniform) corrosion, localized corrosion, and stress corrosion cracking. The corrosion resistance is due to the presence of a chromium-rich passive film formed on the alloy surface in a wide range of environments from oxidizing to reducing conditions at various pH and temperatures. In the absence of environmental conditions leading to localized corrosion, Alloy 22 is expected to corrode uniformly with very low corrosion rates in aqueous environments (Dunn, et al., 2005; Pensado, et al., 2002). Low corrosion rates are dependent on passive film characteristics.

The passive film is composed of a multi-layered structure, with a chromium-rich inner layer, and metal oxi-hydroxides on successive layers. Macdonald (1992) describes the passive film predominantly as a bilayer system, with a compact inner layer and a porous outer layer that incorporates precipitated corrosion products. The inner layer, or barrier layer, forms by solid state reactions and it is mostly responsible for the phenomenon of passivity. The outer layer is believed to play only a secondary role in alloy passivation (Macdonald, 1992). In this report, the term passive film is used for the overall, multi-layered oxi-hydroxide developed on the alloy surface. If the passive film persists for an extended time, the waste package could last very long. For example, in the Total-system Performance Assessment (TPA) model developed by the Center for Nuclear Waste Regulatory Analyses (CNWRA) and the NRC (Mohanty, et al., 2002), waste package failure by general corrosion is estimated to occur well beyond 10,000 years.

General corrosion rates could increase substantially, however, if the passive film becomes unstable, depending on material alteration states and exposure conditions during the disposal period. Loss of passivity (i.e., depassivation) could lead to general corrosion rates that are orders of magnitude higher than those corresponding to passive dissolution, resulting in shorter waste package lifetimes and potential release of radionuclides in waste forms. Thus, the long-term persistence of the passive film on Alloy 22 is considered of high significance to waste isolation (NRC, 2004). Certain aggressive water chemistries characterized by high chloride concentration, low pH, and high temperature may disrupt the Alloy 22 passive dissolution. For example, Alloy 22 exhibits depassivation either in strong acidic solutions (Gray, et al., 2006a) or in concentrated brines at 155 °C [311 °F] (Rodríguez, et al., 2007). Alloy 22 can also undergo localized corrosion in the form of crevice corrosion in chloride solutions containing low concentrations of inhibitors, such as nitrate, bicarbonate, and sulfate, if high enough corrosion

potentials are attained. Localized corrosion of Alloy 22 is analyzed in another CNWRA report of this series (Dunn, et al., 2005).

Besides localized corrosion or depassivation driven by environmental conditions (i.e., high temperatures or aggressive water chemistries), it is possible that the passive film on Alloy 22 could deteriorate in relatively benign environments {i.e., in neutral pH solutions below 100 °C [212 °F]} by gradual action of detrimental corrosion processes occurring over a long time span (i.e., hundreds to thousands of years). These potential processes may eventually disrupt the integrity of the passive film on Alloy 22 resulting in enhanced corrosion rates or increased localized corrosion susceptibility of the waste package outer container.

In this report, processes that may disrupt the passive film on Alloy 22 are considered such as anodic sulfur segregation, effects of base metal chromium depletion at the metal-film interface, film spallation by void formation, anion-selective sorption into the porous outer layer promoting localized corrosion due to local chemistry changes, increased cathodic kinetics (e.g., large cathodic surface area development and production of oxidizing species by radiolysis), and alteration of passive film by dry–wet cyclic processes.

1.1 Objective and Scope

The focus of this report is an assessment of the long-term persistence of the passive film on Alloy 22. The existence of low-temperature {less than 100 °C [212 °F]} processes capable of altering the passivity of Alloy 22 is analyzed, under environmental conditions commonly associated with passive dissolution. This report draws conclusions from currently available DOE, CNWRA, and published literature data. More specifically, the areas of review in this report are (i) general corrosion rate data; (ii) passive film stability-evolution of film thickness, composition, and structure with time; (iii) potential degradation processes under environmental conditions commonly associated with passive dissolution, and (iv) effect of these processes on the long-term persistence of the passive film on Alloy 22.

1.2 Prelicensing Review of the DOE Approach and Relevant DOE and NRC Agreements and Guidances

The DOE approach related to the long-term stability of the passive film on the waste package outer container material has been previously assessed as part of NRC prelicensing review activities. The assessments are provided in the Integrated Issue Resolution Status Report (NRC, 2005).

NRC considered the prelicensing activities associated with Key Technical Issue agreements between NRC and DOE on Container Life and Source Term 1.08 and 1.09, which are directly related to the long-term passivity of waste package and drip shield materials (Kokajko, 2004). This was based on the NRC/CNWRA staff review of the DOE response to these Key Technical Issue agreements in Technical Basis Document No. 6, Appendix N (Bechtel SAIC Company, LLC, 2004a). Agreements pertaining to degradation of container materials are listed in Table 1-1; these agreements are considered complete (Dunn, et al., 2005).

Table 1-1. U.S. Department of Energy (DOE) and U.S. Nuclear Regulatory Commission (NRC) Agreements Related to This Report	
Agreement	**Agreement and Statement**
CLST.1.02* [Container Life and Source Term]	"Provide the documentation for the path forward items listed on slide 12. (Surface elemental analysis of alloy test specimens is necessary for determination of selective dissolution; surface analysis of welded specimens for evidence of dealloying; continue testing including simulated saturated repository environment to confirm enhancement factor). DOE will provide the documentation in a revision to the Analysis Model Report [AMR] General and Localized Corrosion of Waste Package Outer Barrier by license application [LA]."
CLST.1.03*	"Provide documentation that confirms the linear polarization resistance measurements with corrosion rate measurements using other techniques. DOE will provide the documentation in a revision to AMR General and Localized Corrosion of Waste Package Outer Barrier by LA."
CLST.1.05*	"Provide additional details on sensitivities, resolution of measurements, limitations, and deposition of silica for the high sensitivity probes. DOE will document the results of the sensitivity probes including limitation and resolution of measurements as affected by silica deposition in the Alloy 22 AMR and Ti Corrosion AMR (ANL–EBS–MD–000003 and ANL–EBS–MD–000004) prior to LA."
CLST.1.06*	"Provide the documentation on testing showing corrosion rates in the absence of silica deposition. DOE will document the results of testing in the absence of silica deposits in the revision of Alloy 22 AMR (ANL–EBS–MD–000003) prior to LA."
CLST.1.07*	"Provide the documentation for the alternative methods to measure the corrosion rate of the waste package material (e.g., ASTM G–102 testing) or provide justification for the current approach. DOE will document the alternative methods of corrosion measurement in the revision of Alloy 22 AMR (ANL–EBS–MD–000003), prior to LA."

Table 1-1. DOE and NRC Agreements Related to This Report (continued)	
CLST.1.08*	"Provide the documentation for Alloy 22 and titanium for the path forward items listed on slide 16 and 17 [calculate potential-pH diagrams for multi-component Alloy 22; grow oxide films at higher temperatures in autoclaves, in air and/or electrochemically to accelerate film growth for compositional and structural studies below; resolve kinetics of film growth: parabolic or higher order, whether film growth becomes linear, and if, as film grows it becomes mechanically brittle and spalls off; determine chemical, structural, and mechanical properties of films, including thicken films; correlate changes in Ecorr [corrosion potential] measured in LTCTF [Long-Term Corrosion Test Facility] with compositional changes in passive film over time; perform analyses on cold-worked materials to determine changes in film structural properties; perform examination of films formed on naturally occurring Josephinite; compare films formed on Alloy 22 with other similar passive film Alloys with longer industrial experience]. DOE will provide the documentation in a revision to AMRs (ANL–EBS–MD–000003 and ANL–EBS–MD–000004) prior to LA."
CLST.1.09*	"Provide the data that characterize the passive film stability, including the welded and thermally aged specimens. DOE will provide the documentation in a revision to Analysis and Model Reports (ANL–EBS–MD–000003 and ANL–EBS–MD–000004) prior to license application."
TSPAI.3.01†	"Propagate significant sources of uncertainty into projections of waste package and drip shield performance included in future performance assessments. Specific sources of uncertainty that should be propagated (or strong technical basis provided as to why it is insignificant) include: (1) the uncertainty from measured crevice and weight-loss samples general corrosion rates and the statistical differences between the populations, (2) the uncertainty from alternative explanations for the decrease in corrosion rates with time (such as silica coatings that alter the reactive surface area), (3) the uncertainty from utilizing a limited number of samples to define the correction for silica precipitation, (4) the confidence in the upper limit of corrosion rates resulting from the limited sample size, and (5) the uncertainty from alternative statistical representations of the population of empirical general corrosion rates. The technical basis for sources of uncertainty will be established upon completion of existing agreement items CLST.1.4, 1.5, 1.6, and 1.7. DOE will then propagate significant sources of uncertainty into projections of waste package and drip shield performance included in future performance assessments. This technical basis will be documented in a future revision of the General and Localized Corrosion of Waste Package Outer Barrier AMR (ANL–EBS–MD–000003) expected to be available consistent with the scope and schedules for the specified CLST agreements. The results of the AMR analyses will be propagated into future TSPA [Total System Performance Assessment] analyses for any potential license application."

Table 1-1. DOE and NRC Agreements Related to This Report (continued)	
TSPAI.3.04†	"Provide the technical basis that the representation of the variation of general corrosion rates (if a significant portion is 'lack of knowledge' uncertainty) does not result in risk dilution of projected dose responses (ENG1.3.3). DOE will provide the technical basis that the representation of the variation of general corrosion rates results in reasonably conservative projected dose rates. The technical basis will be documented in an update to the WAPDEG Analysis of Waste Package and Drip Shield Degradation AMR (ANL–EBS–PA–000001). This AMR is expected to be available to NRC in FY 2003. These results will be incorporated into future TSPA documentation for any potential license application."

NOTE: Information in this table was compiled directly from the cited sources.
*Schlueter, J.R. "U.S. Nuclear Regulatory Commission/U.S. Department of Energy Technical Exchange and Management on Container Life and Source Term (September 12–13, 2000)." Letter (October 4) to S. Brocoum, DOE. Washington, DC: NRC. 2000.
†Reamer, C.W. "U.S. Nuclear Regulatory Commission/U.S. Department of Energy Technical Exchange and Management on Total System Performance Assessment and Integration (August 6–10, 2001)." Letter (August 23) to S. Brocoum, DOE. Washington, DC: NRC. 2001.

The technical basis for assessing the long-term passivity of waste package materials was previously presented in CNWRA technical reports (Brossia, et al., 2001; Dunn, et al., 2005; Pensado, et al., 2002). After agreement of completion, Ahn, et al. (2007) further reviewed more recent DOE and related literature information. This current report will present more detailed review and evaluation of the recent information.

Under 10 CFR Part 63, NRC's licensing review of the potential Yucca Mountain repository will be risk informed and performance based. Requirements for performance assessment in 10 CFR 63.114 include information on the design of the engineered barrier system, parameters, and conceptual models used in the NRC TPA. The requirements also include technical bases for either inclusion or exclusion of degradation, deterioration or alteration processes of engineered barriers, and technical bases for the models and parameter values used in the performance assessment. Similarly, in the NRC Yucca Mountain Review Plan (NRC, 2003), the waste package is considered in the section of Degradation of Engineered Barriers. The review areas in this section for the performance assessment include description of engineered barrier, sufficiency of data and parameters, data uncertainty and uncertainty propagation, model uncertainty and uncertainty propagation, comparison of the total-system performance assessment output to process-level model outputs and empirical studies, and use of expert elicitation.

1.3 Organization of the Report

This report is organized into five chapters to address the objective and scope identified in Section 1.1. Chapter 1 is an introduction. Chapter 2 is a compilation of long-term corrosion rate data reported in the literature. In addition, the validity of DOE assumptions for the general corrosion model of the waste package outer container to support the DOE Total System Performance Assessment (Betchel SAIC Company, LLC, 2004b) is examined. In Chapter 3, an assessment is provided on the long-term stability of the passive film on Alloy 22 considering film

thickness, structure, and chemical composition as functions of time. Film growth models are briefly discussed to provide insight on the long-term passive behavior of Alloy 22. In Chapter 4, degradation processes potentially compromising the Alloy 22 passive film stability, resulting in enhanced corrosion rates or localized corrosion susceptibility, are discussed. Among these potential processes, anodic sulfur segregation process might be detrimental and requires further experimental evaluation. The other considered processes are not expected to appreciably affect the long-term stability of the passive film on Alloy 22. Other suggested processes are briefly discussed including detrimental effects of base metal chromium depletion at the metal-film interface, film spallation by void formation, anion-selective sorption, increased cathodic kinetics, and alteration of passivation by dry–wet cyclic processes. Chapter 5 summarizes the main conclusions.

2 GENERAL CORROSION RATE OF ALLOY 22

Alloy 22 is the currently proposed container material for the waste package outer container (CRWMS M&O, 2000). Alloy 22 is a nickel-based alloy that contains a high concentration of chromium to promote formation of a protective passive film. Alloying additions of molybdenum and tungsten are also included to promote enhanced resistance against localized forms of corrosion. This alloy is highly resistant to corrosion in a wide range of environments, from oxidizing to reducing conditions, at various pH values, and temperatures. Additional information on Alloy 22 and similar nickel-based alloys has been reported by Cragnolino, et al. (1999).

The long-term passivity of Alloy 22 is significant for the extended containment of nuclear waste (CRWMS M&O, 2000). Estimates of the waste package lifetime are derived from extrapolation of relatively short-term experimental data (Bechtel SAIC Company, LLC, 2004b). In justifying and explaining extrapolations, changes to the passive film over time and the possible range of environments in the repository setting should be accounted for. Characterization of the dependence of corrosion rates on ranges of possible environmental conditions is important to supporting long-term assessments of waste package performance.

In the absence of environmental conditions conducive to localized corrosion or loss of passivity, Alloy 22 is expected to exhibit low corrosion rates characteristic of passive dissolution. A chromium-rich layer formed by solid state reactions next to the alloy is responsible for the passive dissolution of Alloy 22. In this chapter, general corrosion rates associated with passive dissolution reported in the literature are compiled for a range of temperatures. This chapter focuses on tests spanning weeks or longer at temperatures less than 110 °C [230 °F]. However, some data at 155 °C [311 °F] is listed to provide comparison to values obtained by Arrhenius extrapolations from low temperature corrosion rates. The general corrosion model used by the U.S. Department of Energy (DOE) in the repository performance assessment is discussed. Data and models developed at Center for Nuclear Waste Regulatory Analyses (CNWRA) are briefly discussed as well. The chapter concludes with an assessment of the DOE approach with respect to observations/critiques expressed in U.S. Nuclear Regulatory Commission (NRC) (2005) related to the appropriate assessment of general corrosion rates and extrapolation to elevated temperatures.

The measurement of corrosion rates for passive materials such as Alloy 22 can be conducted using many methods. Electrochemical methods include steady-state passive current density measurement, direct current polarization resistance measurement, and alternating-current electrochemical impedance spectroscopy (Pensado, et al., 2002). All of these techniques have limitations, particularly for the measurement of very low corrosion rates, close to instrumentation resolution limits. Another limitation of electrochemical methods is the test time required to obtain steady-state corrosion rates (rates that slowly change due to aging and annealing of the passive film). Nonelectrochemical methods are mainly confined to gravimetric (weight-loss) measurements. Although this method is simple in principle, accurately determining corrosion rates for passive materials becomes difficult owing to the limited resolution of the measuring equipment for very thin films and artifacts (such as thickening of the film and the accumulation of deposits on the metal surface) (Pensado, et al., 2002).

2.1 Review of Literature Data

Alloy 22 corrosion and other similar corrosion-resistant nickel-chromium-molybdenum alloys are generally used in harsh environments that may promote localized forms of corrosion such as pitting corrosion, crevice corrosion, and stress corrosion cracking. General corrosion rates, under conditions where a passive film is stable, are generally not a limiting factor for the expected lifetime of industrial components manufactured with corrosion-resistant alloys. In these cases, the thickness of materials used is typically defined by requirements other than corrosion allowance (e.g., operating pressure and stress fields). Sridhar and Cragnolino (2002) reported corrosion rates of nickel-chromium-molybdenum alloys used in industrial applications.

DOE-supported studies have been conducted using environments that are purported to be similar to water chemistries that may be found in the repository setting. These studies include both electrochemical tests and gravimetric determinations of the corrosion rates of Alloy 22 under passive conditions. Dunn, et al. (2005) have reviewed many of these studies. The results of these studies, as well as the results from more recent studies in the literature, are included in Table 2-1.

Hua and Gordon (2004) reported corrosion rates measured via weight loss after 4- and 8-week exposures in basic saturated water at temperatures of 60 and 105 °C [140 and 221 °F]. Corrosion rates were found to be a function of time and temperature. The corrosion rates after 8 weeks were a factor of 2 lower than those after 4 weeks. Weight loss measurements for the annealed specimens were similar to the welded material. Considering all specimens, regardless of differences in metallurgical condition, the activation energy for general corrosion was determined to be 25.3 kJ/mol [24.0 Btu/mol] based on the 8-week exposure data.

Lloyd, et al. (2003) measured the passive corrosion rate of Alloy 22 and C276 in 1 M NaCl + 0.1 M H_2SO_4 solutions. They reported an activation energy that was dependent on potential, ranging from 32 to 46 kJ/mol [30 to 44 Btu/mol] for Alloy 22. Potentiostatic tests showed that the current density decreased with time over a period of 12 hours. No measurements of the oxide film thickness as a function of time were reported; however, the oxide layer thickness and the compositions of the oxide as a function of potential were examined. Passive corrosion current densities at potentials of 500 mV versus saturated Ag/AgCl at 85 °C [185 °F] were in the range of 3×10^{-7} A/cm^2. These current densities translate into rather high corrosion rates of the order of 3×10^{-3} mm/yr [0.12 mpy]. However, these data were collected from tests lasting hours and, as time elapses, corrosion rates tend to decrease. At lower potentials, accurate measurement of the anodic current density was not possible (instead, a net cathodic current was measured).

Gray, et al. (2006a) reported corrosion rates of Alloy 22 in acidified 1 and 4 m NaCl solutions with nitrate-to-chloride {$[NO_3^-]/[Cl^-]$} ratios up to 0.5 using a polarization resistance method after 2 hours of exposure. Increased nitrate concentrations decreased the corrosion rate of Alloy 22. For solutions with pH values greater than 1, corrosion rates were below 10^{-3} mm/yr [3.9×10^{-2} mpy] at 90 °C [194 °F]. At pH values less than 1, the corrosion rates increased to values greater than 2×10^{-2} mm/yr [0.79 mpy] due to depassivation in solutions with low nitrate concentration. Depassivation was observed in all solutions, independently of the nitrate concentration and temperature, for pH<0. In hydrochloric and sulfuric acids without nitrate

Table 2-1. A Summary of the Corrosion Data of Alloy 22 in the Literature (Test of Duration of Days or Longer)						
Solution	**Temperature °C [°F]**	**Material**	**Method**	**Corrosion Rate (Testing Duration)**	**Activation Energy**	**Reference**
Simulated acidified water	90 [194]	Mill-annealed	Polarization resistance	3.6×10^{-4} to 7.9×10^{-4} mm/yr [0.0142 to 0.0311 mpy]	Not Applicable	Lian, et al. (2003)
Simulated acidified water	90 [194]	Mill-annealed	Electrochemical impedance spectroscopy	4.6×10^{-4} to 3.0×10^{-3} mm/yr [0.018 to 0.118 mpy]	Not Applicable	Lian, et al. (2003)
1 M NaCl	60, 90 [140, 194]	Mill-annealed	Polarization resistance	9.4×10^{-4} to 3.0×10^{-3} mm/yr [0.037 to 0.118 mpy]	Not Applicable	Meck, et al. (2003)
0.5 M NaCl + 0.5 M NaF	60, 90 [140, 194]	Mill-annealed	Polarization resistance	1.6×10^{-4} to 4.7×10^{-4} mm/yr [0.0063 to 0.0185 mpy]	Not Applicable	Meck, et al. (2003)
Basic simulated water	60 to 105 [140 to 221]	Mill-annealed + welded	Weight loss	7.5×10^{-5} to 2.5×10^{-4} mm/yr [0.00295 to 0.0098 mpy] (8 weeks)	25.3 kJ/mol [24 Btu/mol]	Hua and Gordon (2004)
Basic simulated water	60 to 105 [140 to 221]	Mill-annealed + welded	Weight loss	1.5×10^{-4} to 5.1×10^{-4} mm/yr [0.0059 to 0.02 mpy] (4 weeks)	Not Applicable	Hua and Gordon (2004)
1 M NaCl	30 to 90 [86 to 194]	Mill-annealed	Polarization resistance	2.4×10^{-4} to 1.2×10^{-2} mm/yr [0.00945 to 0.47 mpy]	Not Applicable	Day, et al. (2004)
4 M NaCl	45 to 105 [113 to 221]	Mill-annealed	Polarization resistance	4.0×10^{-4} to 3.1×10^{-3} mm/yr [0.016 to 0.122 mpy]	Not Applicable	Ilevbare (2006)
18 m $CaCl_2$ + 9 m $Ca(NO_3)_2$	155 [311]	Welded	Polarization resistance	3.7×10^{-4} mm/yr [0.014 mpy] (600 days)	Not Applicable	Rodríguez, et al. (2007)
18 m $CaCl_2$ + 9 m $Ca(NO_3)_2$	155 [311]	Welded + solution annealed	Polarization resistance	2.6×10^{-4} mm/yr [0.010 mpy] (600 days)	Not Applicable	Rodríguez, et al. (2007)
18 m $CaCl_2$ + 0.9 m $Ca(NO_3)_2$	155 [311]	Welded	Polarization resistance	9.0×10^{-3} mm/yr [0.35 mpy] (600 days)	Not Applicable	Rodríguez, et al. (2007)

Table 2-1. A Summary for the Corrosion Data of Alloy 22 in the Literature (Test of Duration of Days or Longer) (continued)						
Solution	**Temperature °C [°F]**	**Material**	**Method**	**Corrosion Rate (Testing Duration)**	**Activation Energy**	**Reference**
18 m $CaCl_2$ + 0.9 m $Ca(NO_3)_2$	155 [311]	Welded + solution annealed	Polarization resistance	1.2×10^{-4} mm/yr [0.005 mpy] (600 days)	Not Applicable	Rodríguez, et al. (2007)

References:

Lian, T., J.C. Estill, G.A. Hust, and R.B. Rebak. "Passive and Transpassive Dissolution of Alloy 22 in Simulated Repository Environments." *Corrosion*. Paper No. 694. Houston, Texas: NACE International. 2003.

Meck, N.S., P. Crook, S.D. Day, and R.B. Rebak. "Localized Corrosion Susceptibility of Nickel Alloys in Halide Containing Environments." *Corrosion*. Paper No. 682. Houston, Texas: NACE International. 2003.

Hua, F. and G. Gordon. "Corrosion Behavior of Alloy 22 and Ti Grade 7 in a Nuclear Waste Repository Environment." *Corrosion*. Vol. 60, No. 8. pp. 764–777. 2004.

Day, S.D., M.T. Whalen, K.J. King, G.A. Hust, L.L. Wong, J.C. Estill, and R.B. Rebak. "Corrosion Behavior of Alloy 22 in Oxalic Acid and Sodium Chloride Solutions." *Corrosion*. Vol. 60, No. 9. pp. 804–814. 2004.

Ilevbare, G.O. "Effect of Sulfate on the Passive and Crevice Corrosion Properties of Alloy 22 in 4 M Sodium Chloride." *Corrosion*. Vol. 62, No. 4. pp. 340–356. 2006.

Rodríguez, M.A., M.L. Stuart, and R.B. Rebak. "Long Term Electrochemical Behavior of Creviced and Non-Creviced Alloy 22 in $CaCl_2$ + $Ca(NO_3)_2$ Brines at 155 °C." *Proceedings of the CORROSION 2007.* Conference Paper No. 07577. Houston, Texas: NACE International. 2007.

(Gray, et al., 2006b), the critical values of pH for depassivation where corrosion rates exceeded 100 mm/yr at 60 °C [140 °F] in 1 m NaCl and 90 °C [194 °F] in 4 m NaCl had a pH of 0.5 and 2.5, respectively.

Evans, et al. (2005) measured the corrosion rates of Alloy 22 in 1 to 6 m NaCl solutions with different $[NO_3^-]$ /$[Cl^-]$ ratios of 0.05 to 0.15 at 100 °C [212 °F] using the polarization resistance method. The initial corrosion rate of 6×10^{-4} mm/yr [0.024 mpy] in concentrated NaCl solutions decreased with time, and the rate after 50 days was less than 6×10^{-6} mm/yr [2.4×10^{-4} mpy]. The measured corrosion rate was not strongly dependent on chloride concentration but was dependent on the $[NO_3^-]$ /$[Cl^-]$ ratio. The lowest corrosion rates were measured in 6 m NaCl with $[NO_3^-]$/[Cl−] of 0.15. After more than 280 days, the corrosion rate was approximately 2×10^{-5} mm/yr [8×10^{-4} mpy].

Ilevbare (2006) measured the corrosion rates of Alloy 22 exposed to 4 M NaCl solutions with and without Na_2SO_4 additions (0.04 and 0.4 M Na_2SO_4) using the polarization resistance method. Corrosion rates were determined to be a function of temperature over the range from 45 to 105 °C [113 to 221 °F]. The addition of sulfate decreased the general corrosion rate. The resultant decrease was most noticeable at temperatures at or above 75 °C [167 °F]. At lower temperatures, corrosion rates in all solutions were low. After 300 days of immersion, corrosion rates were measured between 4×10^{-4} and 3.1×10^{-3} mm/yr [0.016 and 0.122 mpy].

With respect to elevated temperature tests, Rodríguez, et al. (2007) measured the corrosion rates of the as-welded and welded plus solution heat treated Alloy 22 samples in concentrated solutions containing 18 m $CaCl_2$ with either 0.9 or 9 m $Ca(NO_3)_2$ at 155 °C [311 °F] for 600 days. Corrosion rates were measured using the polarization resistance method. The corrosion rate for the as-welded crevice samples was 3.7×10^{-4} mm/yr [0.015 mpy]. Samples that were solution annealed after welding had a slightly lower corrosion rate of 2.6×10^{-4} mm/yr [0.010 mpy] in 18 m $CaCl_2$ with 9 m $Ca(NO_3)_2$. The corrosion rate of the as-welded samples had greater variation in corrosion rates over 600 days. The final corrosion rate of the solution-annealed sample was similar in the 18 m $CaCl_2$ with 0.9 m $Ca(NO_3)_2$ solution, although greater variations were observed with time. Much higher corrosion rates were observed with the as-welded crevice samples when the $Ca(NO_3)_2$ concentration was reduced from 9 to 0.9 m $Ca(NO_3)_2$. After 600 days, the as-welded crevice sample suffered uniform transpassive dissolution, and the corrosion rate increased to 9.0×10^{-3} mm/yr [0.35 mpy]. These experimental data are consistent with the notions that (i) nitrate is an effective corrosion inhibitor even at elevated temperatures and (ii) thermal treatment of welds enhances the material resistance against general corrosion.

2.2 Review of DOE Data and Approach

DOE investigated the general corrosion rate of Alloy 22 using both mill-annealed and welded material (Bechtel SAIC Company, LLC, 2004b). Tests were conducted in the long-term corrosion test facility using two coupon types: weight-loss coupons and crevice coupons. The nominal specimen dimensions of two coupon types were approximately 50 × 25 × 3 mm [2 × 1 × 0.125 in] and 50 × 50 × 3 mm [2 × 2 × 0.125 in], respectively. The coupons had a 7.9-mm [0.31-in]-diameter hole in the center for sample mounting. For both coupon types, two metallurgical conditions were used (i.e., wrought material as the base metal and welded material). The coupons were fabricated from Alloy 22 plate stock. All weight-loss coupons were affixed using an insulating 12.7-mm [0.5-in]-diameter polytetrafluoroethylene or ceramic washer,

while all crevice coupons were affixed using a 19.1-mm [0.75-in]-diameter polytetrafluoroethylene or ceramic crevice former. Tests were conducted in 2,000-liter [528 gal] tanks that were filled with approximately 1,000 liters [264 gal] of test solution. The temperature of the solutions was controlled at either 60 or 90 °C [140 or 194 °F]. The test solution in each tank is covered with a blanket of air flowing at approximately 150 cm^3/min [9.15^3 in/min] and agitated. The general corrosion rates were determined using weight-loss specimens exposed for periods ranging from 6 months to 5 years in test solutions derived from the composition of J–13 well water including simulated dilute water, simulated concentrated water, simulated acidified water, and simulated saturated water.

Based on weight-loss measurements, there were no significant differences in the corrosion rates for mill-annealed and welded specimens. Corrosion rates decreased with exposure time. For an exposure time of 2 years, corrosion rates were −31 to 37 nm/yr [-1.2×10^{-3} to 1.5×10^{-3} mpy] for specimens with no crevices and −9 to 73 nm/yr [-3.5×10^{-4} to 2.9×10^{-3} mpy] with crevices. Negative corrosion rates were attributed to the accumulation of silica scale on test specimens. Tests conducted for shorter periods yielded higher corrosion rates. For the 5-year specimens, the range of corrosion rates varied from 0 to 12 nm/yr [0 to 4.7×10^{-4} mpy] for the weight-loss specimens and 0 to 23 nm/yr [0 to 9.1×10^{-4} mpy] for the crevice specimens. Average corrosion rates were 50 nm/yr [2.0×10^{-3} mpy] for the specimens exposed for 6 months, 30 nm/yr [1.2×10^{-3} mpy] after 1 year, 10 nm/yr [3.9×10^{-4} mpy] after 2 years, and 7.9 nm/yr [3.1×10^{-4} mpy] for the 5-year specimens. Although the data for the 5-year specimens were treated collectively, the effects of the individual test variables are provided in Table 2-2. The specimen type (i.e., crevice or weight loss) had more significant effects on corrosion rate than on temperature and metallurgical conditions. The crevice coupons showed higher corrosion rates than weight-loss coupons.

In addition to the weight-loss tests, corrosion rates of Alloy 22 were also measured using electrochemical techniques, such as polarization resistance and anodic current measurement methods in multi-ionic solutions including simulated acidified water, simulated dilute water, and simulated concentrated water (Bechtel SAIC Company, LLC, 2004b). Samples were held at the open circuit potential for 24 hours prior to measuring the polarization resistance. Average values and standard deviations for the base metal samples are $2.1 \pm 1.2 \times 10^{-4}$ mm/yr [0.0083 ± 0.0047 mpy], $0.3 \pm 0.3 \times 10^{-4}$ mm/yr [0.0012 ± 0.0012 mpy], and $1.5 \pm 0.4 \times 10^{-4}$ mm/yr [0.0059 ± 0.0016 mpy] for pH 3, 8, and 11, respectively. Average values and standard deviations for the weld metal samples are $1 \pm 0.5 \times 10^{-4}$ mm/yr [0.0039 ± 0.00197 mpy], $0.11 \pm 0.03 \times 10^{-4}$ mm/yr [0.0004 ± 0.00012 mpy], and $0.17 \pm 0.03 \times 10^{-4}$ mm/yr [0.00055 ± 0.00012 mpy] for pH 3, 8, and 11, respectively. Based on the results, corrosion rates were lower in near-neutral and alkaline solutions, and the corrosion rate of the welded metals was similar to the wrought base metals.

Short-term tests under potentiostatic conditions showed that the passive current decreased over time prior to reaching a steady state value when Alloy 22 was held at fixed potential within the passive region. The initial current decrease was attributed to the passive film growth. The transition to the steady-state current was attributed to a balance between dissolution and reformation of the passive film. Based on the steady state current value, general corrosion rates were determined as a function of solution pH. The average values and standard deviations for the base metal were $1.9 \pm 3.0 \times 10^{-4}$ mm/yr [0.0075 ± 0.012 mpy], $2.0 \pm 1.7 \times 10^{-4}$ mm/yr [0.0079 ± 0.0067 mpy], and $1.9 \pm 1.6 \times 10^{-4}$ mm /yr [0.0075 ± 0.0063 mpy] for pH 3, 8, and 11, respectively. A limited number of welded specimens were also tested. Samples that

Table 2-2. Measured Corrosion Rates of Alloy 22 for 5-Year Long-Term Corrosion Test Facility by the U.S. Department of Energy*							
Variable	Variable Range °C [°F]	Corrosion Rate of Weight-Loss Specimens nm/yr (Rates at 10, 50, and 90 Percent Distribution			Corrosion Rate of Crevice Specimens nm/yr (Rates at 10, 50, and 90 Percent Distribution)		
		10	50	90	10	50	90
Temperature	60 [140]	0	2.2	3.5	2.5	6.8	14.5
	90 [194]	1	2.5	10	1	6	16
Position	Aqueous	0.07	2.7	10.5	3	7	14.8
	Vapor	0	1.5	3.5	1	4.8	16
Metallurgical Condition	Mill-annealed	0	1.3	5.9	3	6.5	16
	Weld	0	2.5	10.7	0.4	6	16
Solution Composition	Simulated acidified water	0	2.7	4.5	5.8	8	16
	Simulated concentrated water	0	2.3	10.6	2	7	13.5
	Simulated dilute water	0	1.3	2.8	0.5	3	6.4

*Bechtel SAIC Company, LLC. "General Corrosion and Localized Corrosion of Waste Package Outer Barrier." ANL–EBS–MD–000003. Rev 02. Las Vegas, Nevada: Bechtel SAIC Company, LLC. 2004.

were tested at pH 3 had final current corrosion rates below 0.31×10^{-4} mm/yr [1.22×10^{-3} mpy] at both 200 and 400 mV versus saturated Ag/AgCl potentials. At pH 8, the final current corrosion rates were below 0.8×10^{-4} mm/yr [3.15×10^{-3} mpy] at both 200 and 400 mV versus saturated Ag/AgCl.

2.2.1 Conceptual Model in Total System Performance Assessment–License Application

The DOE conceptual model (Bechtel SAIC Company, LLC, 2004b) for the general corrosion of Alloy 22 uses the corrosion rates for specimens exposed for 5 years in the long-term corrosion test facility. All specimens regardless of the metallurgical conditions (mill-annealed and welded), specimen types (i.e., weight loss or crevice), solution chemistry, or temperature were grouped together. The temperature dependence of the general corrosion rate was determined in separate tests where the corrosion rate of Alloy 22 was determined using polarization

resistance techniques in 1 and 1.25 M NaCl solutions and 1.25 to 9 M $CaCl_2$ solutions at temperatures ranging from 45 to 175 °C [113 to 347 °F]. Based on the polarization resistance data, the activation energy of Alloy 22 was determined to be 25.9 ± 2.46 kJ/mol [24.5 ± 2.33 Btu/mol]. The resulting distribution for the general corrosion rate is shown in Figures 2-1 and 2-2 as a function of the temperature considering effective activation energies equal to 33.29 and 18.53 kJ/mol [31.55 and 17.56 Btu/mol], respectively.

The DOE distribution functions suggest that the median general corrosion rate at 25 °C [77 °F] could range from 1.7 to 3.2 nm/yr [6.7×10^{-5} to 1.3×10^{-4} mpy], accounting for uncertainty in the effective activation energy (Bechtel SAIC Company, LLC, 2004b). The 99th percentile ranges from 5.6 to 10.4 nm/yr [2.2×10^{-4} to 4.1×10^{-4} mpy]. For 100 °C [212 °F], the median general corrosion rate could range from 14.5 to 25.7 nm/yr [5.7×10^{-4} to 9.8×10^{-4} mpy] and the 99th percentile rate from 46.7 to 82.7 nm/yr [1.8×10^{-3} to 3.3×10^{-3} mpy]. Extrapolating corrosion rates to 150 °C [302 °F] and assuming the passivity of the alloy is maintained, the median general corrosion rate could range from 29.4 to 91.3 nm/yr [1.2×10^{-3} to 3.6×10^{-3} mpy] and the 99th percentile rate from 94.6 to 294 nm/yr [3.7×10^{-3} to 1.2×10^{-2} mpy]. The extrapolated corrosion rates at 150 °C [302 °F] are underestimated with respect to data by Rodríguez, et al. (2007), who measured corrosion rates of the order of 300 nm/yr [0.012 mpy] at 155 °C [311 °F] after 600 days. The extrapolated data is consistent with corrosion rates measured by Smailos (1993) of the order of 60 nm/yr [0.0024 mpy] in 25.9-percent NaCl solutions at 150 °C [302 °F] after 18-month exposures in Alloy C–4, which is an alloy similar to Alloy 22 in its dominant Ni-Cr-Mo contents.

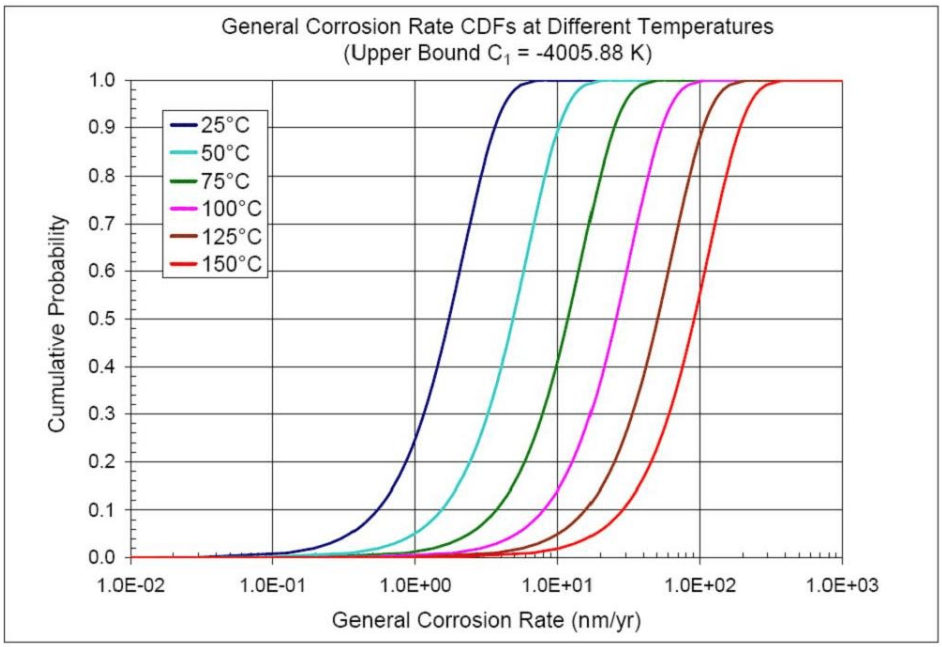

Figure 2-1. Calculated Model Outputs of the Basecase Temperature-Dependent General Corrosion Model With the Upper-Bound Activation Energy of 33.29 kJ/mol [31.55 Btu/mol] at 25, 50, 75, 100, 125, and 150 °C [77, 122, 167, 212, 257, and 302 °F] (Bechtel SAIC Company, LLC, 2004b). CDF = Cumulative Distribution Function.

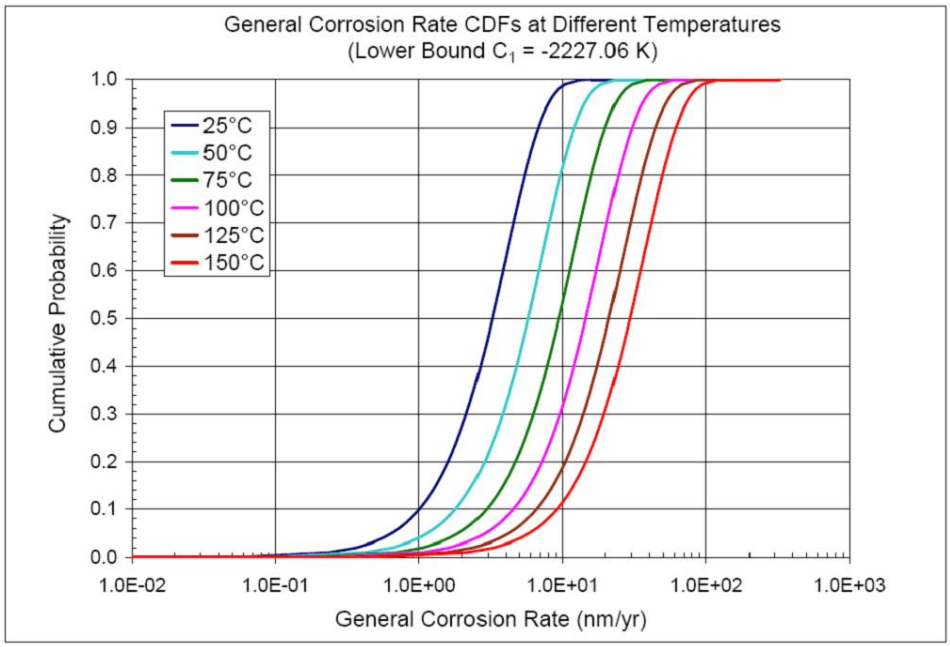

Figure 2-2. Calculated Model Outputs of the Basecase Temperature-Dependent General Corrosion Model With the Lower-Bound Activation Energy of 18.53 kJ/mol [17.56 Btu/mol] at 25, 50, 75, 100, 125, and 150 °C [77, 122, 167, 212, 257, and 302 °F] (Bechtel SAIC Company, LLC, 2004b). CDF = Cumulative Distribution Function.

2.2.2 Alternative Data Treatment

2.2.2.1 Time-Dependent Corrosion Rate

The DOE general corrosion model assumes that the general corrosion rate is time independent. Actual test data obtained using primarily weight-loss specimens over a period of 5 years indicate that the general corrosion rate tends to decrease with time. Decreasing corrosion rates are also noted in passive current density measurements reported by other authors over shorter terms (Dunn, et al., 2005; Hua and Gordon, 2004; Lloyd, et al., 2003; Pensado, et al., 2002). Figure 2-3 shows corrosion rate data obtained over a period of 5 years using a combination of measurement techniques. The decreasing trend in the corrosion rate fits a power law equation. DOE has argued that it is reasonable to expect that the decreasing trend will continue. Although a steady-state corrosion rate could be reached, the value has not been established yet. Thus, distribution functions derived with 5-year data bound corrosion rates expected in the repository setting over long terms (longer than 5 years). Because the corrosion rate for extremely long times is unknown, DOE adopted the approach in its performance assessment model of ignoring any time dependence.

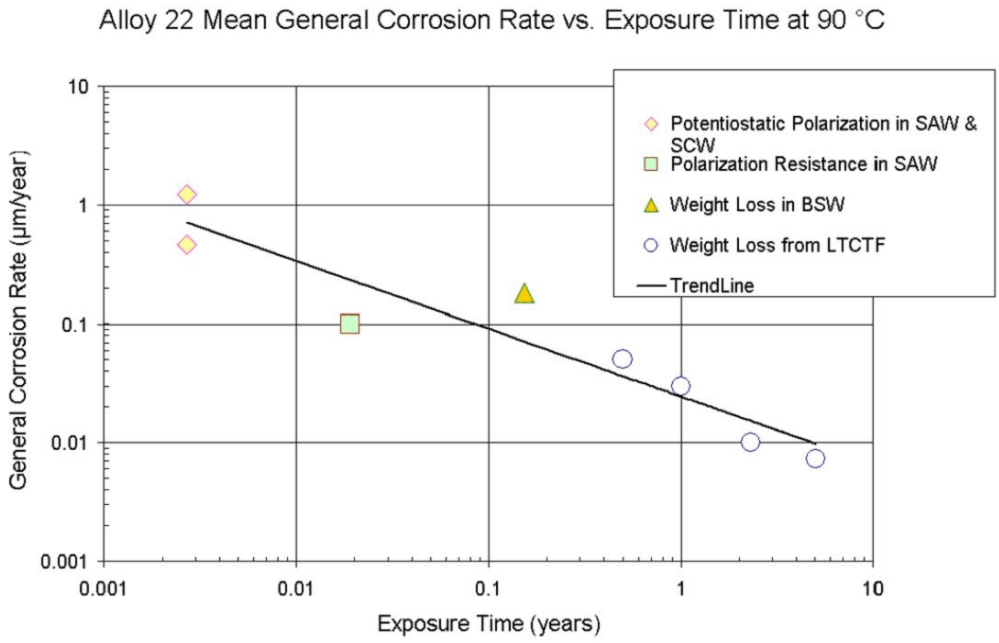

Figure 2-3. Decrease of the Mean General Corrosion Rate of Alloy 22 With Time (Bechtel SAIC Company, LLC, 2004b). SAW = Simulated Acidified Water, SCW = Simulated Concentrated Water, BSW = Basic Simulated Water, LTCTF = Long-Term Corrosion Test Facility.

2.2.2.2 Crevice Sample Corrosion Rates

In the analysis of the weight-loss measurement data, the general corrosion rates of the crevice samples were found to be higher than the weight-loss samples. Several possible reasons may explain this observed behavior. Although the cause for this is not clear, it may be related to surface polishing treatments or higher corrosion rates in the area under the crevice former (i.e., the crevice area). To develop an alternate interpretation of crevice specimen data, DOE performed different data treatment to estimate the corrosion rate of the area under the crevice former (Bechtel SAIC Company, LLC, 2004b):

(i) The average weight loss per unit area of weight-loss geometry samples was calculated.

(ii) The “true” weight loss of the boldly exposed area of the crevice samples was estimated with the corrosion rate of the plain weight-loss samples.

(iii) The weight loss from the crevice area under the crevice former was determined by subtracting the computed weight loss of the boldly exposed area from the total weight loss measured for the crevice samples.

(iv) The corrosion rate of the crevice area only (the area under the crevice former) was calculated using the calculated weight loss from the crevice area.

The empirical cumulative distribution function of the estimated corrosion rates of the crevice area only under the crevice former is shown in Figure 2-4, along with the cumulative distribution functions of the weight-loss samples and crevice samples for comparison. The median corrosion rate of the crevice area only is 51 nm/yr [0.002 mpy] and is about 10 times the mean of the crevice samples. Modified distributions of corrosion rates, from this alternative treatment of data of crevice samples as function of the temperature, are shown in Figure 2-5. The corrosion rates are one order of magnitude higher than in Figures 2-1 and 2-2. If the corrosion rate in the crevice region is about 10 times higher than in the boldly exposed area, microscopic examination would show the differences in the corrosion fronts between the two areas. However, examinations by optical microscopy and scanning electron microscope did not reveal such differences (Bechtel SAIC Company, LLC, 2004b). Therefore, the higher corrosion rates in the crevice samples cannot be explained solely by higher corrosion rates in the crevice regions. The reason for the apparently higher general corrosion rates measured in crevice samples is currently unknown. Therefore, the alternative interpretation of the Alloy 22 general corrosion rate is not considered in the waste package corrosion model for the DOE Total System Performance Assessment, because it is inconsistent with experimental microscopic observations.

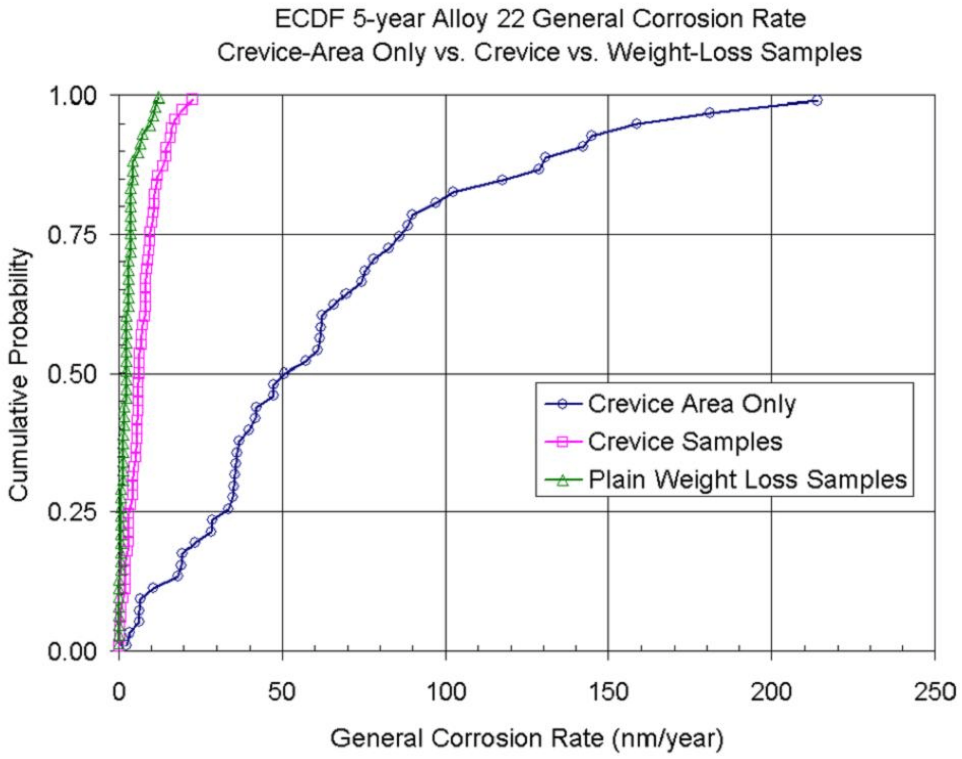

Figure 2-4. Empirical Cumulative Distribution Functions (ECDF) for General Corrosion Rates of Crevice Area Only, Crevice Samples, and Weight-Loss Samples After 5-Year Exposure in the Long-Term Corrosion Test Facility (Bechtel SAIC Company, LLC, 2004b)

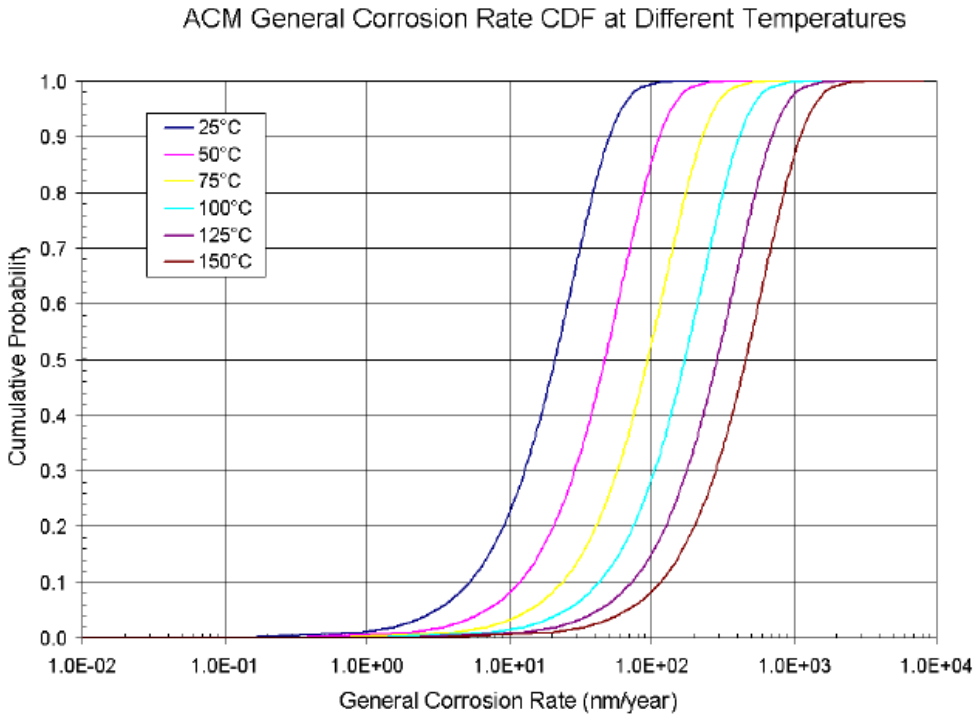

Figure 2-5. Calculated Model Outputs of the Temperature-Dependent General Corrosion Model Based on the Crevice-Area-Only Case at Temperatures of 25, 50, 75, 100, 125, and 150 °C [77, 122, 167, 212, 257, and 302 °F] (Bechtel SAIC Company, LLC, 2004b). ACM = Alternative Corrosion Model, CDF = Cumulative Distribution Function.

2.3 Review of CNWRA Data and Approach

2.3.1 Electrochemical Measurements

Corrosion rate determinations under passive conditions have been conducted using electrochemical methods including the measurement of quasi-steady-state passive current densities, polarization resistance, and electrochemical impedance spectroscopy (Dunn, et al., 2005). The experimental data are summarized in Table 2-3. Corrosion rates were found to be a function of temperature and time.

Based on the passive current density measurements, the corrosion rate of Alloy 22 in 5.5 M NaCl solution at 100 °C [212 °F] decreased by a factor of 2 over a 100-day period. The final corrosion rate, 50 nm/yr [0.002 mpy], is similar to the 1-year corrosion rate DOE obtained in the long-term corrosion test facility. The corrosion rates from 1-day tests for the welded and thermally aged materials tended to be higher than those of the mill-annealed alloys in 0.028 M NaCl solution.

Note that activation energies in Table 2-3 are higher than those DOE considered {of the order of 25 kJ/mol [23.7 Btu/mol]}.

Table 2-3. A Summary of Corrosion Data of Alloy 22 Performed by the Center for Nuclear Waste Regulatory Analyses*					
Solution	**Temperature °C [°F]**	**Material**	**Test Method (Duration)**	**Corrosion Rate**	**Activation Energy**
0.028 M NaCl	25 to 95 [77 to 203]	Mill-annealed	Passive Current Density (2 days)	1.9×10^{-6} to 1.2×10^{-4} mm/yr [7.5×10^{-5} to 4.7×10^{-3} mpy]	44.7 kJ/mol [42.4 Btu/mol]
0.028 M NaCl	25 to 95 [77 to 203]	Mill-annealed	Electrochemical impedance spectroscopy (1 day)	6×10^{-6} to 2×10^{-4} mm/yr [2.4×10^{-4} to 7.9×10^{-3} mpy]	46.3 KJ/mol [43.9 Btu/mol]
0.028 M NaCl	25 to 95 [77 to 203]	Welded, thermally aged 870 °C [1598 °F] /5min	Electrochemical impedance spectroscopy (1 day)	10^{-5} to 2×10^{-3} mm/yr [3.9×10^{-4} to 7.9×10^{-2} mpy]	N/A
4 M NaCl	40 to 150 [140 to 302]	Mill-annealed	Electrochemical impedance spectroscopy (1 day)	2×10^{-4} to 2×10^{-3} mm/yr [7.9×10^{-3} to 7.9×10^{-2} mpy]	41.8 KJ/mol [39.6 Btu/mol]
35 % $MgCl_2$	20 to 120 [68 to 248]	Mill-annealed	Electrochemical impedance spectroscopy (1 day)	2×10^{-4} to 10^{-2} mm/yr [7.9×10^{-3} to 0.039 mpy]	49.6 KJ/mol [47 Btu/mol]
5.5 M NaCl	100 [212]	Mill-annealed	Passive Current Density (100 days)	5×10^{-5} mm/yr [2×10^{-3} mpy]	N/A

*Dunn, D.S., O. Pensado, Y.-M. Pan, R.T. Pabalan, L. Yang, X. He, and K.T. Chiang. "Passive and Localized Corrosion of Alloy 22—Modeling and Experiments." CNWRA 2005-02. Rev. 1. San Antonio, Texas: CNWRA. 2005.

2.3.2 Conceptual Model in the NRC Total-system Performance Assessment

A description of the waste package corrosion model is included in Dunn, et al. (2005). The passive dissolution rate is based on corrosion rates determined as a function of temperature using electrochemical methods. Because the general corrosion rates were not determined to be a strong function of test solution, as long as passivity was maintained, passive dissolution rates are assumed independent of solution chemistry in the performance assessment model.

Note that the environmental composition is considered in the determination of the corrosion mode (i.e., general corrosion or localized corrosion). Specifically, the environmental chemistry determines the corrosion potential and the critical potential for localized corrosion initiation. General corrosion under passive conditions is assumed to prevail indefinitely if the conditions for localized corrosion are not met. Details of the environmental and corrosion model for the Total-system Performance Assessment is described in Dunn, et al. (2005).

In the Total-system Performance Assessment model, it is assumed that welded material exhibits the same general corrosion rate as the mill-annealed Alloy 22. This approach is justified by noting that the corrosion potential is more likely controlled by the current density of the most

abundant material—mill-annealed alloy. Stochastic variability in the corrosion rate is accounted for in the Total-system Performance Assessment model by using an uncertainty distribution function for general corrosion rates at a reference temperature {e.g., 95 °C [203 °F]}. A randomly sampled corrosion rate is adjusted as a function of the temperature, assuming an Arrhenius dependence (Dunn, et al., 2005; Pensado, et al., 2002). The depth of the general corrosion front is computed in the Total-system Performance Assessment model by integrating the corrosion rate with time (as time elapses, the waste package temperature changes because of the radioactive decay heat source). Waste package failure by corrosion is assumed to occur when the corrosion front propagates a depth exceeding the thickness of the waste package wall. Assuming corrosion rates ranging from 50 to 200 nm/yr [2×10^{-3} to 8×10^{-3} mpy] at 95 °C [203 °F] results in waste package breach times by general corrosion well beyond hundreds of thousands of years. Corrosion rates are sampled in the Total-system Performance Assessment code from the uncertainty distribution function, and statistics on waste package failure and radionuclide releases are derived from multiple Monte Carlo realizations.

For the sake of comparison with the DOE data, the median corrosion rate in the Total-system Performance Assessment code at 95 °C [203 °F] is 66 nm/yr [2.6×10^{-3} mpy]. Considering an effective activation energy of 44.7 kJ/mol [42.4 Btu/mol] and an Arrhenius dependence of the corrosion rate on the temperature, a corrosion rate equal to 442 nm/yr [0.017 mpy] is estimated by extrapolation to 150 °C [302 °F]. This extrapolated corrosion rate is slightly higher than the 600-day measurements by Rodríguez, et al. (2007) and higher than the DOE corrosion rates in Figures 2-1 and 2-2. On the other hand, extrapolating to 25 °C [77 °F] results in a median corrosion rate equal to 2.1 nm/yr [8.3×10^{-5} mpy], which compares well to the DOE data in Figures 2-1 and 2-2.

2.4 Assessment of General Corrosion Rates

NRC (2005) previously reviewed the assessment of the DOE approach including the model for general corrosion and the supporting data. At that time, the data and model abstraction for passive dissolution and general corrosion of the waste package outer container were generally considered adequate. However, aspects related to the conditions of the tests and the extent of passive dissolution, and passive film stability and corrosion rates in concentrated solutions with elevated boiling temperatures required additional explanation. There was no evidence at that time whether general corrosion rates could be extrapolated to higher temperatures. Thus, additional information was deemed necessary to evaluate the corrosion rates in concentrated solutions that may disrupt passivity, as well as information to support calculated passive corrosion rates over the entire temperature range of intended use.

The long-term corrosion rates measured by weight-loss methods were lower than the corresponding rates measured using electrochemical methods or techniques. Factors that may have contributed to this observation include (i) the thickening and aging of the passive film with time, resulting in apparently decreased corrosion rates; (ii) deposition of silica and other deposits such as corrosion products from less corrosion-resistant materials used in the test vessels that may have shielded the specimen surfaces from corrosion; (iii) the resolution of the weight-loss measurements; and (iv) the shorter timeframes used in the electrochemical tests.

Since the NRC (2005) assessment, multiple studies have been conducted to measure the general corrosion rate of Alloy 22. The results of these studies are summarized in Table 2-1. The testing Hua and Gordon (2004) reported supports the notion that corrosion rates tend to

decrease with time. Samples were in the passive state at temperatures of 105 °C [221 °F] in basic saturated water. Thus, additional evidence was generated indicating that the decrease in time may be an intrinsic feature of passive dissolution of Alloy 22. Therefore, it is possible that true "steady-state" passive dissolution may take a very long time to be established, if at all. The effective general corrosion rate is the result of complex processes such as oxide film formation and dissolution, ionic transport in the oxide film, solid-state diffusion of metallic elements in the bulk alloy, precipitation of secondary corrosion products, and aging and alteration of the oxide film. It would be beneficial to implement a fundamental study program, beyond the measurement of corrosion rates, aimed at the understanding of long-term passive dissolution via tracking of the evolution of relevant variables over time (e.g., oxide thickness and composition, alloy composition at the metal–oxide interface, solution composition near the oxide) accompanied by modeling aimed at rationalizing the observed time evolution.

Hua and Gordon (2004) also confirmed that in solutions where passive film stability is maintained, the corrosion rate closely follows an Arrhenius dependence on the temperature.

Also significant is the recent work by Rodríguez, et al. (2007), who showed that the passive film can be sustained in concentrated chloride solutions containing oxyanions that are known to inhibit localized corrosion initiation. Corrosion rates were dependent on the metallurgical condition, particularly in aggressive solutions. Corrosion rates in welded Alloy 22 were slightly higher than in a welded and solution-annealed sample in a solution with significant inhibiting oxyanion concentrations. However, when the nitrate ion concentration was decreased, the welded sample exhibited a corrosion rate 10 to 100 times greater than the welded plus solution-annealed material. Therefore, the beneficial effect of solution annealing with respect to general corrosion resistance was confirmed by Rodríguez, et al. (2007).

The corrosion rates Rodríguez, et al. (2007) measured bound extrapolated corrosion rates from the long-term corrosion test facility and an apparent activation energy derived with electrochemical methods (Figures 2-1 and 2-2). Extrapolated corrosion rates to elevated temperatures from DOE may be within a factor of 10 of actual experimental values. Although the discrepancy appears high, note that waste packages in the repository setting are expected to experience temperatures above the boiling point of pure water only for 1,000 or 2,000 years—a period over which general corrosion damage is expected to be limited to a small fraction of the waste package surface.

Based on a more complete set of data that is now available, several conclusions can be drawn about the general corrosion rate of Alloy 22.

- The values of the corrosion rate for Alloy 22 have been successfully measured using multiple methods such as weight-loss measurement and electrochemical techniques from short-term to 5-year long-term time periods in multi-ionic solutions in the temperature range of 25 to 155 °C [77 to 311 °F].

- Many experimental data from DOE, CNWRA, and the open literature show that the measured general corrosion rates of Alloy 22 are, in general, low {i.e., less than 100 nm/yr [0.004 mpy] at 95 °C [203 °F]} and tend to decrease with time at relatively low temperature {i.e., less than 100 °C [212 °F]}. The decreasing rate is observed in all solutions tested where passivity is maintained.

- Several studies have confirmed that general corrosion rates are dependent on temperature and tend to follow an Arrhenius dependence. Estimated values of the apparent activation energy vary from author to author, approximately in the range of 25 to 45 kJ/mol [23.7 to 42.7 Btu/mol]. Some authors have reported that the apparent activation energy appears partially dependent on test conditions.

- Passivity can be maintained in concentrated chloride solutions with low concentrations of inhibitors in most ranges of solution pH and temperatures. However, in certain environments such as concentrated chloride solutions with minimal nitrate at elevated temperatures {e.g. 155 °C [311 °F]} or in strong acidic solutions (i.e., pH <1) at relatively low temperatures {e.g., 60 and 90 °C [140 and 194 °F]}, Alloy 22 can experience depassivation, with resulting high general corrosion rates. Varying corrosion rates as a function of metallurgical condition have also been reported; however, this kind of variation appears within uncertainty bounds in the general corrosion rate.

- Extrapolated corrosion rates in the DOE Total System Performance Assessment model to 150 °C [302 °F] tend to be lower than measured rates. Two points should be noted: (i) it is unclear whether corrosion rates in the elevated temperature system would also show a decreasing trend in time and (ii) waste packages in the repository setting may be above 100 °C [212 °F] only for a limited term (of the order of 1,000 or 2,000 years). Therefore, it appears that the elevated temperature corrosion damage may be restricted to a small fraction of the waste package surface.

- There is no fundamental understanding of passive dissolution over the long term, and in particular, of processes causing the apparent corrosion time decrease. Annealing and thickening of the passive film, formation of precipitated oxihydroxides, as well as changes in the metal at the alloy–oxide interface (e.g., formation of element gradients, accumulation of defects) may contribute to decrease the corrosion rate as time elapses. It would be beneficial to implement an experimental program aimed at tracking the evolution of relevant variables over time (e.g., oxide thickness and composition, alloy composition at the metal–oxide interface, solution composition near the oxide) supported by modeling to rationalize the observed time evolution.

3 SIGNIFICANCE AND STABILITY OF PASSIVE FILM ON ALLOY 22

Passivity occurs when an alloy forms a very thin and protective passive film on its surface in aqueous solutions, significantly decreasing the general corrosion rate. Insoluble compounds that form on the surface of an alloy by precipitation generally do not provide as much protection as an oxide formed by solid-state anodic oxidation of the base metal. Chromium-containing alloys form a very stable passive film. The structure and composition of the passive film has been difficult to determine because the film is thin. In many instances, the passive film is considered to have a bi-layer structure. The inner layer is considered to be a chromium-rich oxide that conforms to the surface of the base metal. An outer film is typically considered to be made up of nickel and iron oxide/hydroxide. The outer layer is usually considered to form by dissolution and precipitation. The outer layer may contribute to the overall low corrosion rate of the alloy, but the inner chromium-rich layer is usually considered to play the major role.

The long-term stability of the passive film formed on Alloy 22 can be evaluated using different approaches. One of these approaches is to examine the corrosion rate and interpret the data to determine what may be happening to the passive film. This type of analysis was presented in Chapter 2. Another approach for examining the passive film is to conduct time-dependent measurements of thickness, composition, and structure. Recent laboratory long-term data has evaluated the film formation up to a period of 5 years. This information would have to be extrapolated to longer times, taking into account changes in temperature and environment. Knowledge of how the passive film is affected by time-dependent changes in the potential repository environment is an important aspect for assessing the passive film stability within the repository timeframe.

Determining the properties of passive film may be conducted using various techniques. These techniques include Auger electron spectroscopy, transmission electron microscopy, x-ray photoelectron spectroscopy, and electron energy loss spectroscopy. These tools can be used in conjunction with some sort of sputtering technique, allowing for the through-film analysis of the oxide. All of these techniques have some limitations regarding spatial resolution along the thickness because the inner layer is usually a couple of nanometers thick. An additional limitation is the possibility of a thick contamination or porous oxide layer forming on the surface of the alloy/passive film. The thick contamination layer could make it difficult to characterize or even sense the presence of a thin passive film. Thus, while these techniques can gather information on the composition and structure of the passive film, supporting data (e.g., corrosion rate) is needed to make any judgment on the long-term stability of the passive film.

This chapter presents a review of the properties of the passive film in environments restricted to temperatures below 100 °C [212 °F]. This is reasonable because the container materials will spend a majority of the time at these temperatures. This chapter examines the work that has been conducted during short-term tests and long-term tests (>2 years).

3.1 Review of Short-Term Test Data

The U.S. Department of Energy (DOE) and the Center for Nuclear Waste Regulatory Analyses (CNWRA) have generated most of the literature on the passive film formed on Alloy 22, primarily because Alloy 22 is the candidate material for the waste package outer container. Some results on the properties of the passive film on Alloy 22 are reported in the literature. A description of short-term test results is presented in this section. Additionally, the Sridhar and Cragnolino (2002) analysis of passive films on industrial analogs to Alloy 22 will also be examined.

A few studies have been conducted on Alloy 600 (Ni-18Cr-8Fe) at temperatures that were less than 100 °C [212 °F]. Hur and Park (2006) examined Alloy 600 exposed to deaerated 0.282 M NaCl between 90 °C [194 °F] and 280 °C [536 °F] using x-ray photoelectron spectroscopy and transmission electron microscopy. The oxide films were formed in the environment by polarizing the sample from the open circuit potential to 50 mV below the pitting potential. At 90 °C [194 °F], metallic chromium and Cr^{+3} corresponding to chromium oxide (Cr_2O_3) and hydroxide {$Cr[OH]_3$} were present in the film. In addition, metallic Ni and Ni^{2+} were identified, but were much weaker than the chromium species. The Alloy 600 passive film had an amorphous structure. The amorphous oxide structure can decrease the corrosion susceptibility because it contains fewer imperfections such as grain boundaries and dislocations.

Lloyd, et al. (2004) evaluated various nickel-chromium-molybdenum alloys, including C2000 (Ni-23Cr-16Mo-2Cu), C276 (Ni-16Cr-16Mo-5Fe-4W), C4 (Ni-16Cr-16Mo-3Fe), 625 (21Cr-9Mo-5Fe), and Alloy 22 for their passive corrosion properties. These alloys were passivated potentiostatically in a deaerated 1 M NaCl + 0.1 M H_2SO_4 solution that was ramped from 25 to 85 °C [77 to 185 °F] during the test. The data indicated that there was a decrease in the passive current density when the chromium content in the base alloy was increased. X-ray photoelectron spectroscopy on all of the tested alloys indicated the presence of Cr(III) in the oxide films. Most of the chromium spectra were from Cr_2O_3 characteristic films. However, some of the chromium spectra were in the form of a hydroxide. A parallel increase in Cr(III) concentration in the film occurred with the increase in potential. No Cr(VI) was observed, indicating that any Cr(VI) produced at the higher potentials must have dissolved or no Cr(VI) was formed. While molybdenum was present in all the oxides, its concentration increased with potential, similar to the chromium. Of all the materials, Alloy 22 had the lowest concentration of molybdenum in the oxide. The alloys with higher concentrations of chromium had a tendency to form a chromium-rich inner layer. At lower potentials (200 mV with respect to a Ag/AgCl reference electrode), the alloys with the higher chromium concentration (Alloy 22, C2000, and 625) showed a significant chromium signal from the outer edges of the film. At higher potentials, there was no chromium signal from the solution-film interface. For Alloy 22 and C2000, there was an enhanced chromium concentration in the inner layer and an enhancement in molybdenum in the outer layer. Lloyd, et al. (2004) also observed nickel in the inner chromium layer, which suggested that a nickel chromite may have existed at the surface of the base alloy.

In the same experiments, the thickness of the oxide film was also analyzed. The data from this study by Lloyd, et al. (2004) indicated that the oxide film thickness increased as the potential increased. In addition, the alloys with a lower chromium concentration had a thinner passive film and as the concentration of tungsten increased in the alloys, the oxide film thickness increased at the higher potentials. The corrosion rates measured in the tests indicated that the

higher chromium alloys had a lower corrosion rate. Additions of tungsten also decreased the corrosion rate, but not to the same extent as additions of chromium to the base alloy.

Rajeswari, et al. (2001) characterized the surface and pitting behavior of Alloy 59 (Ni-23Cr-16Mo-6Fe), C276, and Inconel 825 (Ni-31Fe-22Cr-3Mo). These samples were studied in a solution at 55 °C [131 °F] and contained 1,000 ppm chloride, 1,000 ppm sulfate, and 50 ppm thiosulfate with a pH of roughly 3.5. While all these alloys were evaluated, Alloy 59 was the only nickel-based alloy where x-ray photoelectron spectroscopy in conjunction with argon ion sputtering was utilized to conduct a depth profile evaluation of the passive film. On Alloy 59, a chromium(III) oxide was present mostly in the outer layer, while the inner layer was mostly composed of chromium(III) hydroxide. Nickel oxide was found at the metal–oxide interface, while a nickel hydroxide was found on the outer oxide. The pitting resistance performance of Alloy 59 was attributable to the role played by the chromium and other alloying elements. Interestingly, an increased nickel concentration was observed in the base metal under the passive film. The concentrated nickel may aid in the formation of molybdenum-chromium intermetallic bonds. The reduced anodic dissolution was thought to be due to the enriched passive film in MoO_4^{2-} species and the intermetallic layer below the passive film. This may have provided a source for oxide-forming metallic species, which improved the corrosion resistance of the nickel-chromium-molybdenum alloys.

Lloyd, et al. (2003) examined the behavior of both Alloy C276 and Alloy 22 in acidic solutions. These acidic conditions are not expected in the repository but were used to simulate the balance between the oxide film formation and dissolution, expected over a longer period of time. The materials were examined in a 1.0 M NaCl + 0.1 M H_2SO_4 solution at a temperature ranging from 25 to 85 °C [77 to 185 °F]. Polarization scans were conducted under these conditions, which showed that the Alloy 22 had a lower current density than C276 at 25 °C [77 °F]. Otherwise, the anodic scans for the two samples looked similar. In the reverse direction, the current density for Alloy 22 switched signs at 220 mV (with respect to a Ag/AgCl reference electrode in 0.1 Mol L^{-1} KCl), while C276 switched at 50 mV. As the temperature increased, the potential also increased for both samples. The Alloy 22 samples showed a slight increase in film thickness with voltage, while C276 showed no increase. The overall chromium content of the film increased with potential on the Alloy 22 and was predominantly in the inner layer. However, the nickel content was observed to decrease with potential. The overall molybdenum content in the oxide was greater in the C276 alloy, indicating that it is the chromium that plays a key role for passivity in these environments. At higher potentials on Alloy 22, it seemed that Cr(VI) was released into the solution, while molybdenum was retained as the dominant cation species in the oxide film.

Birn, et al. (1999) examined how the addition of molybdenum affects the passive film properties on nickel and iron-based alloys. Three materials were examined with concentrations of molybdenum at 3.5, 6.3, and 15.6 weight percent. The two alloys with the lower concentration of molybdenum were iron based, while the higher molybdenum concentrated alloy was balanced in nickel. The electrolyte used to evaluate these materials consisted of 0.5 M H_2SO_4 with various additions of NaCl from 0 to 2 M at temperatures of 25, 50, and 75 °C [77, 122, and 167 °F]. This electrolyte was deaerated with pure argon. Auger electron spectroscopy and ion milling was used to evaluate the surface of these films. The passivating films on all of the alloys were rather thin. Molybdenum in the passive film was depleted and not oxidized. The results

suggested that the role that molybdenum plays in corrosion resistance was in stabilizing the passive film and not as a passivity promoter. It was suggested that molybdenum acts as a dissolution moderator.

Miyagusuku and Devine (2007) evaluated the passive film properties of Alloy 22 in acidic conditions at room temperature {approximately 20 °C [68 °F]} and 90 °C [194 °F]. Polarization tests and impedance spectroscopy were both utilized to examine Alloy 22. The results from the room temperature tests indicated that Cr(VI) was the most likely product in the transpassive oxidation, suggesting that Cr(III) was probably a significant component in the passive film. At 90 °C [194 °F], the polarization curves results indicated that Alloy 22 did not form any Cr(VI). Results from a pure molybdenum sample in the same solution suggested that molybdenum may have a critical role in the properties of the passive film. Because it is believed that the oxidation of Cr(III) to Cr(VI) will decrease the pitting corrosion resistance of alloys with passive films mainly composed of Cr(III), the passive film on Alloy 22 was expected to be more resistant at 90 °C [194 °F] than at 20 °C [68 °F] in these types of acidic solutions. The results did not address the question of whether the oxidation of molybdenum at higher temperatures results in a soluble molybdenum compound or a species that remains in the passive film. The results also indicated that the capacitance decreased as this passive film formed, which, if the film was uniform and of identical composition, would suggest that there was a change in thickness of the film's space charge region. However, additional results would be needed to validate this concept. In addition, current capacitance measurements indicated that the film thickness was "very thin."

Macdonald, et al. (2004) measured the capacitance changes with applied potential of Alloy 22, represented by a Mott-Schottky plot, and postulated that the barrier layer of passive film in the passive region (i.e., lower than 0.6 V_{SHE}) is a defective chromium oxide ($Cr_{2+x}O_{3-y}$) with n-type electronic character and the passive film in the transpassive regions (i.e., higher than 0.6 V_{SHE}) is the p-type semiconductor. Based on the positive slope observed in the Mott-Schottky plot in the passive ranges, the authors concluded that the interstitial cations are the principal defect, unequivocally, with oxygen vacancies. If the barrier layer is cation rich, the oxide phase close to the metal–film interface was estimated to have the composition $Cr_{2.028}O_3$. If the barrier layer is oxygen deficient, the stoichiometry was estimated to be $Cr_2O_{2.981}$ at the same location. Carranza, et al. (2005) also reported the n-type characteristic of the passive film that formed on Alloy 22 tested in 1 M NaCl (pH 6) at 90 °C [194 °F]. The Mott-Schottky plot demonstrated two linear regions with a flat band potential of around 0.0 V_{SCE}. Below the flat band potential, Alloy 22 behaved as an n-type semiconductor (positive slope) possibly due to chromium interstitials and/or oxygen vacancies, which was originally postulated by Macdonald, et al. (2004). When the polarization was in a more noble potential region (e.g., above 0.0 V_{SCE}), its behavior was that of a p-type semiconductor (negative slope). Note that the change in electronic property of passive film occurred around 0.0 V_{SCE} and was found to be 300 mV below the initiation of transpassive dissolution 0.3 V_{SCE}. However, the difference of 300 mV might indicate either a p-type of chromium oxide or another p-type oxide that is not chromium in this potential region between 0.0 to 0.3 V_{SCE}.

While the n-type of chromium oxide formed on Alloy 22 has been postulated by Macdonald, et al. (2004) and Carranza, et al. (2005), other studies have shown the p-type character of chromium oxides formed on either iron-based chromium containing alloys such as Type 304 and 316 stainless steels in buffered solution at pH 9.2 (Hakiki and Da Cunho Belo, 1998), pure Cr and Fe-18Cr alloys in sulfuric acidic solution (Tsuchiya, et al., 2002), AISI 304 stainless steel

in concentrated $MgCl_2$ solution at 142 °C [288 °F] (Rangel and Da Cunho Belo, 2004) or Alloy 600 (Ni-16.3Cr-7.8Fe-0.28Mo-0.65Si) in a buffered solution at pH 9.2 at room temperature (Da Cunho Belo, et al., 1999), and Alloy 600 and Alloy 690 (Ni-292Cr-10.3Fe-0.31Mn-0.01Mo) in buffered solutions at pH of 8 and 10 at 350 and 320 °C [662 and 608 °F], respectively. This discrepancy related to the semiconducting properties of chromium oxide (i.e., n-type postulated by Macdonald and p-type observed by other investigators as noted) may be ascribed to the different material properties (e.g., chemical compositions and microstructure) or test conditions (e.g., solution chemistry, pH, temperature, surface roughness).

Gray, et al. (2006a) examined the influence of pH, anion concentration, and temperature on the corrosion behavior of Alloy 22. The samples were examined in 1 and 4 M NaCl containing HCl, H_2SO_4, or HNO_3 at 25, 60, and 90 °C [77, 140, and 194 °F]. By using impedance spectroscopy and assuming a parallel plate capacitor, the film thickness was decreased with lower pH in HCl and H_2SO_4, concurring with a lower corrosion resistance. The film thickened in the HNO_3, correlating with a higher corrosion resistance. In this correlation between film thickness and corrosion resistance, it is assumed that the film did not become more stable or change composition in these various environments. X-ray photoelectron spectroscopy analysis indicated that the major contributor to the passive film was Cr(III) with lesser concentrations of molybdenum. The influence of chloride seemed to be its binding with the passive film, which then thinned it out. The effect of the nitrate was to thicken the passive film and inhibit dissolution.

Gray, et al. (2006b) evaluated the inhibiting effect of nitrates by examining the passive film breakdown of Alloy 22 in chloride environments. Alloy 22 was evaluated in a chloride-containing solution at 1 and 4 M NaCl from a pH of 5 to −1 at 60 and 90 °C [140 and 194 °F]. Raman spectroscopy was utilized to determine what may have occurred to the passive film as NO^-_3 was added to the test solution. The results indicated that the corrosion of Alloy 22 in low pH can be inhibited by small amounts of nitrate added to the solution. As suggested by some of the data presented earlier, the passive film may be enriched in molybdenum for these environments. Raman results suggest that the dissolved molybdenum species increased in the transpassive region, while the amount of NO_3^- species in solution decreased with time. As the pH was lowered and potential increased, more molybdenum segregated from the alloy to the oxide that solubilized in the acidic solutions.

DOE considers that the corrosion performance of the waste package outer barrier is dependent upon the integrity of a thin and adherent passive film that forms on the alloy surface (Bechtel SAIC Company, LLC, 2004b). The low general corrosion rates and resistance to localized corrosion will depend upon the long-term stability of the passive film. DOE defines passivity as the “formation of a thin and adherent oxide or oxyhydroxide film that protects a metal or alloy from corrosion degradation.” It is the integrity of this passive film that dictates the corrosion performance of the corrosion-resistant alloys. Some tests were conducted using two techniques to address the film stability (Orme, 2005): (i) polarization resistance and (ii) potentiostatic testing, measuring the current density for a period of time. Both of these electrochemical measurements were converted to a corrosion rate to compare the results from both methods. Testing details follow.

For nickel-chromium-molybdenum alloys, it is believed that the molybdenum provides resistance against reducing environments; chromium against oxidizing environments; chromium and molybdenum against localized attack; and nickel, chromium, and molybdenum against stress

corrosion cracking due to chlorides. A modeling program, EQ3/6, determined the equilibrium oxide phases at two potential and pH points. At pH 2.8, the modeling results predicted that Cr_2O_3 would be the major phase. As the voltage is increased, there should be some contribution from $Fe_2(MoO_4)_3$. Near neutral pH, nickel oxides are expected to be present and chromium will predominantly be in a $NiCr_2O_4$ phase. At higher potentials, the modeling results indicated that there should not be any thermodynamically stable chromium oxides.

Samples of Alloy 22 were tested in complex multi-ionic solutions that were based on the repository groundwater. These solutions are simulated acidic water, simulated concentrated water, and basic saturated water. Buffered 1 M NaCl solutions with pHs of 3, 8, and 11, similar to the simulated waters, were also used. Alloy 22 showed similar potential scans in the buffered NaCl solutions and the simulated solutions at the same pH levels as shown in Figure 3-1. This observation suggested that the oxide films may be mostly a function of pH and not of ionic additions.

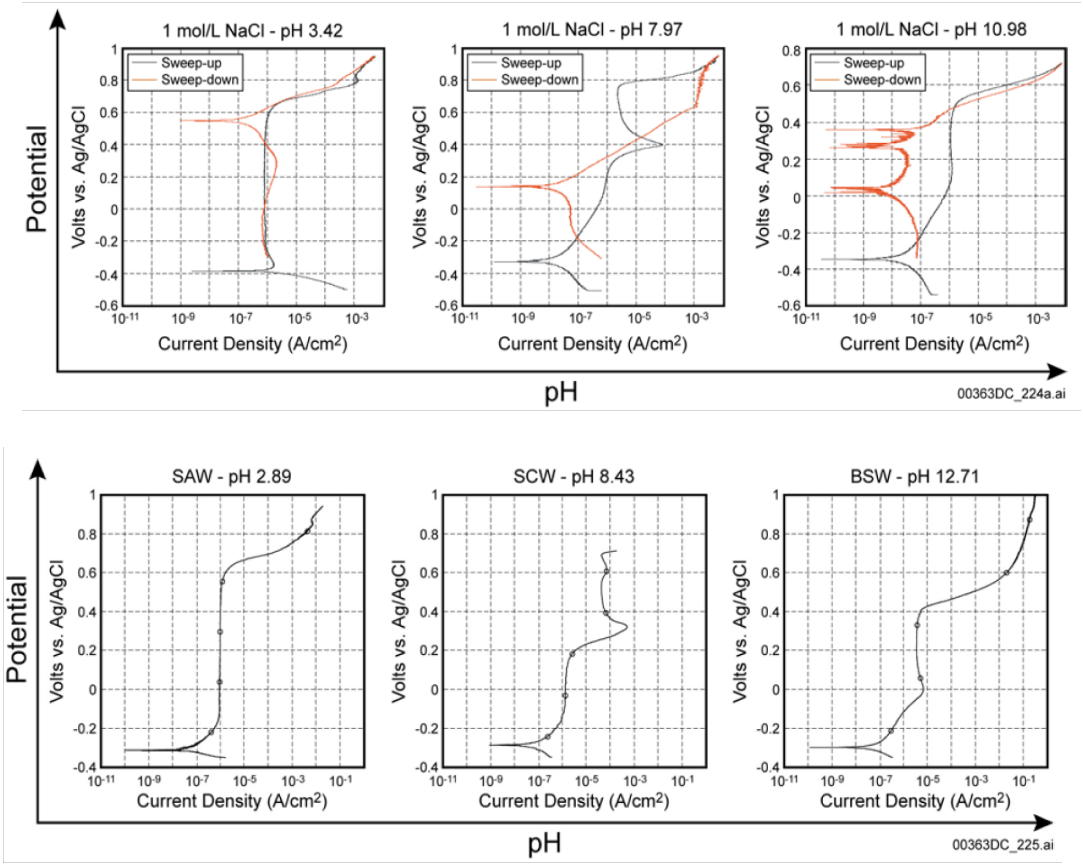

Figure 3-1. Polarization Curves Showing the Similarity Between Buffered Solutions (Top) and Simulated Solutions (Bottom) (Orme, 2005). SAW = Simulated Acidified Water, SCW = Simulated Concentrated Water, BSW = Basic Saturated Water. (Orme, 2005)

Alloy 22 exhibited a classical passive behavior in 1 M NaCl at pH 3 (buffered solutions). The oxide films were examined at 200 and 500 mV (with respect to a saturated Ag/AgCl reference electrode)—two potentials on either side of the passive region. The oxide grown in both potentials was thin, smooth, and conforming to the surface of the material. At the lower potentials, the oxide film thickness was roughly 4.0 ± 0.5 nm [$1.6 \times 10^{-4} \pm 2.0 \times 10^{-5}$ mil], while the film formed at the higher potential was 2.4 ± 0.3 nm [$9.4 \times 10^{-5} \pm 1.2 \times 10^{-5}$ mil]. Electron energy loss spectroscopy images, which are shown in Figure 3-2, indicated that both chromium and oxygen predominated in the oxide film. For the electron energy loss spectroscopy chromium map, there was a slightly dark line in the base metal right below the oxide. This may have indicated that there could be less chromium in that area, which is consistent with nickel enrichment. Chapter 4 discusses how the reduction in chromium concentration below the passive film may affect the long-term stability of the passive film.

In simulated acidic water at pH 3, the passive films were similar to those formed in the buffered NaCl solution. At a potential of 200 mV, the film was roughly 2.9 nm [1.14×10^{-4} mil] thick, and the oxide was predominantly chromium. Nickel enrichment below the oxide film in the base metal was also observed. The signal-to-noise level was low in the test, so no nickel, molybdenum, or tungsten oxides were identified in the oxide layer from the x-ray photoelectron spectroscopy.

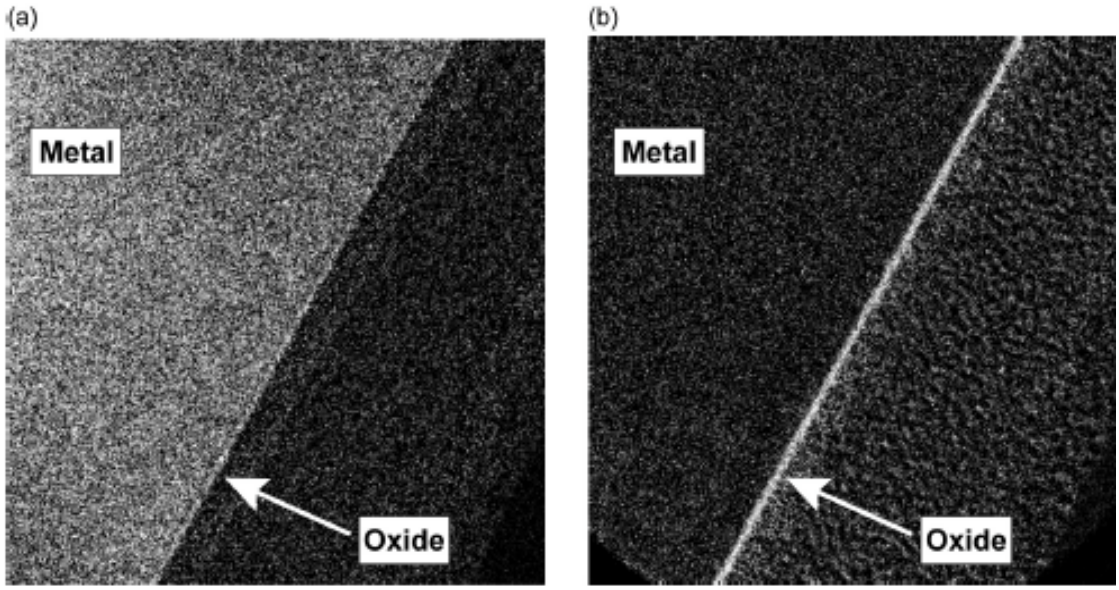

Figure 3-2. (a) Chromium and (b) Oxygen Electron Energy Loss Spectroscopy Indicating a Chromium Oxide Film (Orme, 2005)

There were two distinct oxide film layers observed on the Alloy 22 in the buffered NaCl at pH 7.5. A thin oxide film similar to the pH 3 thin passive films and another outer porous oxide was observed on the Alloy 22. The cyclic potentiodynamic polarization of Alloy 22 in this solution suggested that there may be two distinctive oxide layers, because there were two constant current density regions in the anodic polarization curve separated by a peak. The results suggest that the first region, 0–300 mV, may be associated with the inner layer {approximately 4 nm [1.6×10^{-4} mil] thick}, while the second region, 500–800 mV, may be associated with the porous outer oxide layer. In the first passive region, a thin, smooth oxide film was observed. Oxygen, nickel, and chromium have the highest composition in the oxide film. However, the data suggested that most of the nickel was from the base metal. From x-ray photoelectron spectroscopy, the film at 200 mV appeared to be predominately chromium oxide, with some molybdenum and nickel.

Above the 300–350 mV potential range, a thick porous oxide formed {about 30–40 nm [1.2×10^{-3}–1.6×10^{-3} mil] thick}. This porous oxide consisted of a compact thin layer close to the base metal and a porous structure further away. At 400 mV, the porous layer was irregular and open, while at higher potentials, the pore size had become refined and more uniform. There appeared to be voids that separated the compact and porous oxide interface. The surfaces of the two porous oxides were predominately nickel oxide.

At a potential of 250 mV in the basic (pH~12) solutions, the oxide film on Alloy 22 has a compact inner layer close to the metal and a porous contamination layer. It seems that the solution was contaminated with silica that likely dissolved from the glassware. The porous contamination layer was precipitated silica. Because of the silica contamination layer, Orme (2005) was unable to obtain meaningful results that could be used to evaluate the inner passive film. Orme suggested that Cr(III) was in the inner oxide layer and nickel hydroxide was in the outer porous layer from the data that was available; however, the silica contamination invalidated the usefulness of the analysis.

In tests conducted in 1 M NaCl solutions (pH 2.8 and 7.5) at 90 °C [194 °F], the current density for Alloy 22 was measured as a function of time to evaluate the protectiveness of the passive film (Orme, 2005). Trends of log(I) versus log(t) were plotted and showed a linear trend indicating that the passive film growth was logarithmic for as short as 16 minutes or as long as 6 hours depending upon solution pH and applied potential. Next, the plots deviated from the logarithmic growth rate toward a constant current density approaching the establishment of steady-state conditions. In the less aggressive solutions (pH 7.5), the logarithmic film growth was longer because it takes more time to locally dissolve and repassivate the film to remove its imperfections. In the more aggressive solution (pH 2.8) the logarithmic film growth was shorter, so the defected films are dissolved and repassivated much quicker, which can lead to an oxide film with fewer imperfections. Orme (2005) assumed that the protective nature of the passive film was due to a restructuring of the oxide film that removes imperfections rather than a thickening of the film.

In the same report, Orme (2005) conducted two different studies to examine the long-term stability of the passive film. These tests included the evaluation of polarization resistance and current density after holding the sample at a fixed potential and time. The data from these two methods were converted to corrosion rates so they could be compared; however, these two processes are not directly comparable. Polarization rate measures an instantaneous process,

whereas current density provides a steady-state corrosion rate. Therefore, the data gathered from each of the two methods examines different fundamental behavior of the passive film.

From the polarization resistance test, Orme (2005) stated that the corrosion rates were higher at a pH of 3 and 11 than at 8 and that the corrosion rates did not trend with the open circuit potential that ranged from −400 to −100mV Ag/AgCl as shown in Figure 3-3. However, examination of the data seems to suggest that the corrosion rates actually do have some maximum centered on −300 mV in (b), yet there may be a large uncertainty.

Next, Alloy 22 was held potentiostatically in the passive region while the current that decreased over time was examined. The corrosion rates measured with this method did not have a strong trend with either pH or applied potential for the ranges tested (see Figure 3-4). The currents decayed to the microampere range in 18 hours for all solutions tested between the open circuit potential and the potential for transpassive dissolution. The barrier oxide was predominantly a Cr(III) oxidation state and was most likely to be kinetically stable. On the basis of other authors' findings, Orme (2005) suggested that the outer chromium oxide may have been composed of hydrated chromium hydroxide, acting like a cement to limit transport along grain boundaries. Another suggestion is that the bipolar oxide film formed with a net negative charge at the oxide–solution interface and a net positive charge at the metal–oxide interface. The outer negative charge reduces the diffusion of negative anions to the oxide–hydroxide surface, limiting the reaction with the metal that relies on anodic current flow.

Orme (2005) conducted some additional tests comparing samples with different surface treatments. Since the surface film of the current waste package design will be determined from the solution annealing step, it is important to understand the effect of surface condition. One surface type was polished, while another was left in the annealed condition. The results indicated that the annealed sample had a smaller current density during the polarization scans. In addition, there was no longer an anodic peak in the middle of the passive current region for the annealed sample in the simulated concentrated water, and the porous film associated with this peak was not present.

On the annealed samples, a chromium oxide {0.8 µm [3×10^{-2} mil]} formed in the inner barrier, and an iron and nickel oxide formed in the outer barrier {0.8 µm [3×10^{-2} mil]}. Islands of aluminum also formed during the annealing process.

Passive behavior occurred over a wide range of pH and applied voltage, creating a predominant oxide composed of chromium in the +3 oxidation state. It was suggested that there were two Cr(III) oxides that may have formed in the passive region: Cr_2O_3 at pH 2.8 and $NiCr_2O_4$ at pH 7.5. The characterizations of the film were consistent with these phases. The films should be kinetically stable so the low corrosion rates may be due to the slow dissolution kinetics of the Cr(III) oxides.

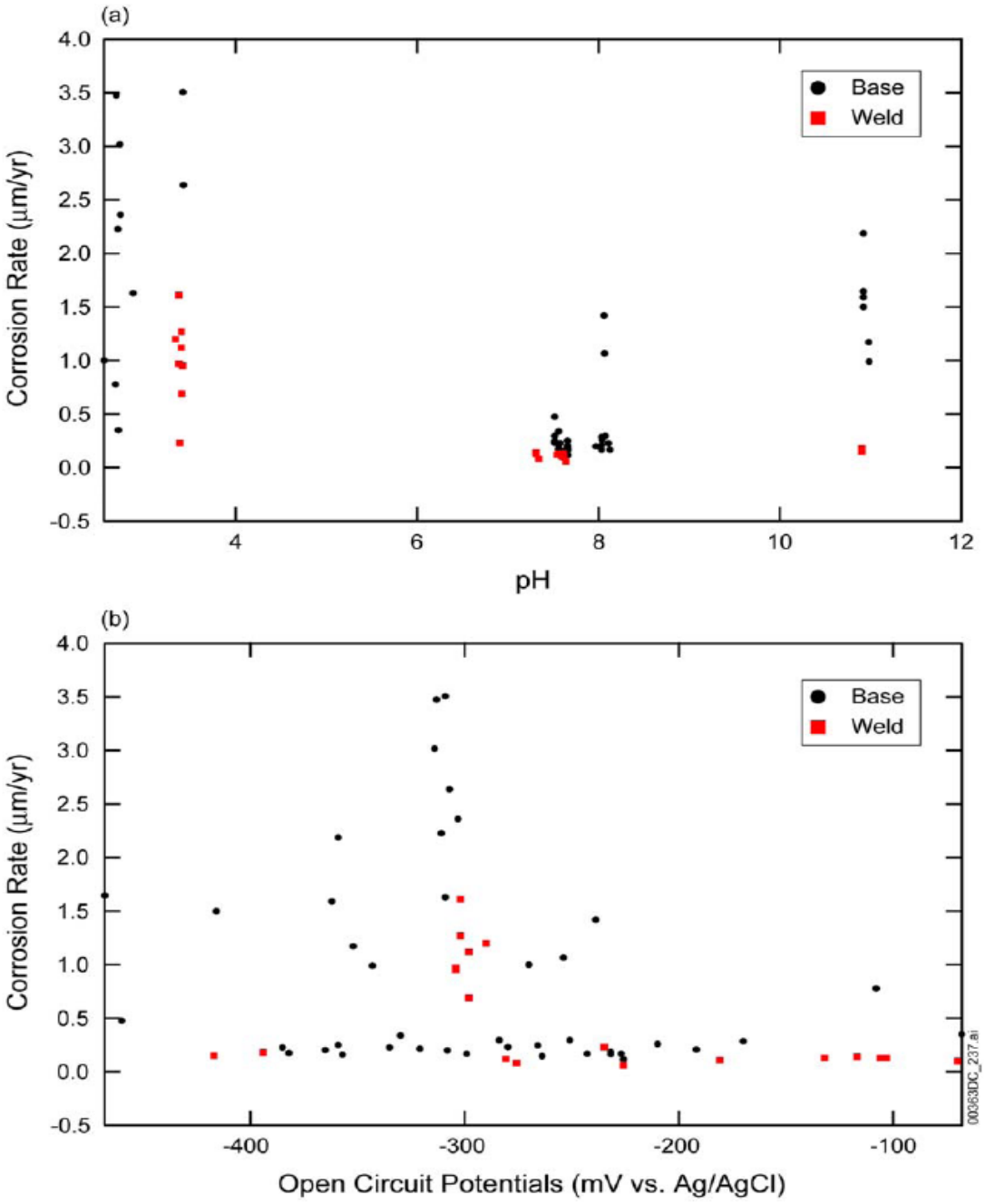

Figure 3-3. Corrosion Rate as Determined by the Polarization Resistance Is Shown as a Function of the (a) Solution pH and (b) Open Circuit Potential (Orme, 2005)

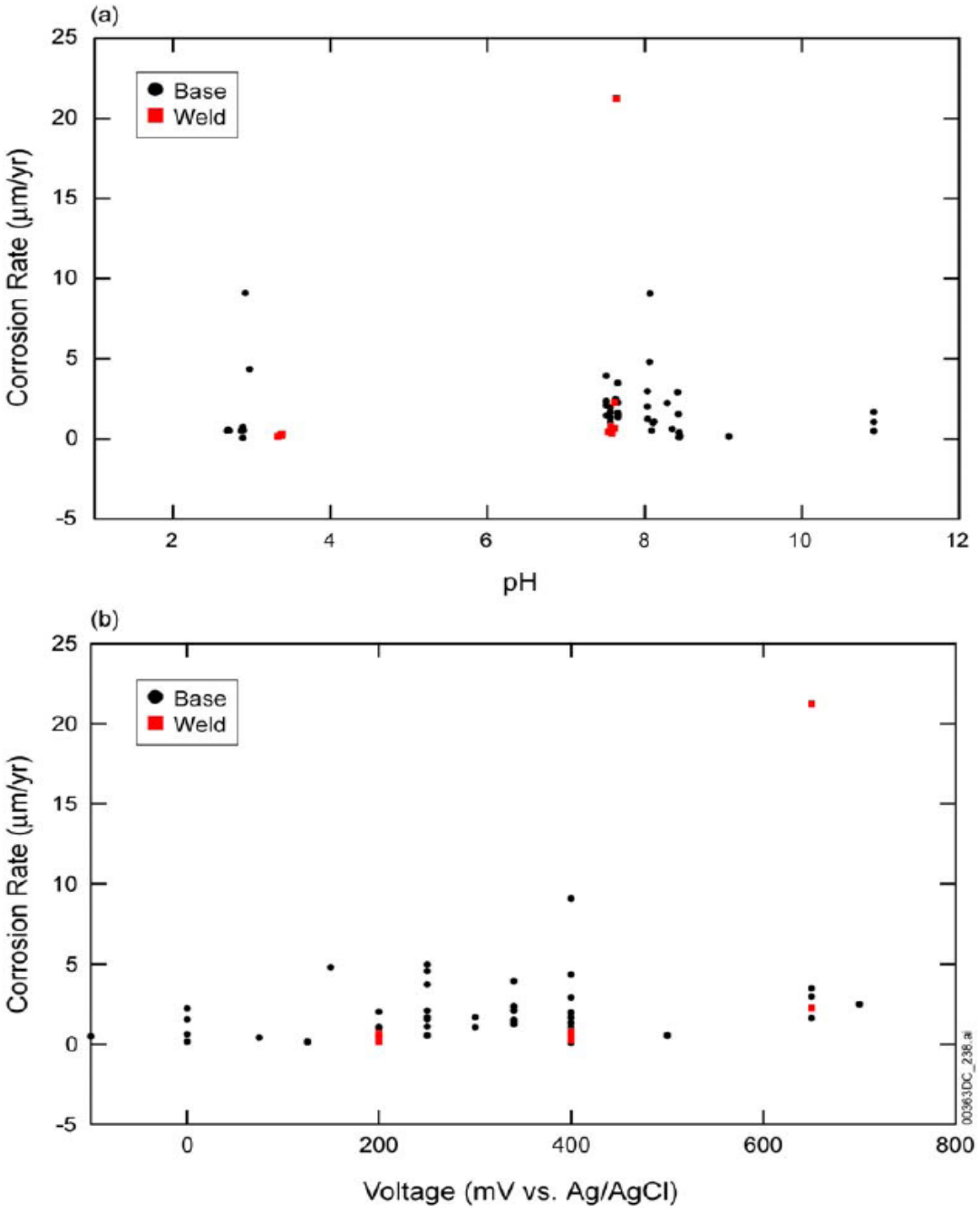

Figure 3-4. Corrosion Rate as Determined by the Current Density Held for a Period of Time Is Shown as a Function of the (a) Solution pH and (b) Open Circuit Potential (Orme, 2005)

It was suggested that the Cr(III) was in an amorphous oxide barrier that isolates the base metal from the environment by limiting ionic and electronic currents (Orme, 2005). If significant current were to flow or the volume was small, then solution saturation would take place and the oxides should be thermodynamically stable. The dissolution rates are expected to become even slower as the solution-oxide system moves closer to equilibrium. However, the concentrations of the metal ions in solution were so small that the films were not likely thermodynamically stable, but rather kinetically stable.

Chiang, et al. (2007) evaluated the passive films formed on Alloy 22 in environments where stress corrosion cracking was either observed or did not occur. Simulated concentrated water with various modifications was used in this testing. In addition, a control sample exposed only to air was evaluated. The specimens were potentiostatically held at either 100 or 400 mV_{SCE} (with respect to a standard calomel electrode) for 7 days. X-ray photospectroscopy was used to analyze the surface of the samples.

The x-ray photoelectron spectroscopy depth profiles of the control specimen and the specimen held at 100 mV_{SCE} in 0.028 M NaCl solution at 95 °C [203 °F] are shown in Figures 3-5 and 3-6, respectively. For both specimens, three regions were observed from the depth profiling analysis: (i) an outer contamination layer, (ii) the inner passive layer, and (iii) the base metal. The outer layer was contaminated with carbon and was assumed to have occurred during the transport through air after the test. There was an inner region, which was the passive film, where a mixture of nickel and chromium oxide was present. The passive film grown in the NaCl solution had a higher chromium-to-nickel ratio on the outer side and decreased ratio on the inner side of the passive oxide. While the concentration profiles showed an increased chromium concentration, there was a decreased nickel and molybdenum concentration in the oxide film compared to the bulk concentration. This film was estimated to have a thickness of 5.4 nm [2.1×10^{-4} mil]. The oxide film on the control sample was nickel-rich with low concentrations of Cr_2O_3. The thickness of the air-formed oxide was only 1.7 nm [6.7×10^{-5} mil].

The samples grown in simulated concentrated water at the same potential and temperature showed a strong carbon signal on the outer oxide as shown in Figures 3-7 and 3-8. The carbon film is considered to be a contamination layer. The passive film under the contamination layer had low signals for chromium, nickel, and molybdenum. There was a significant increase in the nickel concentration at depths greater than 15 nm [5.9×10^{-4} mil]. The chromium concentration in the oxide formed in the saturated concentrated water was lower than the chromium concentration in the dilute chloride solution. The oxide formed in the simulated concentrated water was approximately 40 nm [1.6×10^{-3} mil] thick, which was significantly thicker than the oxide film formed in the dilute chloride solution. At a potential of 400 mV_{SCE}, the oxide film was approximately 280 nm [1.1×10^{-2} mil]. The oxide thickness increased by a factor of seven. Neither of these two cases showed an observable Cr_2O_3 underlayer.

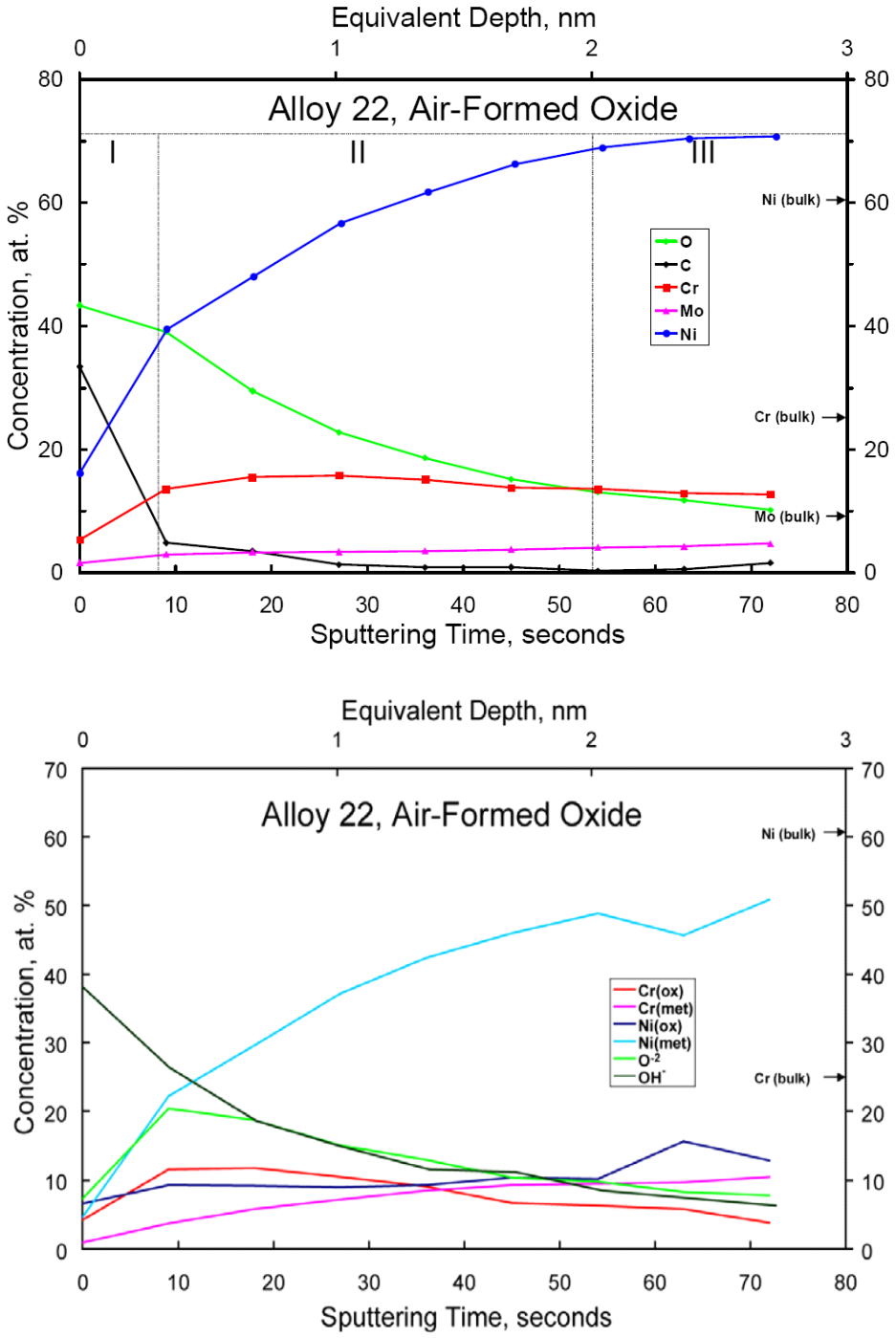

Figure 3-5. X-ray Photoelectron Spectroscopy Depth Profiles of Alloy 22 Control Specimen Air Exposed at Room Temperature for Elemental Concentrations (Top) and Species Concentration (Bottom) (Chiang, et al., 2007)

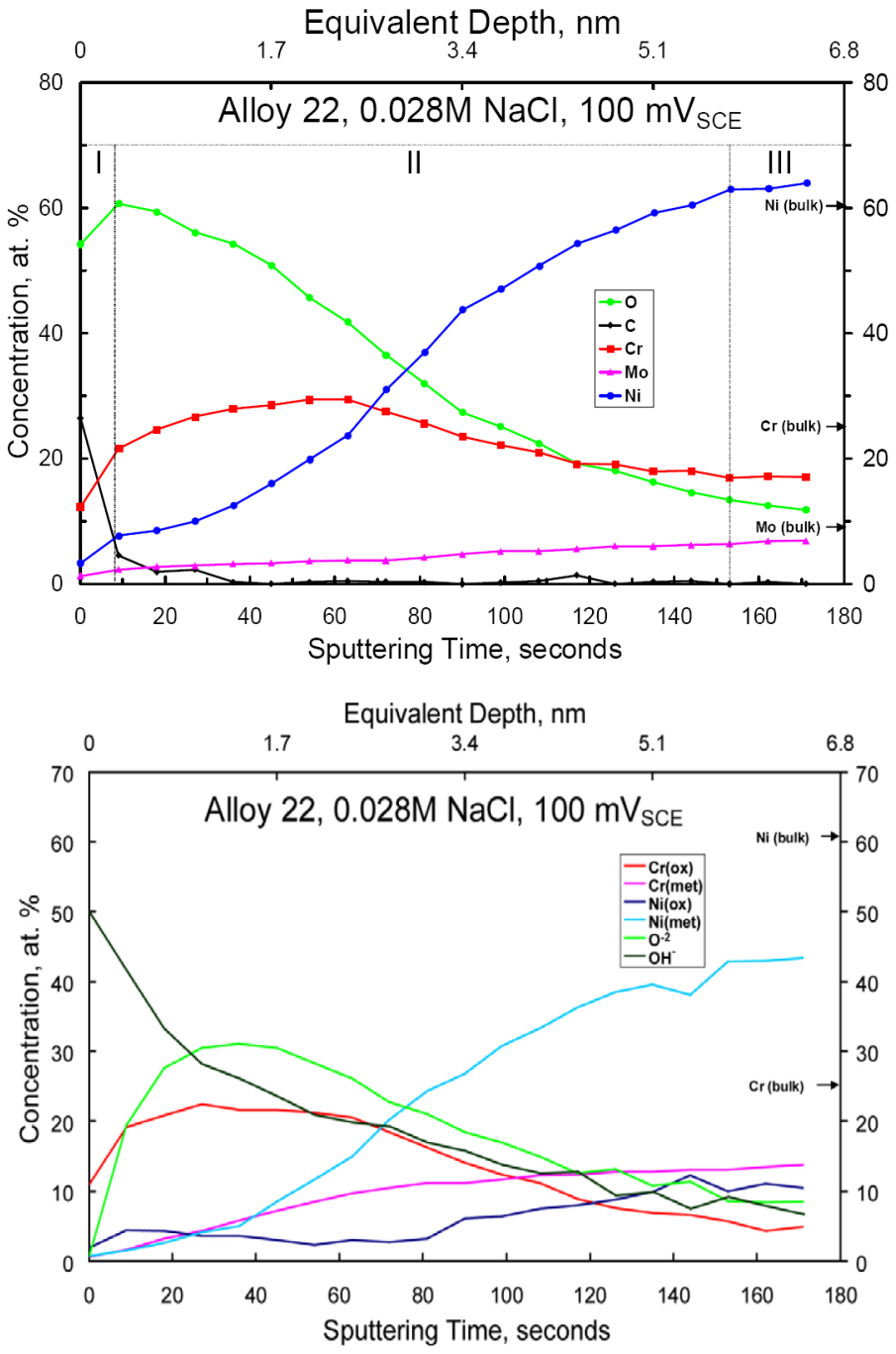

Figure 3-6. X-ray Photoelectron Spectroscopy Depth Profiles of Alloy 22 Electrochemically Treated in Deaerated 0.028 M NaCl at 95 °C [203 °F] With an Applied Potential at 100 mV$_{SCE}$ for Elemental Concentrations (Top) and Species Concentration (Bottom) (Chiang, et al., 2007)

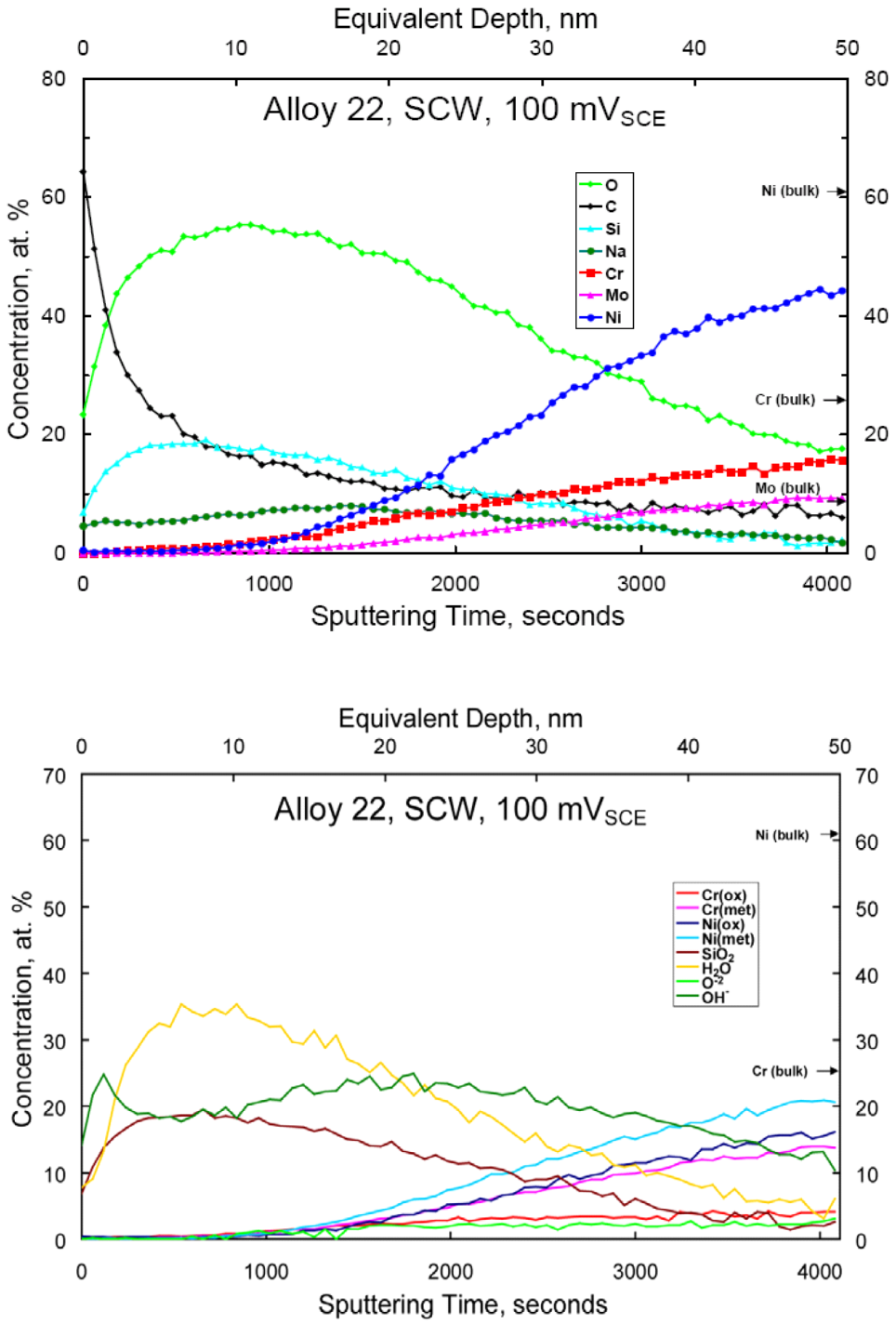

Figure 3-7. X-ray Photoelectron Spectroscopy Depth Profiles of Alloy 22 Electrochemically Treated in Deaerated Simulated Concentrated Water (SCW) at 95 °C [203 °F] With an Applied Potential at 100 mV$_{SCE}$ for Elemental Concentrations (Top) and Species Concentration (Bottom) (Chiang, et al., 2007)

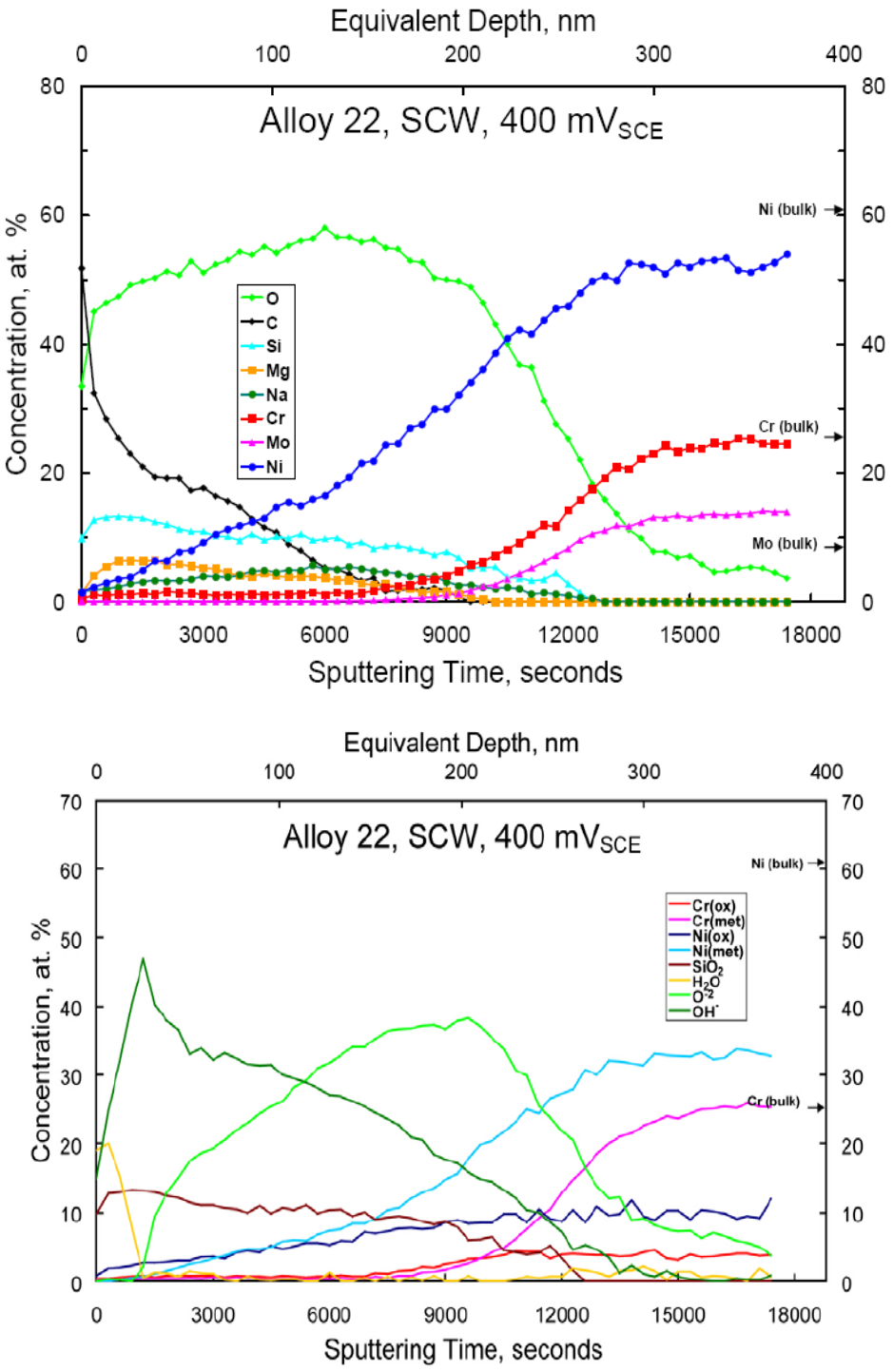

Figure 3-8. X-ray Photoelectron Spectroscopy Depth Profiles of Alloy 22 Electrochemically Treated in Deaerated Simulated Concentrated Water (SCW) at 95 °C [203 °F] With an Applied Potential at 400 mV$_{SCE}$ for Elemental Concentrations (Top) and Species Concentration (Bottom) (Chiang, et al., 2007)

X-ray photoelectron spectroscopy (Figure 3-9) was also utilized to examine samples in a 0.19 M NaCl solution, which contained the same concentration of chloride as the simulated concentrated water solution but without the other anions. At a potential of 400 mV_{SCE}, the oxide was thinner {approximately 150 nm [5.9 × 10^{-3} mil]} than the simulated concentrated water oxide and contained a significant increase in the concentration of chromium. The chromium oxide dominated the outer layer in this solution. However, the chromium concentration was lower than that measured in the dilute solution at 100 mV_{SCE}. The concentration of molybdenum was also lower than that observed in the oxide film developed in the dilute chloride solution.

Samples were also examined in solutions with the same concentration of HCO_3^- as the simulated concentrated water but with no other ions at 95 °C [203 °F]. The results of these studies are shown in Figures 3-10 and 3-11. The oxide film that formed at 100 mV_{SCE} was approximately 15 nm [5.9 × 10^{-4} mil] thick and was rich in chromium oxide. At 400 mV_{SCE}, the oxide film thickness increased to 150 nm [5.9 × 10^{-3} mil] (similar to the oxide film produced in the 0.19 M chloride solution at the same potential). However, in contrast to that solution, the oxide produced in the 1.14 M HCO_3^- solution had a lower chromium and molybdenum concentration. In addition, there was no evidence of a Cr_2O_3 oxide. The oxide film formed in the HCO_3^- solution had a slightly higher nickel content than the oxide formed in the simulated concentration water.

The next solution studied was mixed chloride and HCO_3^- with the same concentrations as the simulated concentrated water. The x-ray photoelectron spectroscopy depth profiles for the specimens tested in this solution at two potentials are shown in Figures 3-12 and 3-13. The oxide films that formed in this solution were almost the same as those formed in the HCO_3^--only solution, except that there was a much thicker oxide at 100 mV_{SCE}. The oxide film thickness was approximately 90 nm [3.5 × 10^{-3} mil] at 100 mV_{SCE} and 170 nm [6.7 × 10^{-3} mil] at 400 mV_{SCE}.

Samples were also studied in 0.19 M chloride and 1.14 M nitrate solution, which were at the same concentrations as the simulated concentrated water. The results of this study are shown in Figure 3-14. The oxide that formed in this solution was much thinner and contained a significant concentration of chromium and a distinct Cr_2O_3 underlayer compared to the solution with only chloride.

The oxide films are dependent upon the potential and solution composition. Thicker oxides were observed at the higher anodic potential of 400 mV_{SCE} than 100 mV_{SCE}. The composition of the solution also affected the films. The films were thinner in the solutions that contained either just chloride or chloride and nitrate. The oxides were thicker in either the HCO_3^- or the HCO_3^- and chloride. The oxides were thickest in the simulated concentrated water solution.

The thin air-formed film contained Cr_2O_3. The oxide films grown in either the chloride or chloride and nitrate solutions contained a significant amount of chromium. The compositions of the oxide films in the solutions that did not contain HCO_3^- were potential dependent. At higher potentials, the oxide contained significant chromium, but the concentration of nickel was reduced. A distinct chromium oxide underlayer was evident on all the Alloy 22 specimens at 100mV_{SCE}, except for the simulated concentration water condition. In the chloride or the chloride and nitrate solutions, the presence of the distinct Cr_2O_3 underlayer was evident, and no stress corrosion cracking was observed.

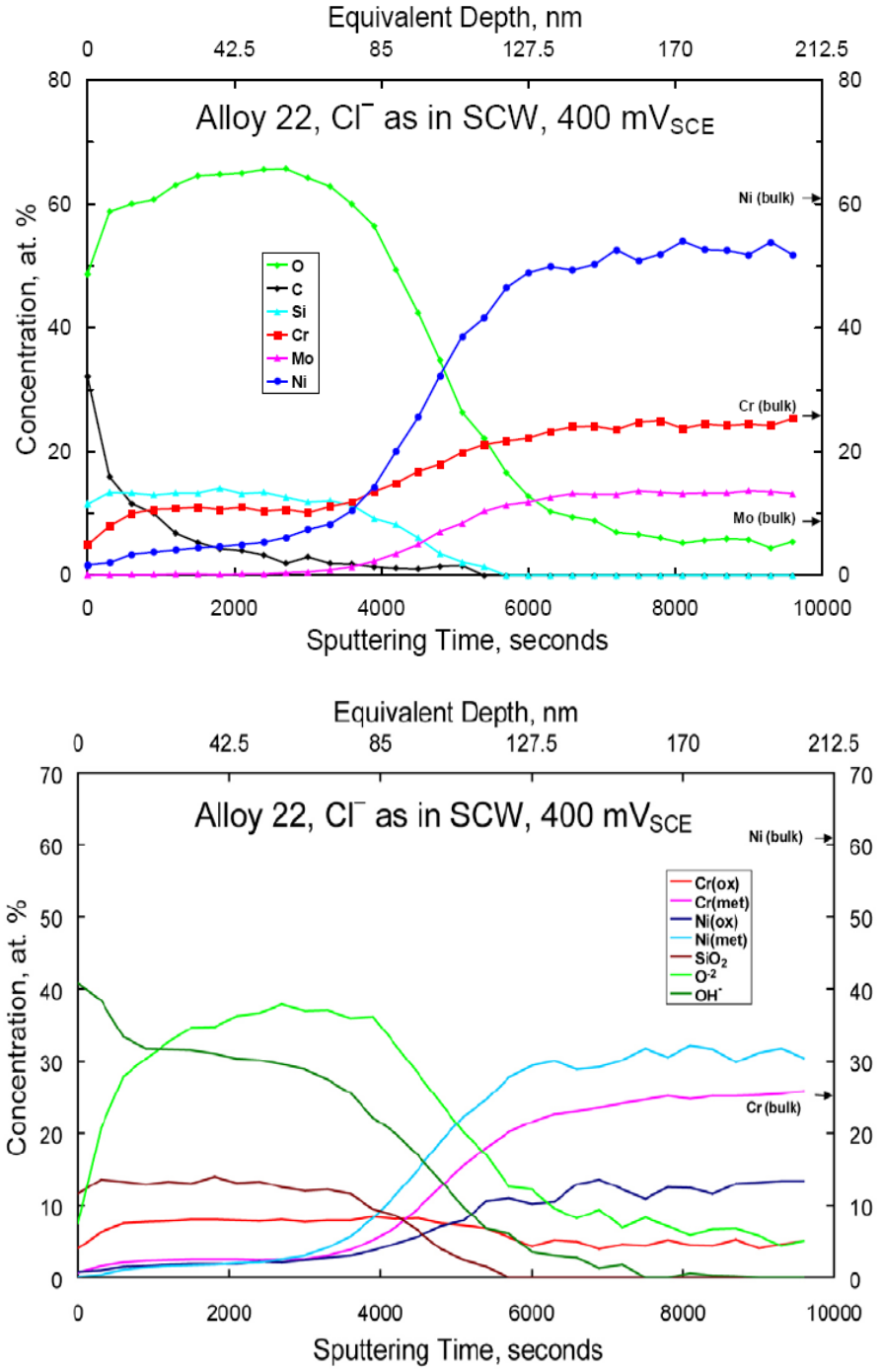

Figure 3-9. X-ray Photoelectron Spectroscopy Depth Profiles of Alloy 22 Electrochemically Treated in Deaerated 0.19 M NaCl {Same [Cl$^-$] as in Simulated Concentrated Water (SCW)} at 95 °C [203 °F] With an Applied Potential at 400 mV$_{SCE}$ for Elemental Concentrations (Top) and Species Concentration (Bottom) (Chiang, et al., 2007)

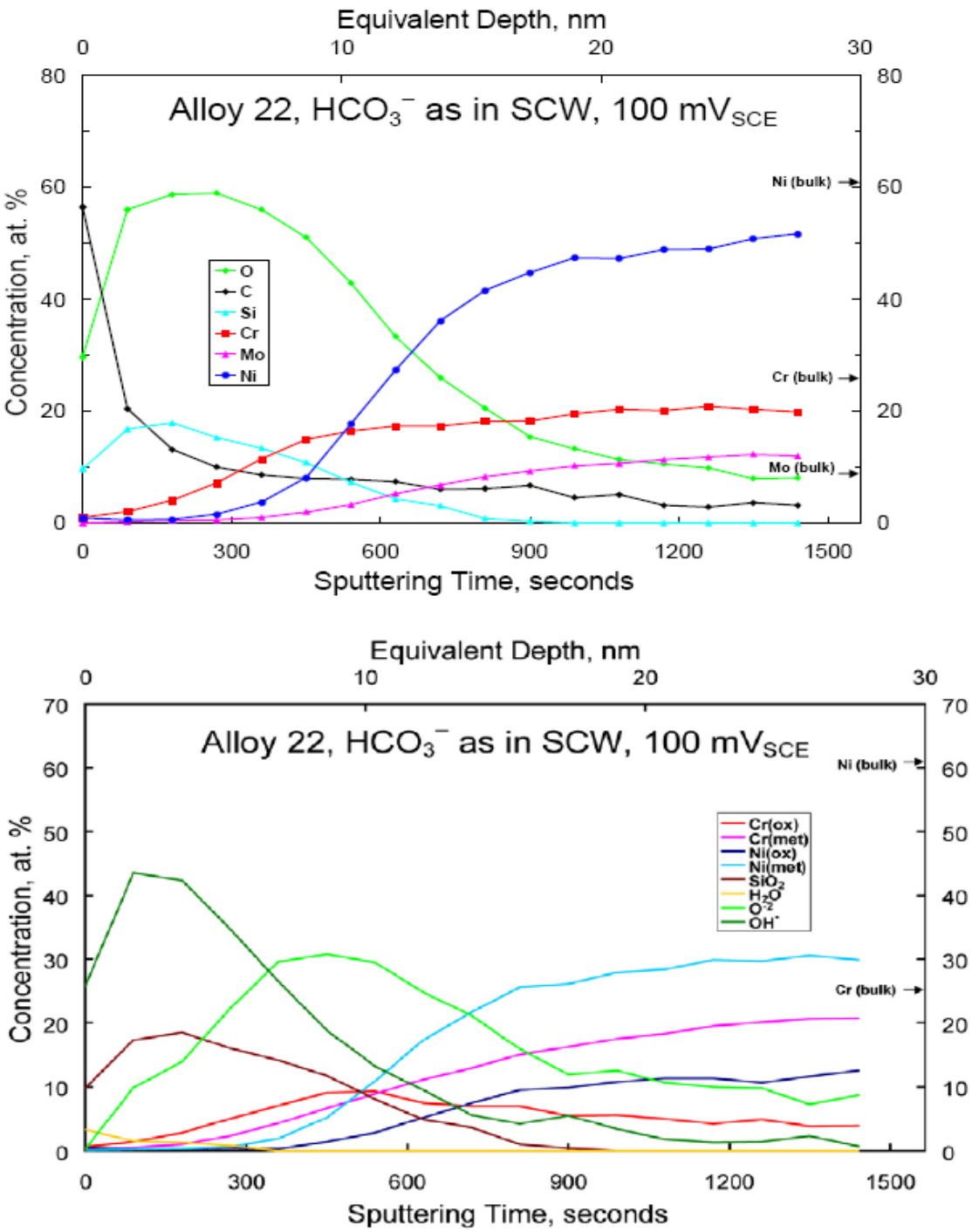

Figure 3-10. X-ray Photoelectron Spectroscopy Depth Profiles of Alloy 22 Electrochemically Treated in Deaerated 1.14 M $NaHCO_3$ {Same [HCO_3^-] as in Simulated Concentrated Water (SCW)} at 95 °C [203 °F] With an Applied Potential at 100 mV_{SCE} for Elemental Concentrations (Top) and Species Concentration (Bottom) (Chiang, et al., 2007)

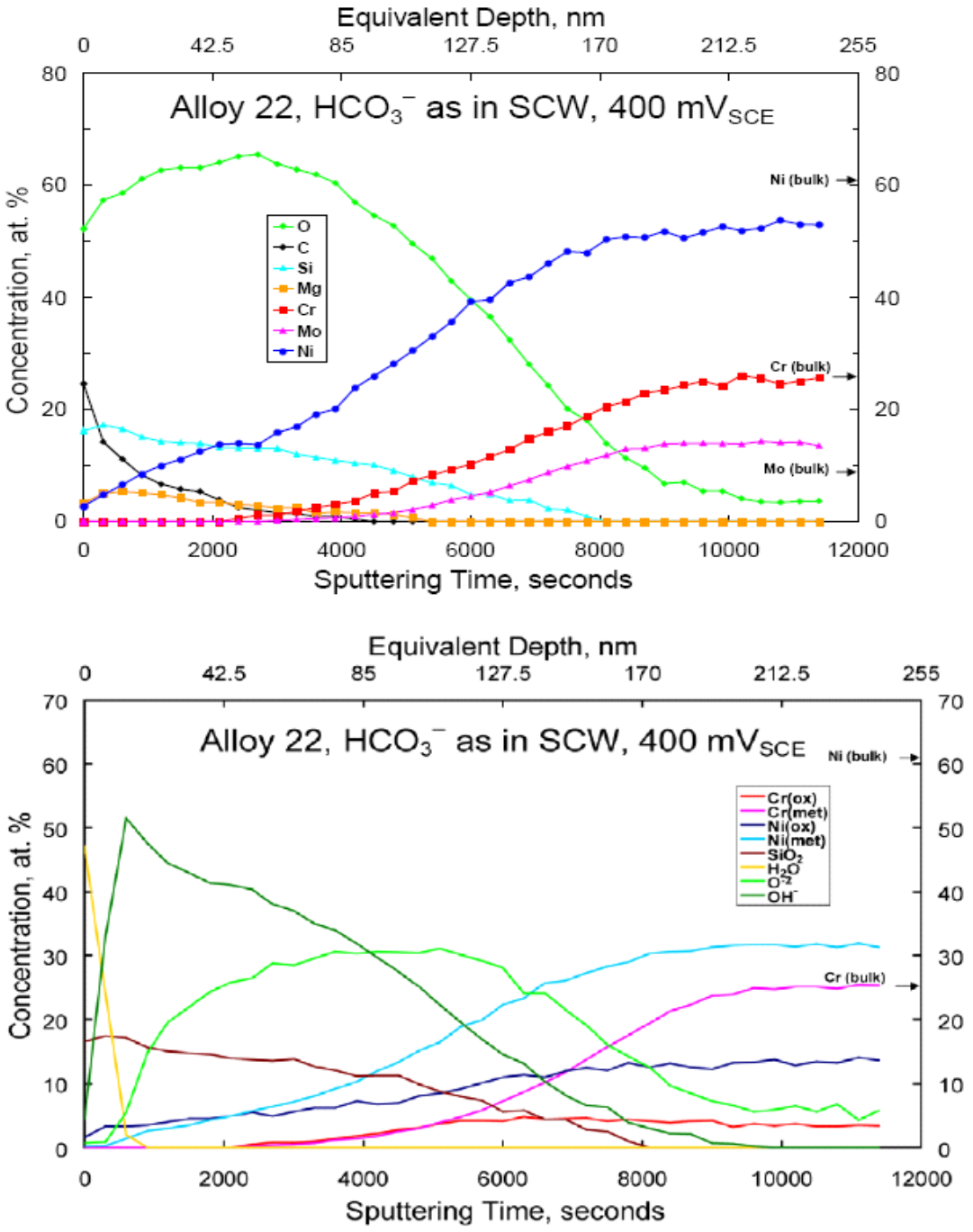

Figure 3-11. X-ray Photoelectron Spectroscopy Depth Profiles of Alloy 22 Electrochemically Treated in Deaerated 1.14 M $NaHCO_3$ {Same [HCO_3^-] as in Simulated Concentrated Water (SCW)} at 95 °C [203 °F] With an Applied Potential at 400 mV_{SCE} for Elemental Concentrations (Top) and Species Concentration (Bottom) (Chiang, et al., 2007)

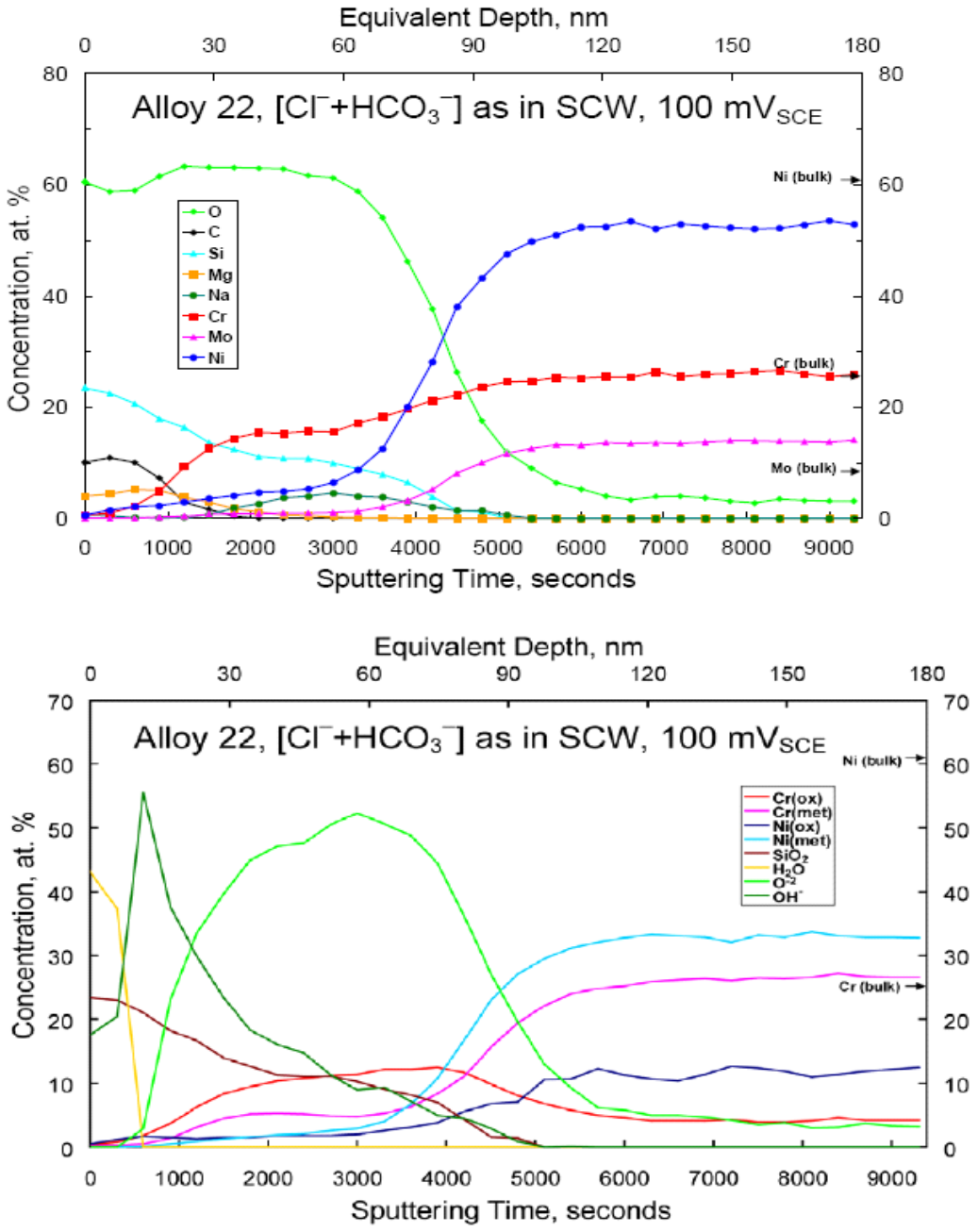

Figure 3-12. X-ray Photoelectron Spectroscopy Depth Profiles of Alloy 22 Electrochemically Treated in Deaerated 0.19 M NaCl and 1.14 M $NaHCO_3$ {Same $[Cl^-]$ and $[HCO_3^-]$ as in Simulated Concentrated Water (SCW)} at 95 °C [203 °F] With an Applied Potential at 100 mV_{SCE} for Elemental Concentrations (Top) and Species Concentration (Bottom) (Chiang, et al., 2007)

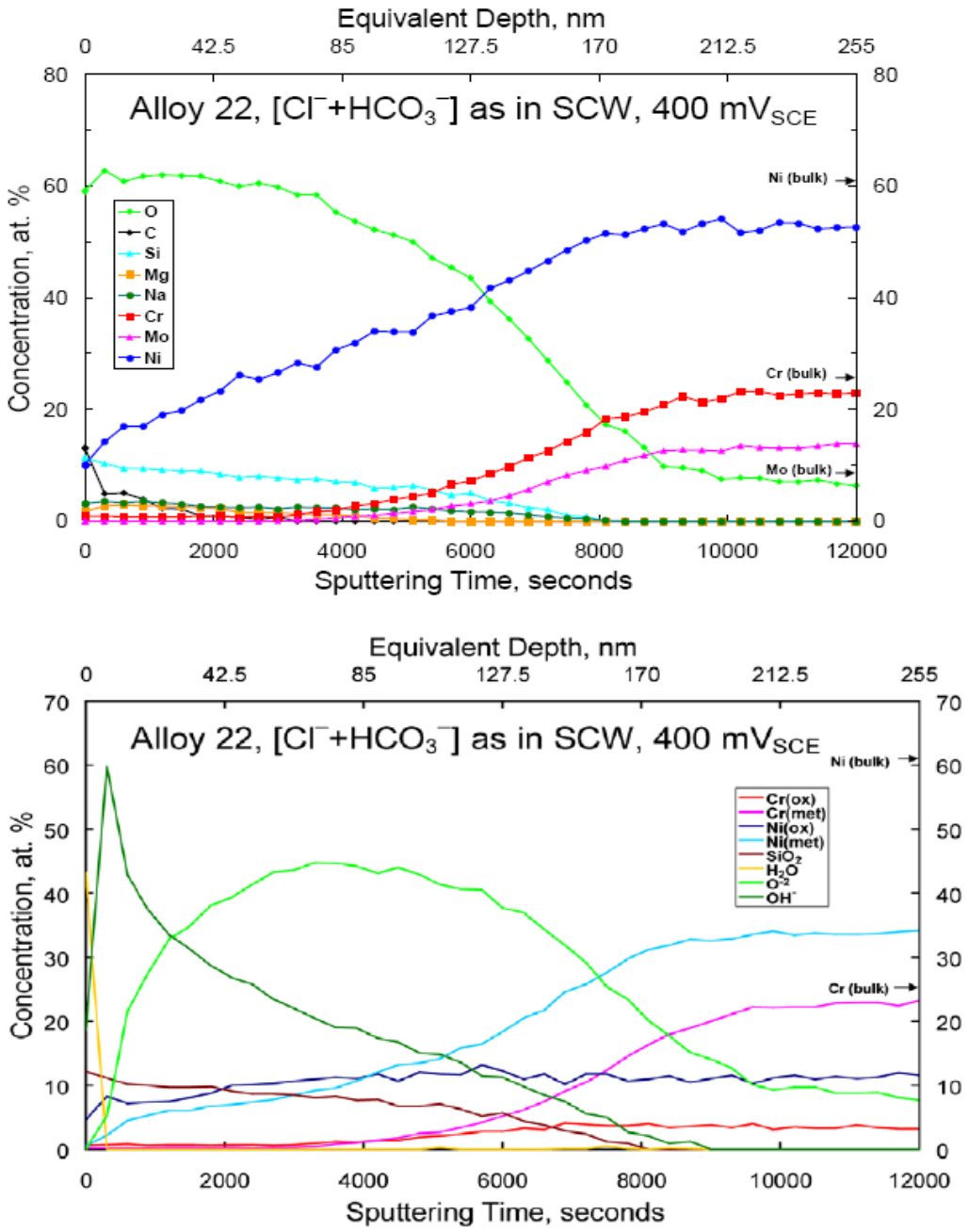

Figure 3-13. X-ray Photoelectron Spectroscopy Depth Profiles of Alloy 22 Electrochemically Treated in Deaerated 0.19 M NaCl and 1.14 M $NaHCO_3$ {Same $[Cl^-]$ and $[HCO_3^-]$ as in Simulated Concentrated Water (SCW)} at 95 °C [203 °F] With an Applied Potential at 400 mV_{SCE} for Elemental Concentrations (Top) and Species Concentration (Bottom) (Chiang, et al., 2007)

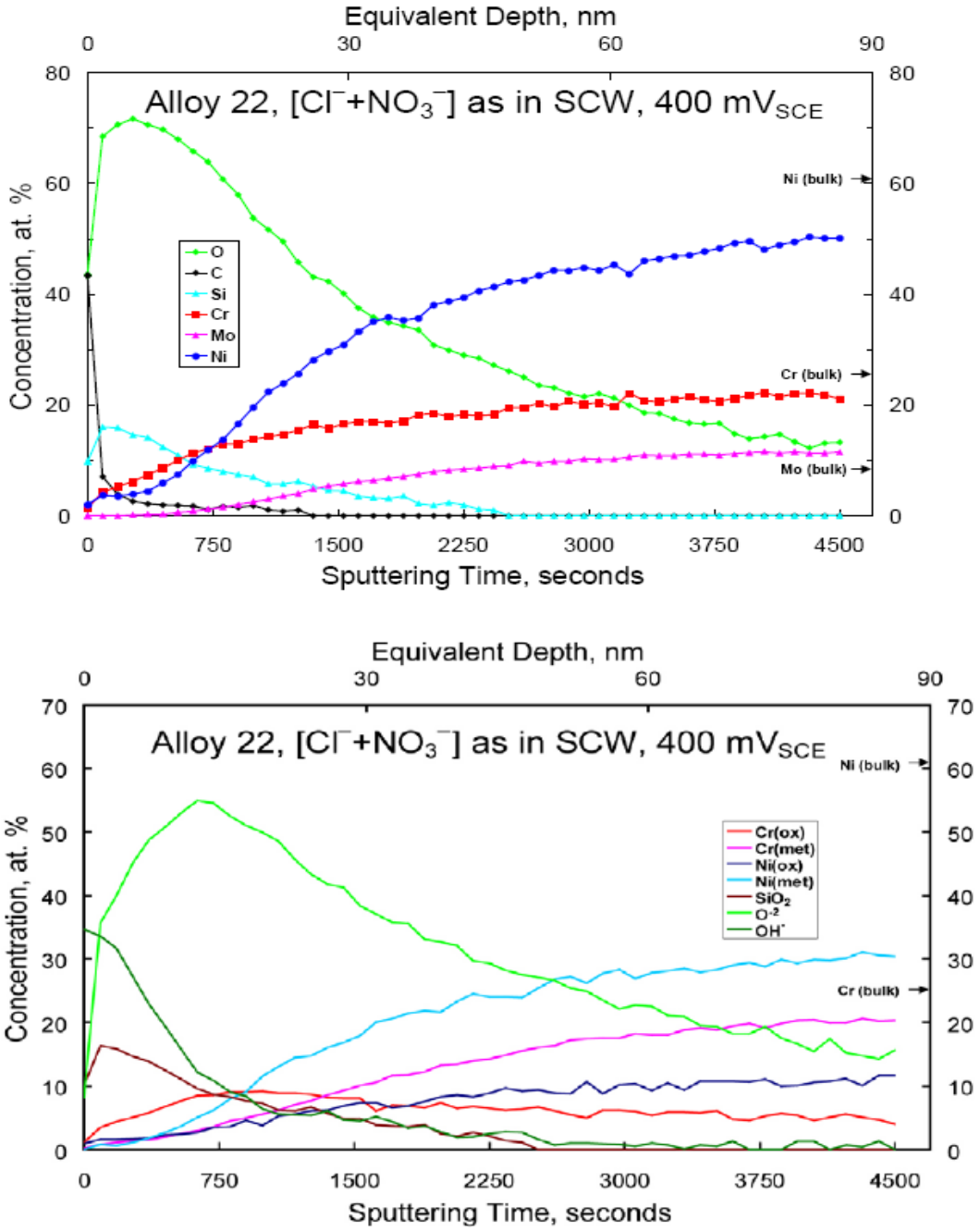

Figure 3-14. X-ray Photoelectron Spectroscopy Depth Profiles of Alloy 22 Electrochemically Treated in Deaerated 0.19 M NaCl and 1.14 M $NaNO_3$ {Same $[Cl^-]$ and $[NO_3^-]$ as in Simulated Concentrated Water (SCW)} at 95 °C [203 °F] With an Applied Potential at 400 mV_{SCE} for Elemental Concentrations (Top) and Species Concentration (Bottom) (Chiang, et al., 2007)

The results indicate that the oxide films formed in the HCO_3^- solutions at potentials that promote stress corrosion cracking were significantly thicker and had a reduced chromium and molybdenum concentration compared to passive films grown under benign conditions. HCO_3^- may also play a role in the loss of protective Cr_2O_3 film on the alloy surface, implying that the loss of Cr_2O_3 can be correlated with stress corrosion cracking.

Alloy 22 had also been evaluated in Dunn, et al. (2005) study using 0.028 M sodium chloride solution at 95 °C [203 °F], which was similar to a solution used in the stress corrosion cracking tests previously mentioned. Similar to this study, three layers were observed on the surface of Alloy 22. These layers include the outer contamination layer, the inner passive layer, and the base material.

The transpassive conditions were also examined in this study, with the potential being applied at 600 mV_{SCE}. In this region, a thick chromium-rich oxide surface layer formed. The thickness of the film was greater than 23 nm [9.1×10^{-4} mil]. The profile in Figure 3-15 shows that the measured concentration of chromium to nickel in the surface layer was much higher than that in the bulk alloy. In addition, high iron concentrations were noted in the surface layer. An examination of the surface morphology was conducted, showing that the film was in elongated patches that were indicated by the discontinuous surface in the transpassive region. Note that the Cr(III) is expected to convert to a Cr(IV) in the transpassive region; however, there was no evidence of Cr(IV) in the passive film.

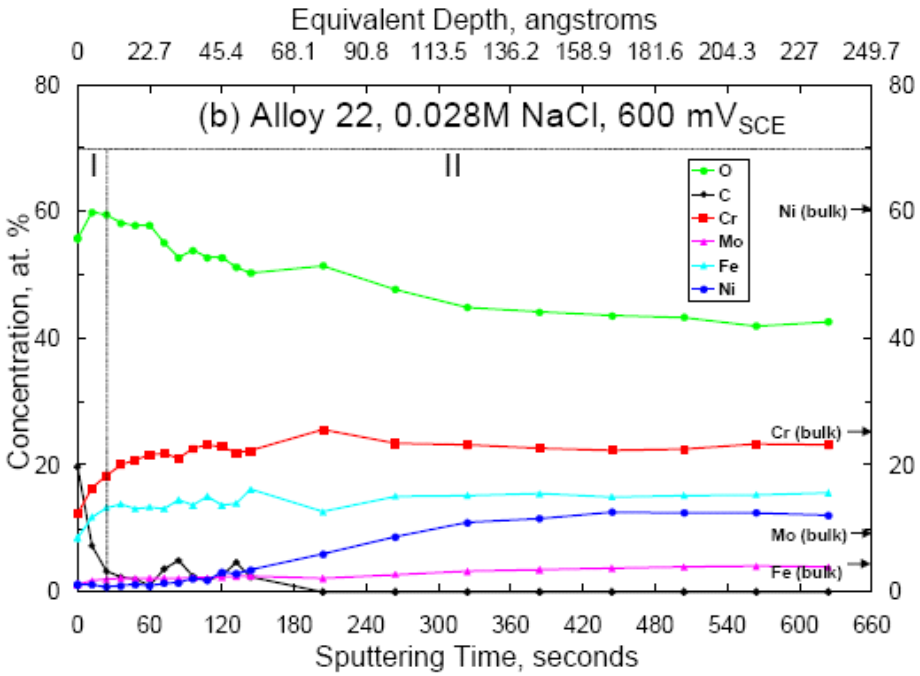

Figure 3-15. Concentration Depth Profile of Alloy 22 Electrochemically Treated in Deaerated 0.028 M NaCl at 95 °C [203 °F] with an Applied Potential of 600 mV_{SCE} (Dunn, et al., 2005)

In the passive region, the outer side of the film was rich in chromium oxides. The chromium oxide on the outer part of the film was hydrated, consistent with the observation of past examination of nickel-chromium-iron alloys (Marcus and Grimal, 1992).

3.2 Review of Long-Term Test Data

Orme (2005) examined the oxide film formed on U-bend samples of Alloy 22 that were exposed to simulated acidic water, simulated concentrated water, and simulated dilute water at 90 °C [194 °F] for roughly 5 years in the long-term corrosion test facility (see Section 2.2). These samples were evaluated using transmission electron microscopy and electron energy loss spectroscopy. The passive oxide film remained less than 5 nm [2.0×10^{-4} mil] for these exposure times and environments.

The results from a nonimmersed control Alloy 22 sample indicated that there was a very thin air-formed oxide film on the surface. A high concentration of carbon was detected in the oxide with some oxygen, but no nickel. This suggested that there was a hydrocarbon film on the surface of the alloy. These images showed no evidence of any metal-oxide type of film.

The results of Alloy 22 held in simulated acidic conditions indicated the presence of a thick {(0.2 to 0.4-μm) [7.9×10^{-4} to 1.6×10^{-4}-mil]} iron oxide scale. Orme (2005) suggested that this scale was deposited from the solution rather than being a corrosion product. In addition to the iron oxide, there were several holes in the film from an unknown source. Figure 3-10 indicated that these holes were surrounded by carbon. Because of this, Orme suggested that these may have been formed by oil-coated dust particles that had incorporated into the film. There was no obvious chromium oxide layer, but the weight loss sample from this test indicated a low corrosion rate.

The Alloy 22 examined in simulated concentrated water had a 50 to 150-nm [2.0×10^{-3} to 6.0×10^{-3}-mil]-thick carbon film at the metal interface. There was no observable metal oxide on the surface. Because of the low corrosion rates, Orme (2005) indicated that there was an undetected chromium passive film. The results from the simulated dilute water were very similar to the results observed in the simulated concentrated water. The main difference between these two solution results was that the film thickness was greater in the simulated dilute water.

CNWRA conducted some long-term (approximately 2 years) testing in simulated groundwater at a pH of 7.5 under open circuit potential and at 250 mV_{SCE}. The results for these samples are shown in Figures 3-16 and 3-17. The results indicated that there were two layers in the oxide film. The initial layer had silica as a result of glass cell dissolution. The layer underneath the silica was found to be rich in all elements from the base alloy. The inner layer contained metallic species of nickel and chromium with low concentrations of the oxide species. A high contribution of water species was measured in the middle of the outer layer, suggesting the silica was porous. Because of the lack of evidence of a chromium oxide underlayer from the data, the stability of the passive film in these types of environments is not truly understood.

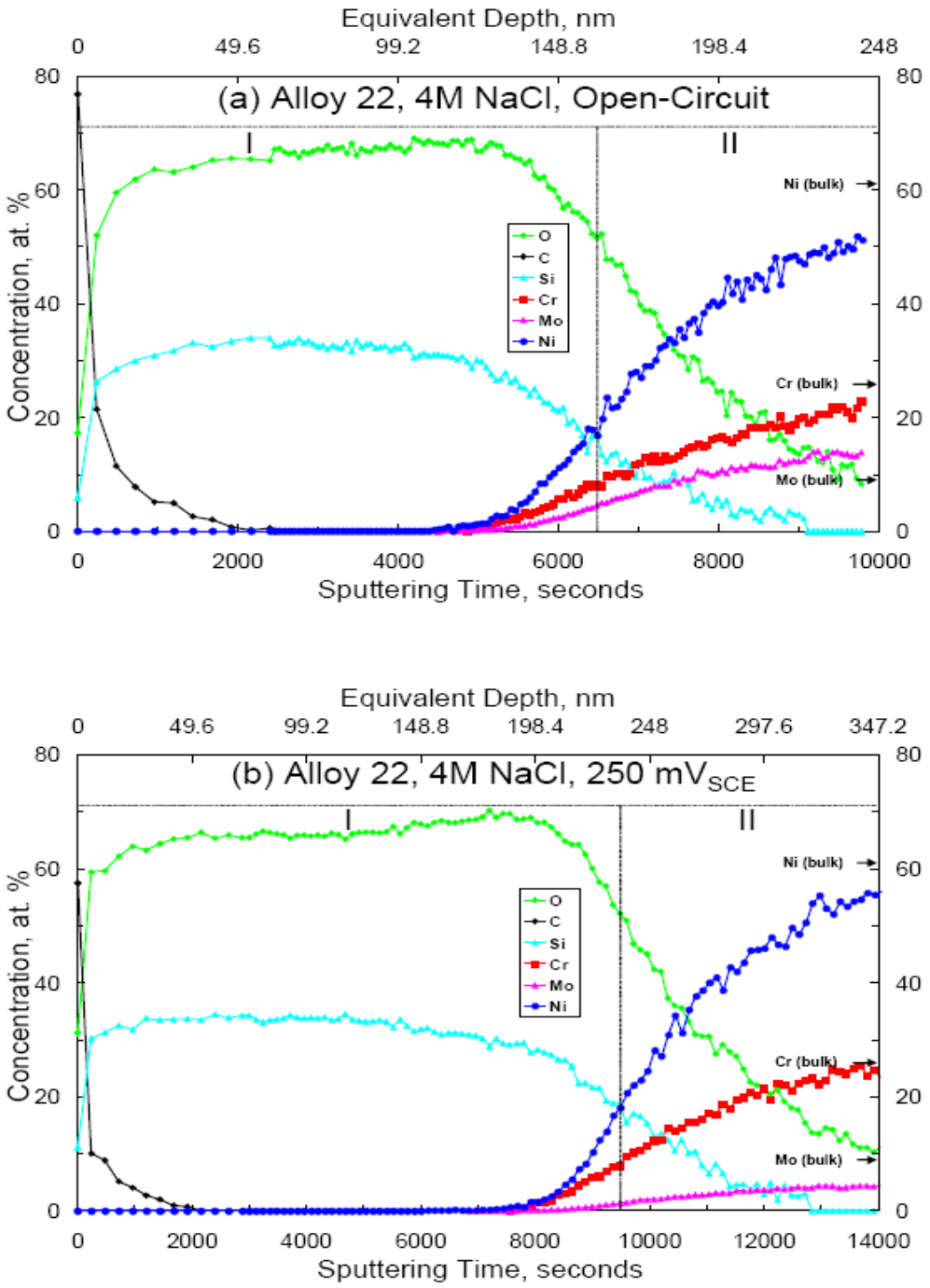

Figure 3-16. Concentration Depth Profiles of Alloy 22 Electrochemically Treated in Deaerated 4 M NaCl Multi-Ionic Solution at 95 °C [203 °F] (a) Under Open-Circuit Condition and (b) With an Applied Potential of 250 mV_{SCE} (Dunn, et al., 2005)

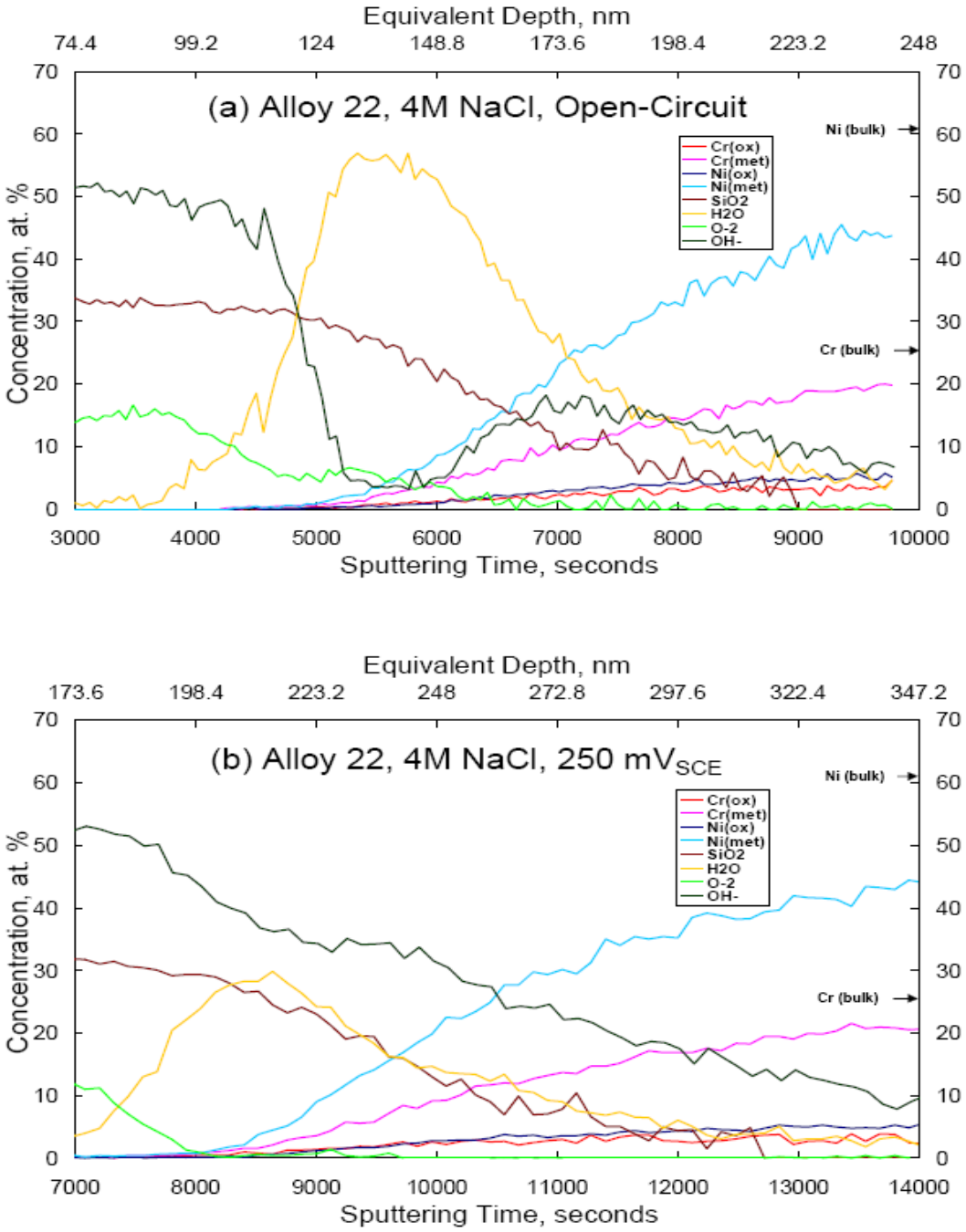

Figure 3-17. Species Concentration Depth Profiles of Alloy 22 Electrochemically Treated in Deaerated 4 M NaCl Multi-Ionic Solution at 95 °C [203 °F] (a) Under Open-Circuit Condition and (b) With an Applied Potential of 250 mV_{SCE} (Dunn, et al., 2005)

3.3 Assessment of the Significance and Stability of Passive Film on Alloy 22

It is important to determine whether the long-term stability of the passive film formed on Alloy 22 in the repository environment can be assured, based on existing information. To accomplish this task, short-term (maximum 5 years) testing needs to be extrapolated to the repository time scale. This includes not only time, but changes in environment such as temperature and solution chemistry.

The passive film has three main features that can limit the amount of corrosion: composition, thickness, and physical structure. Universities, industrial laboratories, DOE, and CNWRA qualitatively and quantitatively have evaluated these properties. These features have been tested for Alloy 22 and its industrial analogs in various environments. The long-term oxide film formed on Alloy 22 consists of a bilayer. The bilayer normally consists of a nickel/iron outer oxide or hydroxide with an inner chromium oxide-rich passive layer.

One of the features that characterizes a passive film is its thickness. The growth of the passive film is evident by the decrease in the passive current density. This decrease with time can be based on a linear, parabolic, and logarithmic rate law. The passive current density is proportional to the rate of the passive film formation as can be expressed by Eq. (3-1).

$$i_{\text{pass}} = k\frac{dx}{dt} \tag{3-1}$$

where

i_{pass} — passive current density
k — proportionality constant
dx/dt — rate of film thickening

In the passive region, the films usually grow by the logarithmic rate law, so that $i_{\text{pass}} = k'/t$, where k' is another proportionality constant. Substitution for i_{pass} in Eq. (3-1) and integrating the equation produces the logarithmic film growth law shown in Eq. (3-2) (Jones, 1996).

$$x = A + B \log t \tag{3-2}$$

where

x — thickness of the film
t — time
A, B — proportionality constants

From Eq. (3-2), it would seem that the passive film, as $t \rightarrow \infty$, would be infinitely thick, which is physically impossible. However, it is a basic growth-rate equation that has been useful in the

past to analyze the results of short-term potentiostatic tests. Macdonald and Sun (2006) recently examined the film growth properties utilizing the point defect model. In this work, the calculations suggest that for a particular set of electrochemical conditions, the passive film will have a given thickness. The thickness equation for this method is elaborate, so the details of the equation will not be described here. However, the thickness is a function of the pH, electrochemical potential, and rate constants for the reactions that occur at the interfaces between the alloy-film and the film-solution.

Urquidi-Macdonald and Macdonald (2002) conducted a study that predicted the film thickness and current density associated with film growth for Alloy 22. For a given pH, the steady-state film thickness was predicted to vary linearly with voltage. Furthermore, for a given voltage, the film thickness will vary linearly with pH. The point defect model assumed that the metal-to-metal oxide reaction is irreversible so that film thinning is totally due to the dissolution of the film. The control of the film growth rate is due to the injection of charge into the film at the metal/oxide layer, which occurs by generating oxygen vacancies at this interface. Thickness and current were examined as a function of voltage for the steady-state case. The thickness was calculated to increase linearly with potential until the transpassive region was entered (+3 oxidation state to +6 oxidation state). Because the film thickness decreased instantly in the transpassive region, the potential drop across the metal–film interface increased, which led to a higher current density. The thinning and thickening of the film with changes in potential was predicted to have an asymmetrical rate. This is because the film growth and dissolution result from two different processes. Therefore, the point defect model suggests that the change in current with time is due to a change in the film thickness. However, some Orme (2005) results do not relate directly to the point defect model in some instances, which indicates that there may be other aspects of the passive film affecting growth and corrosion resistance of Alloy 22.

One of the other corrosion prevention features is the physical structure of the passive film. Over time, dissolution will occur at local defects (e.g., grain boundaries and dislocations) in the passive film. These sites will repassivate, leading to less imperfect oxide structure. Orme (2005) evaluated this by plotting the passive current over time on a log plot. The passive current always started with logarithmic growth, but at some later time, deviated from this rate. Orme attributed this rate change to a change in the passive film structure. The data showed that the corrosion rates did not necessarily correlate directly to the film thickness, which indicates that some type of passive film restructuring likely plays a role in the corrosion resistance of Alloy 22. The slow decrease in corrosion rate may not only be a restructure of the passive film, but also of the outer porous film. The data indicated that the porous film can have different porosity depending on the environmental conditions. It is also possible that the porosity could change over time. Therefore, the slow decrease in corrosion rate over time may be a slowly evolving change in the porosity of the outer film. It is likely that the inner passive film leads to the initial low corrosion rate and the change in the outer film may affect the slow decrease in corrosion rate with time.

In evaluating the long-term stability of the passive film to the repository timeframe, it is difficult to make predictions based on short-term data. However, the results indicate that it is important to maintain the chromium oxide passive film. In most of the environments, a chromium oxide film was always detected. However, there were few environments where a contaminated silica layer or carbon layers were present and no passive chromium oxide film could be observed. This result was observed in both Orme (2005) data and CNWRA data (Dunn, et al., 2005). It was assumed that the chromium oxide film was still present due to the low and decreasing corrosion

rate over time. It may be possible that the large silica layer interfered with the ability to resolve any thin conformal chromium layer. However, this is left as an unresolved question and is currently being evaluated. In addition, there are some possible degradation mechanisms that may have a long initiation time, and they may not be observed during these relatively short-term tests. These potential long initiation time processes will be discussed in Chapter 4.

Based on the data presented in this chapter, several conclusions can be drawn about the significance and stability of the passive film on Alloy 22.

- The passive film has been evaluated on Alloy 22 using multiple methods such as Auger spectroscopy, transmission electron microscopy, x-ray photoelectron spectroscopy, Raman spectroscopy, and electron energy loss spectroscopy for short-term tests up to 5 years in multi-ionic solution at various temperatures.

- Most of the experimental data including DOE, CNWRA, and other sources show that a chromium oxide passive film protects against potential corrosion degradation modes that occur at a faster rate. Alloys with lower concentrations of chromium in the base metal have been shown to have fewer passivation properties.

- The chromium oxide passive layer is observed in most of the environments expected in the Yucca Mountain repository, and the film seems to restructure itself with time. However, when heavy silica or carbon deposits were observed on the surface of Alloy 22 in the long-term tests, no chromium passive film could be detected, yet it was assumed to be present due to the low and decreasing corrosion rate. This is currently being evaluated.

- No degradation mechanisms were observed to interfere with the stability of the passive film over the short testing periods. Therefore, the short-term tests indicate that passivity would not be lost in a repository timeframe. However, there may be mechanisms that have long initiation times, which could possibly affect the passivity of Alloy 22. These potential degradation processes are discussed in Chapter 4.

4 EFFECTS OF POTENTIAL CORROSION-RELATED DEGRADATION PROCESSES ON LONG-TERM PERSISTENCE OF PASSIVE FILM ON ALLOY 22

As discussed in Chapter 3, the high corrosion resistance of Alloy 22 is mainly the result of a thin protective passive film that forms in aqueous solutions. Corrosion-related degradation processes causing film breakdown or instability by altering the passive film properties during the postclosure period are important and could significantly affect the long-term waste package performance.

Several corrosion-related potential degradation processes have been suggested and may include enhanced dissolution rate by anodic sulfur segregation, base metal chromium depletion underneath passive film, spallation of passive film by void formation at the metal–film interface and/or within the film, alteration of passive film by dry–wet cyclic process, anion-selective sorption of passive film, and increased cathodic kinetics (i.e., large cathodic area development and hydrogen peroxide formation by radiolysis).

This chapter discusses some details of the previously noted degradation processes and their potential effects on the long-term persistence of the passive film formed on Alloy 22. An anodic sulfur segregation process is evaluated in more detail through literature data analyses and mathematical calculations. Other potential degradation processes warrant additional considerations to reduce associated uncertainties assessing their potential effects on the long-term persistence of the passive film formed on Alloy 22.

4.1 Enhanced Dissolution Rate by Anodic Sulfur Segregation

One of the potential degradation processes is the enhanced corrosion rate as a result of anodic sulfur segregation during passive dissolution of Alloy 22 and the resultant breakdown of the passive film under potential repository environments. This process was identified as a potential factor that could affect the long-term passive film stability of Alloy 22 at the International Workshop on Long-Term Extrapolation of Passive Behavior (U.S. Nuclear Waste Technical Review Board, 2001) and in the NRC's Integrated Issue Resolution Status Report (NRC, 2005). The final report of the Waste Package Materials Performance Peer Review Panel (Beavers, et al., 2002) notes the importance of evaluating the incidence of the anodic sulfur segregation process in the long-term passivity of Alloy 22. The Panel recommended the need for research on this topic for potential license application by the U.S. Department of Energy (DOE). The DOE agreed to address the sulfur effects theoretically and/or experimentally before the license application (Beavers, et al., 2002). However, the work may continue beyond the license application if it is not shown that the detrimental effect of sulfur can be eliminated by reducing the sulfur in alloy during the manufacturing process. This section discusses the potential effects of sulfur in Alloy 22 (maximum 0.02 wt% of sulfur in general) on the long-term passivity of Alloy 22.

4.1.1 Effects of Sulfur on Passivation of Metals

4.1.1.1 Influence of Sulfur on the Passivation of Nickel and Nickel-Iron Alloys

Marcus and coauthors reported detailed studies on the effects of sulfur on the corrosion behaviors of nickel (Marcus, et al., 1988; Marcus, et al., 1980; Oudar and Marcus, 1979) and nickel-iron alloys (Marcus, et al., 1984a,b) using electrochemical, radiotracer, and surface analysis techniques. These studies have shown enhanced corrosion rates due to the detrimental effects of either adsorbed or alloyed sulfur on the corrosion resistance. It has been proposed that the sulfur segregates onto the metal surface and inhibits the formation of a protective oxide film of the metal surface (Marcus and Oudar, 1995). Major findings from their studies are summarized in the following sections.

4.1.1.1.1 Acceleration of Anodic Dissolution by an Adsorbed Monolayer of Sulfur on the Metal Surface

A monolayer of adsorbed sulfur on the metal surface was obtained by doping the specimen with a gaseous H_2S-H_2 mixture at high temperature {e.g., 520 or 550 °C [968 or 1,022 °F] for nickel or Ni-25 at% iron, respectively}. The surface sulfur concentrations varied depending on the metal specimen such as 43, 40, or 20 nanogram/cm^2 on the metal surface for single-crystalline nickel (100), Ni-25 at% iron (100), or polycrystalline nickel, respectively. From the polarization curves for the specimens tested in deaerated 0.05–0.1 N H_2SO_4 at 25 °C, it was clearly demonstrated that (i) a monolayer of adsorbed sulfur on the metal surface enhanced the anodic dissolution rates five to eight times with respect to the sulfur-free surface, (ii) the adsorbed sulfur remained on the metal surface during anodic dissolution of the metal elements and acted as a dissolution catalyst, and (iii) the formation of a passive film could take place only after partial desorption of adsorbed sulfur. According to the proposed mechanism by Marcus and Oudar (1995), the adsorbed sulfur on the metal surface accelerates the anodic dissolution of the metal by weakening the metal–metal bonds and/or by allowing easier transport of the metal cations to the film–solution interface from the metal–film interface due to the changes in the electric field across the passive film. The adsorbed sulfur may also delay the passive film formation by blocking the sites for the adsorption of hydroxyl ion (OH^-), which is generally accepted as a precursor to form hydroxide and oxide films. Above a critical surface coverage by a monolayer of sulfur 70–80 percent complete, the passivation was retarded by shifting the passivation potential to a more anodic potential, and the residual current within the passive range was higher than that for the sulfur-free case. Below the critical surface coverage of adsorbed sulfur, the passive film was still able to form. However, using reflection high-energy electron diffraction, Oudar and Marcus (1979) identified that the film was a less protective polycrystalline film compared to the film observed on the substrate in the absence of sulfur.

4.1.1.1.2 Film Breakdown by Anodic Sulfur Segregation

Samples of nickel or Ni-25 at% iron with different concentrations of sulfur in the alloy ranging from 38 to 90 ppm by weight were prepared and used to investigate the effects of the sulfur content in the alloy. The sulfur-doped samples, using radioactive S-35, were prepared by appropriate treatments at high temperatures {i.e., 1,130 or 1,150 °C [2,066 or 2,102 °F] for Ni or Ni-25 at% Fe, respectively} in a gaseous H_2S (labeled S-35) and H_2 mixture (Marcus and Talah, 1989).

The electrochemical responses of all tested samples in deaerated 0.05–0.1 N H_2SO_4 at 25 °C [77 °F] were drastically changed when sulfur was added in the metal matrix. During the potentiodynamic scan, the active-passive transition was suppressed and passivation was completely precluded. The current density increased with increasing potential over the whole range of anodic potentials. The radiochemical measurements revealed that the metal surface was enriched with sulfur and the sulfur concentration increased continuously as the applied potential increased. By comparing the measured and the calculated concentrations of sulfur on the metal surface, it was found that while the surface concentration of sulfur remained below a monolayer, most of sulfur continued to accumulate on the metal surface by the selective dissolution of the metal elements (e.g., nickel, iron)—a process also known as anodic sulfur segregation. Above a monolayer of sulfur, further sulfur segregation resulted in a precipitation of nickel sulfides, and a thin layer of nickel sulfide was formed on the metal surface. The final measured concentration of sulfur at the potential of 800 mV_{SHE} was about 400 nanogram/cm^2, corresponding to approximately 25 Å of Ni_3S_2. Sulfur exceeding this amount was desorbed from the metal surface by oxidation to SO_2 or SO_4^{2-}. The sulfide layer was not protective due to its high porosity, and thus high corrosion rates were recorded in the potential ranges where sulfur-free nickel or nickel-iron alloys are normally passivated. The rate of anodic sulfur segregation increased as the alloy sulfur concentration and/or the anodic dissolution rate increased. The results also revealed a critical content of bulk sulfur between 30 and 40 ppm by weight above which the passivation was prevented.

Anodic polarization tests were conducted on Ni-25 at% iron alloys containing different sulfur concentrations ranging from 38 to 74 ppm by weight (Marcus and Talah, 1989). These samples were polarized at a constant potential in the passive range, and after a certain induction time, the anodic current density increased remarkably from the low value of 1.5 mA/cm^2 [9.67 mA/ft^2] to the final measured anodic current density of roughly 4.5 mA/cm^2 [29.0 mA/ft^2] after 305 hours for all tested samples. This final measured value was several orders of magnitude higher than the passive current densities for the sulfur-free Ni-25 at% iron alloys. The induction time for passivity breakdown was dependent on the sulfur concentration in the alloy. The metal surface morphologies of the sulfur-segregated samples exhibited numerous pits both in the grains and the grain boundaries after potentiostatic polarization. The sulfur concentration within the pits was much higher than the overall concentration of sulfur as measured by autoradiography.

Assuming that all sulfur present in the alloy accumulates at the metal–film interface, the concentration of sulfur at the interface (θ_s^{interf}) with time was estimated using Faraday's law.

$$\theta_s^{interf}(t) = \frac{MS}{nF}\int_0^t i\,dt \qquad (4\text{-}1)$$

where

M	—	atomic weight of nickel (g/mol)
S	—	alloy sulfur concentration (ppm by weight)
n	—	number of electrons exchanged (2)
F	—	Faraday constant (96,485 Coulomb/mol)
i	—	passive current density (1.5 mA/cm^2)
t	—	time (hours)

The induction time is the time required to reach a critical concentration of sulfur at the metal–oxide interface ($\theta_{s,max}^{interf}$) above which breakdown of the passive film occurs. The induction time (t = τ) was calculated by Marcus and Talah (1989) using Eq. (4-1) and empirical data. Table 4-1 presents the calculated critical concentration of sulfur at the interface for different sulfur concentrations in the alloy along with the experimentally measured induction time using a passive current density of 1.5 mA/cm^2 [9.67 mA/ft^2].

As seen in Table 4-1, the measured induction time decreases from 112 to 45 hours as the alloy sulfur concentration increases; the higher sulfur content results in the shorter induction time. The calculated values of critical concentration of sulfur are mostly in the monolayer range of sulfur concentration and decrease with increasing the alloyed sulfur concentration. The calculated critical concentration of sulfur using Eq. (4-1) was compared to the measured value by direct measurements of sulfur concentration using the radioactive sulfur. For example, after polarization $t \sim 0.75\ t$ (75 percent of the induction time for the passivity breakdown), the measured value of concentration was 28 nanogram/cm^2 (i.e., about 70 percent of the complete monolayer coverage). Assuming that the current density does not change as long as the sample remains passivated, the induction time (t) at a constant passive current density (i) is estimated as

$$\tau = \frac{\theta_{s,max}^{interf}}{iMS} \qquad (4\text{-}2)$$

Equation (4-2) may be applicable to estimate an approximate value of the induction time for other similar sulfur-containing systems where i and S are known. Note that Eqs. (4-1) and (4-2) are currently only valid for Ni or Ni–25 at% Fe alloys.

4.1.1.1.3 Influence of Dissolved Sulfur in the Solution on Passivation

A similar inhibiting effect of sulfur on the passivation was observed when the solution contained dissolved sulfur. Adding 10^{-5} to 10^{-3} M Na_2S to the sulfuric acid solution precluded the formation of the passive film on nickel (Oudar and Marcus, 1979) and Ni-25 at% iron alloys (Marcus, et al., 1984a). Irrespective of the origin of sulfur (i.e., alloyed sulfur in the metal or dissolved sulfur in the aqueous solution), the sulfur played an identical role, which resulted in depassivation of nickel and nickel-iron alloys.

4.1.1.2 Role of Alloying Element in Passivation of Sulfur Containing Alloy

4.1.1.2.1 Chromium

Chromium is known for its beneficial effect on the passivity of chromium containing nickel-based alloys. Corrosion test results show that the chromium in Ni-xCr-10Fe alloys (x = 8, 19, and 34 at%) counteracts the detrimental effects of sulfur by promoting the passivation of the alloys, whereas the passivation is precluded by sulfur in nickel or nickel-iron alloys (no chromium) under similar conditions (Combrade, et al., 1990; Costa and Marcus, 1993; Marcus and Grimal, 1990).

Table 4-1. Calculated Values of the Critical Concentration of Sulfur for Experimental Measured Values of Induction Time at Different Alloy Sulfur Concentrations*		
Alloy Sulfur Concentration, S (ppm in weight percent)	Measured Induction Time, τ (hrs)	Calculated Critical Concentration of Sulfur at the Metal-Oxide Interface (ng/cm^2)
38	112	56
54	102	42
68	68	35
74	45	16
*Marcus, P. and H. Talah. "The Sulfur Induced Breakdown of the Passive Film and Pitting Studied on Nickel and Nickel Alloys." *Corrosion Science*. Vol. 29. pp. 455–463. 1989.		

With a simple schematic model, Marcus and Grimal (1990) and Costa and Marcus (1993) explained that chromium in the presence of sulfur was beneficial because it formed a continuous chromium oxide (Cr_2O_3) layer at the metal–film interface covering the nickel sulfide (Ni_3S_2) islands. The surface analyses using x-ray photoelectron spectroscopy and Auger election spectroscopy show that the passive films formed on the alloys have a bilayered structure with a thickness range of 2 to 3 nm [7.874×10^{-5} to 1.181×10^{-4} mils]. In the presence of sulfur, the inner layer consists of Cr_2O_3, Fe_3O_4, Fe_2O_3, and NiO, which is thinner and less enriched in the chromium oxide compared to the sulfur-free case. The outer layer consisting of $Cr(OH)_3$ and $Ni(OH)_2$ is thicker than in the sulfur-free case. It seems that the nickel sulfide (Ni_3S_2) coexisted with oxides in the inner layer and most likely was covered by a continuous chromium oxide layer. The passive film in the presence of a monolayer of sulfur on the metal surface was more porous than the sulfur-free case.

Alloy 600 (Ni-17Cr-8-Fe in wt%) was tested in deaerated 0.1 M H_2SO_4 at 25 °C [77 °F] with an adsorbed monolayer of sulfur on the metal surface (Combrade, et al., 1990). The potentiodynamic polarization curve for this alloy showed an active peak followed by a passivity range with an increase of the passive current densities compared to the sulfur-free case. The active peak current density and the passive current density increased to 1,200 and 5 $\mu A/cm^2$ [7,741 and 32.2 $\mu A/ft^2$] with sulfur and from 94 and 1.2 $\mu A/cm^2$ [606 and 7.7 $\mu A/ft^2$] without sulfur, respectively. A sample of Alloy 600 doped with 77 ppm sulfur passivated when it was potentiostatically polarized at 350 mV_{SHE} within the active potential range after reaching current density of approximately 1,200 $\mu A/cm^2$ [7,741 $\mu A/ft^2$].

4.1.1.2.2 Molybdenum

It has been widely observed that molybdenum plays a beneficial role in the localized corrosion resistance of nickel- and iron-based alloys. Marcus and Moscatelli (1989) reported the beneficial effects of molybdenum in the presence of adsorbed sulfur on nickel-iron alloys. For single-crystal Ni-2 or 6 at% molybdenum (100) alloys with a monolayer of sulfur on the surface, the adsorbed sulfur catalyzed the dissolution of the alloys in sulfuric acidic solution. The effect of adsorbed sulfur on the passivation, however, was less pronounced on the molybdenum-containing alloys compared to those on nickel and nickel-iron alloys. The concentration of adsorbed sulfur decreased continuously when the nickel-molybdenum alloys

were polarized at either active potentials or held at the open circuit potential. The loss of adsorbed sulfur was explained by an interaction between sulfur and molybdenum to produce either soluble molybdenum-sulfide such as Mo_2S or a simple form of molybdenum-sulfur complex with water that could be readily dissolved. A similar effect of molybdenum was also observed for Type 316 single-crystalline stainless steel with a composition of Fe-17Cr-14.5Ni-2.3Mo (100) in wt% when the alloys were tested in sulfuric acidic solutions (Elibiache and Marcus, 1992). During the active dissolution of the stainless steel, the adsorbed sulfur on the surface was reduced and could be dissolved in the form of MoS phase.

Betts and Newman (1993) observed similar beneficial effects of molybdenum on the corrosion resistance of stainless steels containing molybdenum concentrations ranging from 0.02 to 3.5 wt%. An increase of molybdenum content decreased the anodic dissolution rate measured in 6 M HCl solution containing 0.5–50 mM thiosulfate. Betts and Newman (1993) explained the role of molybdenum in the dissolution of alloys differently than Marcus, stating that molybdenum could reduce the residence time of the adsorbed sulfur on the surface by desorbing the sulfur and occupying the active sites (e.g., ledge sites) presented on the metal surface. This model was indirectly supported by the observation that molybdenum was enriched on the metal surface during the active dissolution of iron-chromium-molybdenum alloys (Newman, 1985). Newman (1985) proposed that the stable state of an uncharged sulfur bridging two nickel or iron atoms can be unstable when one of the atoms is molybdenum, and then the unstable sulfur can be reduced to $H_2S_{(aq)}$.

4.1.1.3 Passive Film Breakdown of Alloy C-4

It is generally accepted that chloride plays a major role in the development of a critical solution chemistry in occluded regions that can lead to passivity breakdown. The decrease in local pH and the increase in chloride ions to maintain charge neutrality in an occluded region lead to activation of the metal and subsequent localized corrosion (e.g., crevice corrosion or pitting corrosion). In chloride solutions, the combined action of sulfur and chloride promoting localized corrosion was observed on Alloy C-4 (Smailos, 1993).

Smailos (1993) reported passive film breakdown on Alloy C-4 (Ni-19.4 Cr-13.8 Mo-2.4 Fe in wt%) in sulfur containing chloride-rich solution. Alloy C-4 is one of the high corrosion-resistant nickel-based alloys that has a chemical composition very similar to Alloy 22 (Ni-22-Cr-13-Mo-3-Fe in wt%). For the disposal of spent fuel, Alloy C-4 was selected as a candidate material for a spent fuel container in Germany (Closs and Einfekd, 1986). The corrosion test results for a surface-welded Alloy C-4 at 150 °C [302 °F] revealed that the general corrosion rate measured in the NaCl-rich brine remained fairly constant during the entire test period (up to 18 months) and was very low {i.e., 0.1 mm/yr [2.54×10^{-6} mpy]}. In the presence of 6×10^{-4} M Na_2S in the NaCl-rich brine, however, Alloy C-4 was attacked by pitting corrosion with a maximum depth of 200 µm [7.87 mil]. In the $MgCl_2$-rich brines with sulfur addition, the general corrosion rate was higher than in NaCl-rich brine with sulfur, and the final rate was 6 mm/yr [1.52×10^{-4} mpy] after 18 months' immersion. All tested samples in the $MgCl_2$-rich brines also suffered severely from the pitting corrosion, with a maximum 900 µm [35.43 mil] of pit depth and crevice corrosion also occurring below the polytetrafluoroethylene threads.

4.1.2 Short-Term Corrosion Test Data of Sulfur-Doped Alloy 22

Jones, et al. (2005) and Windisch, et al. (2005) investigated the corrosion behaviors of Alloy 22 implanted with sulfur in deaerated 1 M NaCl solution. Sulfur concentrations up to sulfur-to-total metal ratio approximately 0.02–0.03 (equivalent to 2–3 percent coverage of sulfur on the alloy surface) were used. The potentiodynamic polarization curves for the Ar-implanted control sample and the sulfur-doped Alloy 22 sample are presented in Figure 4-1. As seen in this figure, the values of passive currents for both samples are similar. In the presence of sulfur, there was a 100 mV negative shift of the corrosion potential, and the S-to-total metal ratio increased from 0.021 to 0.03 on the alloy surface after a potentiodynamic polarization at a scan rate of 1 mV/sec. Even if the change of passive current density was not noticeable, the sulfur enrichment on the surface was reproducible. The sulfur-doped sample also showed an anodic peak at high anodic potentials (e.g., 0.05 to 0.1 V_{SCE}), indicating a localized corrosion process. No morphological analyses for the localized corrosion were given in this reference.

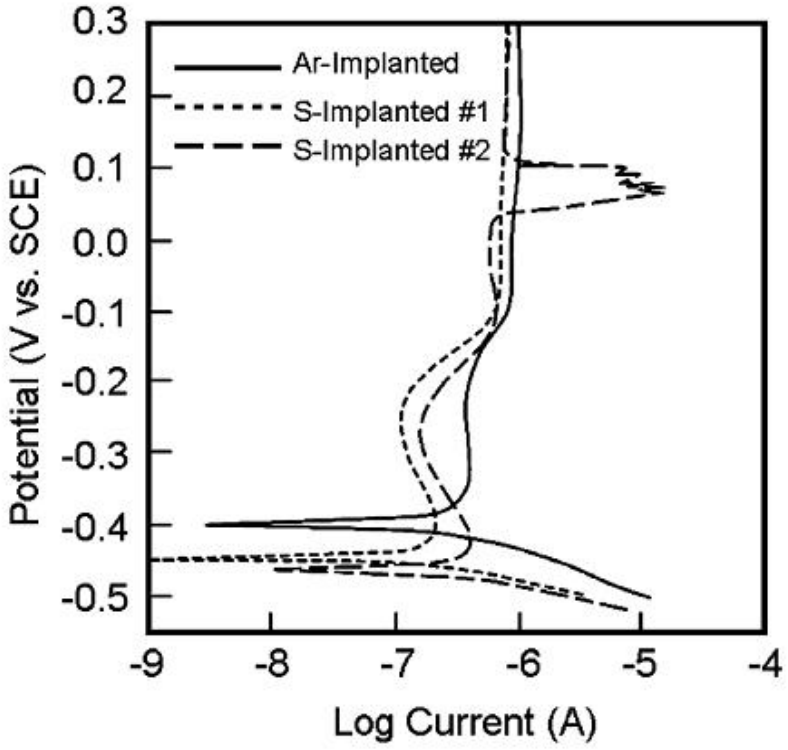

Figure 4-1. Potentiodynamic Polarization Curves for Alloy 22, Implanted With Ar and S (duplicate runs for S) and Subsequently Sputtered to the Implant-Concentration Maximum, in Deaerated 1 M NaCl Solutions Buffered to pH = 3.67 with 0.05 M Potassium Hydrogen Phthalate (KHP) (Windisch, et al., 2005)

Sulfur enrichment was observed in a relatively long-term immersion test at the open circuit potential in 1 M NaCl solution (pH of 3.67) as shown in Figure 4-2. After 29 days immersion, the sulfur concentration on the surface increased up to S-to-total metal ratio of 0.05 measured by x-ray photoelectron spectroscopy. The corrosion rate was estimated to be approximately 0.1–0.25 μA/cm^2 [1.6 μA/ft^2]. Detailed information regarding the corrosion rate measurements, however, is not given in the previously noted references. This result suggests that the long-term exposure (e.g., hundreds years) of the alloy with a low level of bulk sulfur concentration (e.g., 10 ppm by weight) has the potential of raising surface sulfur concentrations higher than that in the alloy currently being tested, which may influence the corrosion processes. Jones, et al. (2005) estimated that it would take approximately 500 years to form a monolayer of sulfur at the metal–film interface in nickel-based alloys containing 100 ppm sulfur in at% at a general corrosion rate of 0.01 μm/yr [2.54 × 10^{-7} mpy] if 100 percent of the sulfur atoms were retained at the surface.

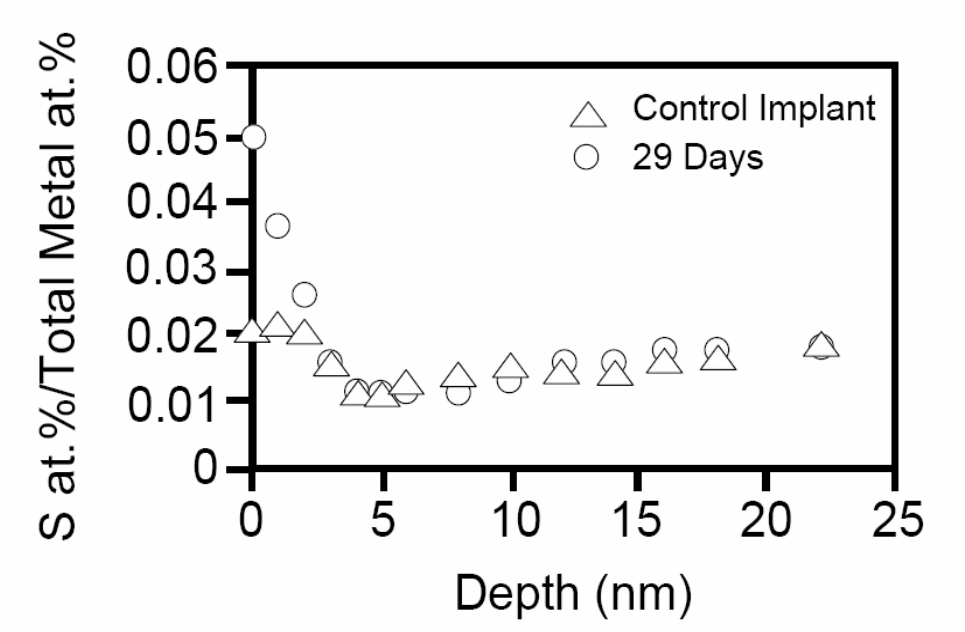

Figure 4-2. Depth Profile Showing the Ratio of Sulfur-to-Metal Concentrations as a Function Depth for the Control Sample Before Corrosion Test and the Tested Sample Exposed to 1 M NaCl Solution (pH 3.67) for 29 days. An Excess Amount of Sulfur Accumulated Near the Surface Region After 29 Days (Windisch, et al., 2005).

4.1.3 Evaluation of Sulfur Effects on the Long-Term Persistence of the Passive Film on Alloy 22

In this section, the preliminary results for the potential sulfur effects on the long-term persistence of the passive film on Alloy 22 are discussed, including thermodynamic stability of metal-sulfur-water systems, the induction time for film breakdown by anodic sulfur segregation, and repassivation processes under potential repository environments.

4.1.3.1 Thermodynamic Stability of Metal-Sulfur-Water System

The potential-pH diagram (Pourbaix diagram) provides a thermodynamic basis for understanding the dissolution and oxide formation phenomena in aqueous solutions under various electrochemical conditions. Regions of thermodynamic stability of solid and soluble species are defined for different activities based on standard free energy data. Figures 4-3, 4-4, and 4-5 show Pourbaix diagrams for nickel-sulfur-water, chromium-sulfur-water, and molybdenum-sulfur-water systems, respectively, at 25 or 90 °C [77 or 194 °F] for 10^{-6} M concentration of ions in the solution.

In Figure 4-3, at 25 °C [77 °F], nickel becomes unstable and forms Ni^{2+} at the anodic potential above -0.42 V_{SHE} in acidic solutions and forms $Ni(OH)_3^-$ in alkaline solutions. With an increase in pH, Ni^{2+} reacts with different valence states of sulfur species such as sulfides ($H_2S_{(aq)}$ at pH 3.29 or HS^- at pH 5.04) in low anodic potentials or sulfate (SO_4^{2-} at pH 6.56) in high anodic potentials and then forms different phases of nickel sulfides (e.g., Ni_3S_2, NiS, and Ni_3S_4) over a wide range of potential and pH regions. The formation of nickel sulfide (Ni_3S_2) was observed on a nickel-sulfur-water system by x-ray photoelectron spectroscopy surface analysis during the corrosion tests (Marcus and Grimal, 1990) (see Section 4.1.1). Above the potential of Ni_3S_2 formation, NiO can be formed in alkaline pHs. The increase of temperature to 90 °C [194 °F] results in a larger NiO stable region than at the low temperature, while there are no significant changes for nickel sulfides.

According to the potential-pH stability diagram for two-dimensional layers of adsorbed sulfur element on the metal nickel system (Marcus and Protopopoff, 1993), the stability domain of adsorbed sulfur can extend beyond the usually predicted range of stability of metal sulfides, and thus it is possible that atomic sulfur can adsorb on the nickel or NiO bulk solid in which bulk sulfides are not stable.

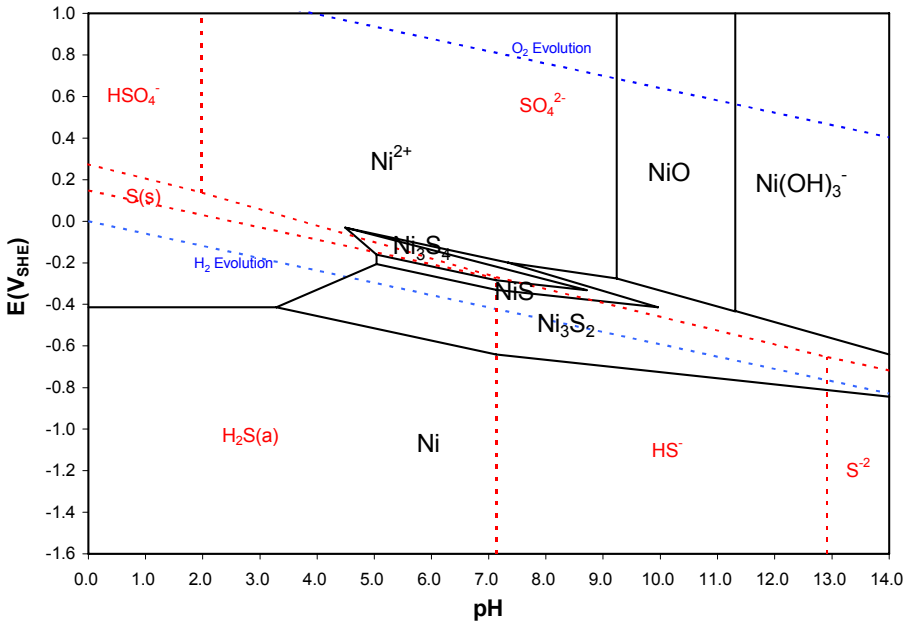

(a)

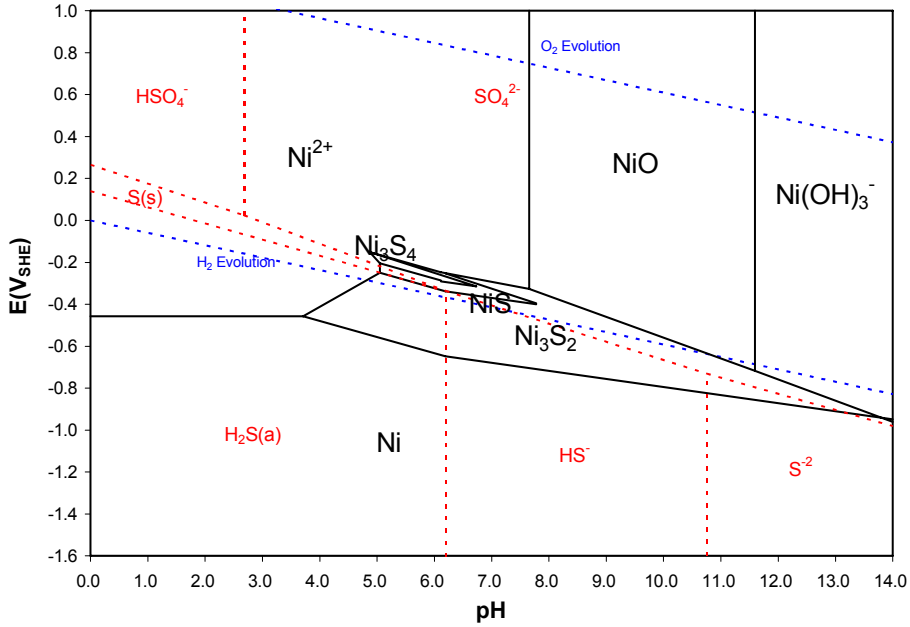

(b)

Figure 4-3. Potential-pH Diagram for Ni-S-H_2O System at (a) 25 °C [77 °F] and (b) 90 °C [194 °F] for 10^{-6} M of Ions

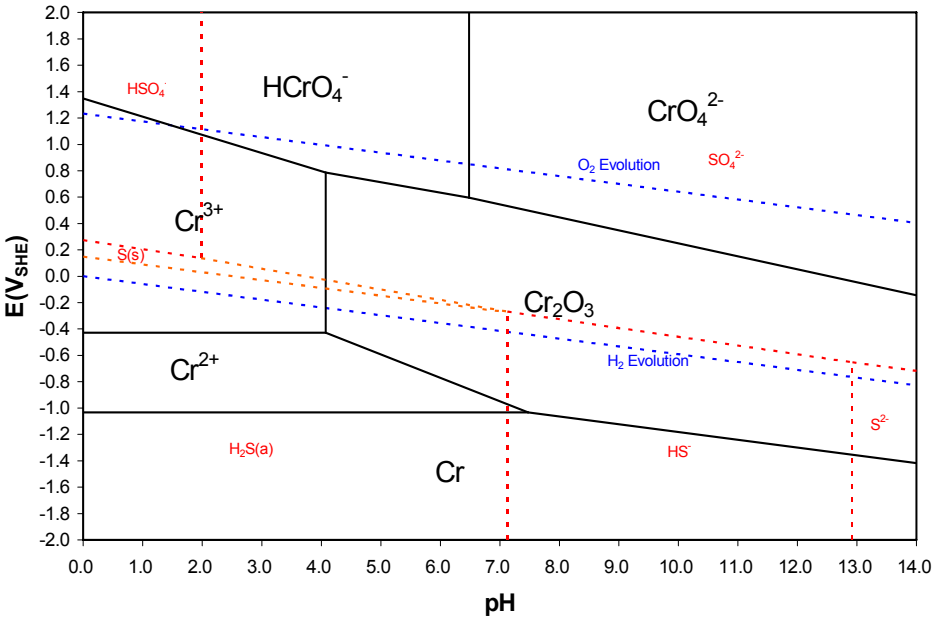

(a)

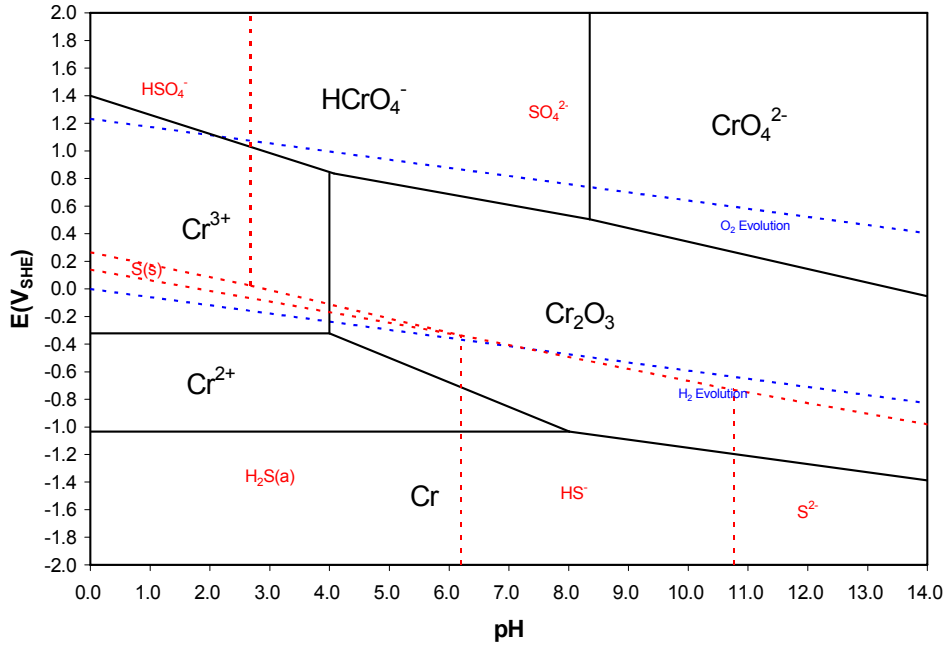

(b)

Figure 4-4. Potential-pH Diagram for Cr-S-H_2O System at (a) 25 °C [77 °F] and (b) 90 °C [194 °F] for 10^{-6} M of Ions

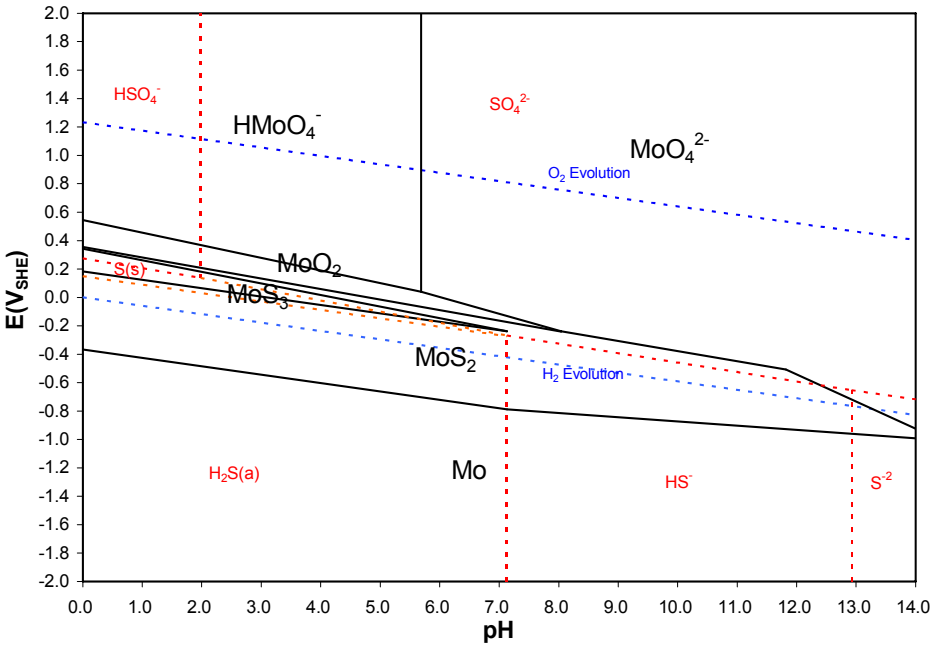

(a)

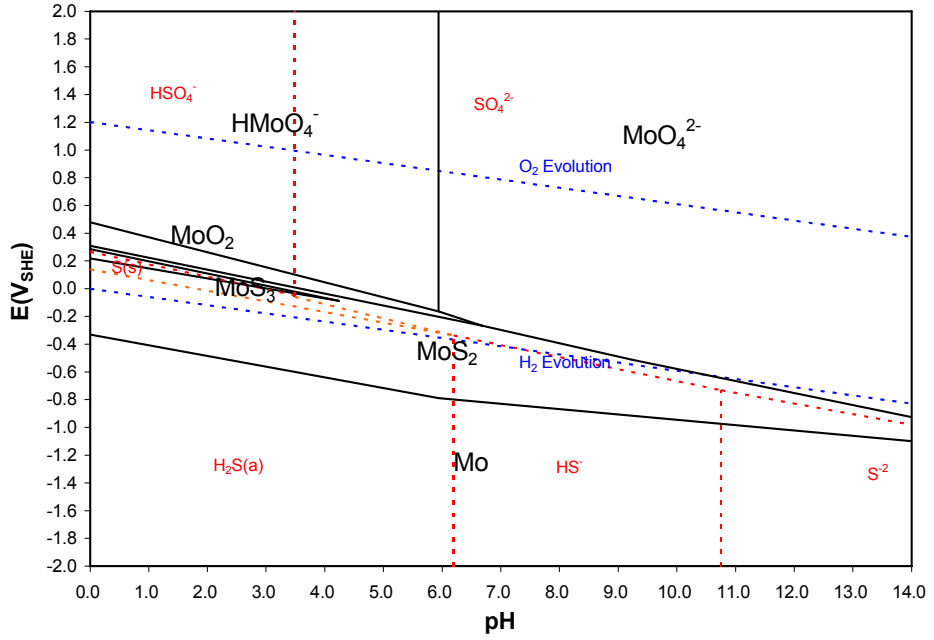

(b)

Figure 4-5. Potential-pH Diagram for Mo-S-H_2O System at (a) 25 °C [77 °F] and (b) 90 °C [194 °F] for 10^{-6} M of Ions

For the chromium-sulfur-water system shown in Figure 4-4, the computational results for sulfide stability are much different than for the nickel-sulfur-water case. The resultant diagrams indicate that the formation of chromium (Cr_2O_3) is strongly favorable in a wide range of potential and pH regions rather than sulfide formation at both 25 and 90 °C [77 and 194 °F]. This superior stability of chromium oxide over any forms of sulfides explains why chromium is beneficial to the corrosion resistance of chromium containing nickel-based alloys with adsorbed or alloyed sulfur (see Section 4.1.1.2).

The potential-pH diagrams for the molybdenum-sulfur-water system at 25 and 90 °C [77 and 194 °F] are presented in Figure 4-5. Similar to nickel, molybdenum also shows a strong tendency to form metal sulfides over a wide range of potential and pH regions at both temperatures. The stable phases of molybdenum sulfides are MoS_2 and MoS_3. The formation of molybdenum sulfides during the anodic dissolution process of nickel-molybdenum alloys and stainless steel with adsorbed sulfur was postulated by Marcus and Moscatelli (1989) with different chemical compositions (see Section 4.1.1.2.1). Marcus and Moscatelli (1989) argued that the adsorbed sulfur on the alloys can be dissolved via soluble molybdenum sulfides (e.g., Mo_2S or MoS for nickel-molybdenum or stainless steel, respectively) or molybdenum-sulfur clusters with water. Due to the absence of thermodynamic data for Mo_2S and MoS from the currently available database, neither sulfide was considered as the species in the reactions. Note that the kinetically observed phases often differ from the thermodynamically stable phases due to different reaction rates for each reaction.

4.1.3.2 Calculation of the Induction Time for Passive Film Breakdown

Assuming the sulfur present in Alloy 22 accumulates at the metal–film interface during the passive dissolution and passive film can break down above a critical sulfur concentration of 40 nanogram/cm^2, the induction time for a film breakdown of Alloy 22 under deaerated conditions is estimated by utilizing Eq. (4-2). Note that the induction time calculation for Alloy 22 would only be valid if similar sulfur effects on passivity degradation mechanisms exist for Ni-Fe alloys and Alloy 22. Equation (4-2) may not be applicable if the sulfur-related degradation mechanism for Alloy 22 is different than that for Ni-Fe alloys. The assumption of film breakdown is partially supported by the observation of pitting corrosion on Alloy C-4 as mentioned previously (see Section 4.1.1.3). In these calculations, the passive current density is a temperature-dependent Arrehnius function with the activation energy of 44.7 kJ/mol [47.1 Btu/mol] and the reference passive current density of 10^{-8} A/cm^2 [6.5×10^{-8} A/ft^2] at 95 °C [203.25 °F] (Dunn, et al., 2005). Figure 4-6 presents the resultant induction time at 10, 50, 100, 200, and 1,000 ppm by weight of sulfur concentrations as a function of temperature and summarized values in Table 4-2 at 25 and 90 °C [77 and 194 °F].

Table 4-2. Calculated Induction Time for Film Breakdown With Various Sulfur Concentrations at 25 and 90 °C [77 and 194 °F] With a Passive Current Density of 10^{-8} A/cm^2 [6.5 × 10^{-8} A/ft^2]		
Sulfur Concentration (ppm by weight)	Induction Time (years)	
	25 °C [77 °F]	90 °C [194 °F]
10	1,278	50
50	255	10
100	127	5
200	63	2.5
1,000	12	0.5
2,000	6	0.25

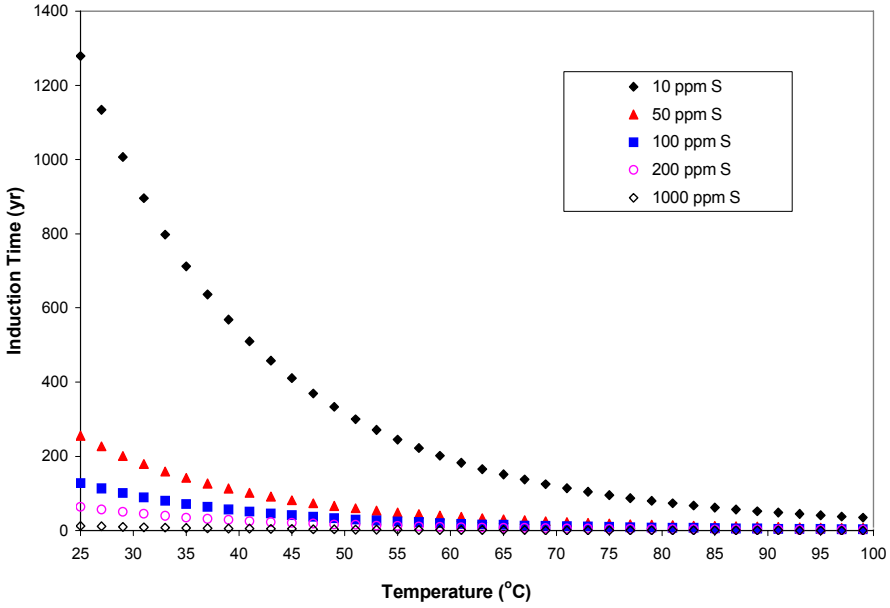

Figure 4-6. Calculated Induction Time of Alloy 22 for Film Breakdown as a Function of Temperature at the Passive Current Density of 10^{-8} A/cm^2 [6.5 × 10^{-8} A/ft^2] and the Activation Energy of 44.7 kJ/mol [47.1 Btu/mol]

As seen in Table 4-2, the induction time decreases linearly as the sulfur concentration increases at both temperatures. At 25 °C [77 °F], the induction time for 10 ppm of sulfur is 1,278 years, but as sulfur concentration increases to 200 ppm, the induction time decreases to 63 years, which is about 20 times smaller than 10 ppm of sulfur. The effect of temperature on the induction time is more significant than sulfur concentration. As the temperature increases, the induction time decreases exponentially at a given sulfur concentration. At 90 °C [194 °F], the

induction times for 10 and 200 ppm by weight of sulfur are 50 and 2.5 years, respectively. Considering a maximum sulfur concentration (e.g., maximum 0.02 wt% = 200 ppm by weight) and a generally low passive current density {e.g., < 10^{-8} A/cm^2 [6.5 × 10^{-8} A/ft^2]} in Alloy 22, the calculation indicates that the film breakdown on Alloy 22 could occur after 2.5 years or longer under deaerated conditions, assuming sulfur in the alloy segregates at the metal–film interface without dissolving into the solution. Based on the currently available long-term corrosion test data for Alloy 22, such as that obtained at the DOE long-term corrosion test facility, there is no evidence or any indication of sulfur-induced film breakdown for Alloy 22, suggesting that the beneficial role of alloying elements (e.g., molybdenum and chromium) overcome any potential anodic sulfur segregation.

As the beneficial effects of chromium and molybdenum have been previously demonstrated in nickel-molybdenum and nickel-chromium-iron alloys as discussed, it can be also expected that the beneficial role of alloying elements (molybdenum and chromium) in Alloy 22 counteract the detrimental sulfur effects. Long-term studies using higher sulfur concentrations in the alloy may be useful to examine the potentially beneficial and/or aggravating effects of these elements on corrosion induced by anodic sulfur segregation in Alloy 22.

4.1.3.3 Film Breakdown and Repassivation Processes of Alloy 22 by Anodic Sulfur Segregation

Based on the observation of sulfur accumulation on Alloy 22 and non-Alloy 22 metal surfaces (i.e., chromium containing nickel-based alloys) as previously discussed, it is possible that the sulfur contents in Alloy 22 can accumulate on the metal surface and segregate at the metal-oxide film interface. This occurs through an anodic sulfur segregation process due to a selective dissolution of metal elements such as nickel, chromium, and molybdenum during the passive dissolution of Alloy 22 in potential repository environments. The segregated sulfur at the metal–film interface may inhibit the formation of the protective passive oxide film and eventually lead to film breakdown at the defected sites preferentially if the concentration of the segregated sulfur reaches a critical concentration. This critical concentration would be approximately a monolayer of sulfur and subsequent formation of metal sulfides (e.g., nickel sulfide and/or molybdenum sulfides) as predicted thermodynamically (see Figures 4-3 to 4-5). Once the passive film is broken down, the subsequent localized corrosion could occur at the defected sites. The anodic dissolution will increase, and the solution chemistry in the pits may change to acidic pH accompanied by a high chloride concentration. This situation may be similar to the localized corrosion that has occurred near the sulfide inclusion (e.g., MnS) in stainless steel (Brossia and Kelly, 1998).

Due to very low solubility products of metal sulfides in general, the dissolution of metal sulfides exposed to the solution may be thermodynamically limited. Thus, metal sulfides such as Ni_3S_2 could stay on the metal surface during a relatively long period, preventing the formation of protective passive oxide film on Alloy 22. On the other hand, it is kinetically possible that the fast dissolution of metal species from the exposed area could enforce and accelerate the dissolution (or desorption) of metal sulfides by breaking the bonds between metal matrix and sulfides. The reduction of adsorbed sulfur concentration on the metal surface has been observed in Ni and Ni-Fe alloys at high anodic dissolution rates (see Section 4.1.1.1.1). Molybdenum in the alloy will also contribute to removing the segregated sulfur as postulated by Marcus and Oudar (1995) and Betts and Newman (1993) (see Section 4.1.1.2.2).

The dissolved sulfur species could be either in the form of the reduced sulfur [e.g., sulfides ($H_2S_{(aq)}$ or HS^-)] or the oxidized sulfur [e.g., sulfate (SO_4^{2-})] in the oxidized conditions along with any possible states [e.g., sulfur, thiosulfate ($S_2O_3^{2-}$), or sulfite (SO_3^{2-})] depending on the solution chemistry and temperature.

In the presence of the reduced sulfur with chloride, the synergistic effects of the reduced sulfur can stabilize localized corrosion processes as previously described in Section 4.1.1.3. If the detrimental combined effects of chloride and reduced sulfur overwhelm the beneficial effects of molybdenum and chromium contents on the surface, the repassivation of Alloy 22 could be difficult. On the other hand, the situation could be reversed because the beneficial effects of alloying elements are more effective, resulting in easy repassivation of Alloy 22. However, chromium may effectively promote passivation and allow repassivation of Alloy 22 to occur; the resultant passive film may be more porous than the unattacked film.

If the sulfur segregation on the metal surface occurs more evenly over the entire metal–oxide interface, a relatively large sulfur segregated area (i.e., more evenly dispersed metal sulfides over the entire metal–oxide interface) can develop, and the passive film could detach due to a possibly large misfitted strain between the sulfides and the metal matrix near the interface and/or a relatively weak bond of metal sulfides to the metal matrix. Thus these mechanically unstable metal sulfides may spall off. The situation under large areas exposed to the solution would be different than the localized small areas.

The role of oxyanions such as nitrates, sulfates, and carbonates/bicarbonates on the film breakdown and repassivation processes should also be considered. The aqueous solution chemistry under the potential repository conditions indicates that the Yucca Mountain environments may contain these oxyanions, which have been known as effective inhibitors for the crevice corrosion of Alloy 22 in a binary solution of 0.5 m NaCl with each inhibitor at 95 °C [203 °F] (Dunn, et al., 2005). Thus these types of anions could reduce or prevent crevice corrosion and then promote the repassivation of Alloy 22. Also, the waste package surface will be subject to dripping groundwater, continuously replenishing the solution. This solution replenishment could reduce (or dilute) the amount of dissolved sulfur species in the aqueous layer, which is potentially beneficial to the repassivation of Alloy 22.

Therefore, the likelihood of repassivation and depassivation of Alloy 22 in potential repository environments would be dependent on several factors, including chemical composition of alloy surface, groundwater chemistry (anion type and quantity, pH, etc.), temperature, and water flow rate on the waste package outer container surface. It is also noted that the influences of dissolved oxygen on the surface sulfur build up and solution chemistry exists. In aerated environments, for example, it is possible that the sulfur may be significantly oxidized and removed by dissolution from the surface, thus ameliorating the long-term sulfur effects on the corrosion process of Alloy 22. Whether the sulfur segregation may cause breakdown of the passive film under potential repository conditions, how quickly Alloy 22 repassivates, and what is the quality of the protective passive film on Alloy 22 to be reformed are currently unknown.

4.2 Base Metal Chromium Depletion on Passive Film Stability

Another potential degradation process that has been suggested to affect the stability of the passive film is the chromium depletion phenomena. This phenomena is described as a reduction in the concentration of a particular alloying element below the baseline value for the

specific material. For Alloy 22, the specified base metal concentration of chromium is 22 wt%. Note that this chromium depletion discussion refers to the concentration of chromium in the base alloy; it does not refer to the concentration of chromium in the passive film on the surface of the alloy. Although stability of a chromium oxide-rich passive film is related to chromium depletion in the base metal, these are two separate topics.

As mentioned in Chapter 3, DOE observed depletion of chromium concentration in the bulk metal of Alloy 22 at the interface of the alloy and the oxide film. Lower concentrations of chromium in bulk alloys below a critical threshold level have been observed to reduce the protective nature of the passive film that forms on various alloys. This part of Chapter 4 will evaluate the chromium depletion in the bulk material underneath the passive film. Initially, the effect of chromium concentration on the performance of passive films with respect to corrosion protection will be examined. Following this discussion, the experiments where chromium depletion was observed to occur in Alloy 22 will be presented. The last part of this section will discuss the implications associated with this degradation phenomenon.

4.2.1 Role of Chromium Concentration on Passivity

The concentration of chromium in bulk alloys can be a direct measure of the corrosion resistance of an alloy. For example, the pitting resistance equivalents are directly related to the amount of an alloy's chromium concentration (Sridhar and Cragnolino, 2002). For this reason, many of the alloys used in highly corrosive environments, such as Alloys 22, 600, 690, and Type 304 stainless steel, contain high concentrations (>18 percent) of chromium. A reduction in the amount of chromium can possibly lead to the loss of passivity, high corrosion rates, or even localized corrosion. Two chromium depletion related examples are discussed below.

In the 1970s and early 1980s, the nuclear industry was dealing with a degradation problem with sensitized stainless steels. Stainless steel could undergo a process called sensitization when it was welded. During the welding process, the pipe material would get heated to high temperatures. While the material is cooling down, chromium and carbon diffuse to and precipitate out in the form of chromium carbides [$(Fe, Cr)_{23}C_6$] at the grain boundaries. This depletes the surrounding grain boundary matrix of chromium (Devine, 1990). The stainless steel alloy could then suffer from intergranular stress corrosion cracking, because the chromium concentration was below a value required to maintain safe operation. The sensitization and thus the reduction of chromium concentration on the grain boundaries of 304 stainless steel has been correlated to a change in the nature of the passive film that forms on this alloy (Kumai and Devine, 2001).

Lloyd, et al. (2003) studied two nickel-based alloys with different concentrations of chromium. Potentiostatic polarization experiments were preformed on Alloys 22 and 276 at temperatures between 22 °C [72 °F] and 85 °C [185 °F] in a solution of 1.0 M NaCl and 0.1 M H_2SO_4. The main difference between Alloy 22 and Alloy 276 is the chromium concentration, which is roughly 22 and 16 percent, respectively. The results from this study indicated that Alloy 276 had a higher passive current density compared to Alloy 22 under all of the conditions evaluated. The overall chromium content in the oxide film was lower for Alloy 276 compared to Alloy 22. In addition, Alloy 276 in this study initiated localized corrosion, while Alloy 22 did not. These results indicated that the higher chromium content in the oxide of Alloy 22, particularly at the oxide/alloy interface, and its persistence is a controlling feature for the resistance to film breakdown.

4.2.2 Chromium Depletion in Alloy 22 and Other Nickel-Based Alloys

Lorang, et al. (1990) examined Alloy 600 (Ni-18Cr-8Fe) and Alloy C4 (Ni-18Cr-10Mo) in deaerated 0.5 M or 5M NaCl at 20 and 90 °C [68 and 194 °F] with Auger electron spectroscopy. The results from both Alloy 600 and Alloy C4 indicated depletion of the chromium concentration in the bulk alloy at the metal/oxide interface, concurrent with an enrichment in the nickel concentration at the same location. This has also been previously detected in stainless steels passivated in neutral to alkaline solutions.

Additional studies on nickel-chromium and nickel-chromium-iron alloys were conducted in 0.05 M H_2SO_4 solution (Boudin, et al., 1994) at room temperature. Depth concentration profiles of chromium, nickel, iron, and oxygen were examined using Auger electron spectroscopy. The composition was modified below the passive films in the bulk alloy. The results indicated that there was chromium concentration depletion in the bulk alloy, which was compensated by an enrichment of nickel concentration in the same location.

Results from short-term potentiostatic tests of Alloy 22 in the potential repository environment showed depletion of chromium concentration in the bulk alloy at the interface between the alloy and the oxide film (Orme, 2005). Chapter 3 initially presented details of this work. The electron energy loss spectroscopy in Figure 3-2 shows a darker line at the metal-oxide interface, which indicates a reduction in chromium concentration in the bulk alloy below the passive film. This reduction in chromium concentration is consistent with nickel enrichment at the metal surface. The results in the simulated acidic conditions indicated that the chromium concentration was depleted with an enrichment in the nickel concentration in the bulk alloy below the passive film. In addition, the chromium depletion and nickel enrichment was observed for Alloy 22 in buffered pH 7.5. The results that Orme (2005) presented for the long-term testing (5 years) showed no chromium depletion or nickel enrichment in the bulk alloy at the metal/oxide interface. However, no chromium oxide film was observable. The source for chromium depletion at the interface is likely due to the formation of the chromium oxide (this will be discussed in the next section). However, the data may have been obscured by the large carbon surface layer present.

Chiang, et al. (2007) also indicated the presence of chromium depletion in the bulk alloy at the alloy/oxide interface on Alloy 22 in the environments examined. X-ray photoelectron spectroscopy for Alloy 22 in 0.028 M NaCl at 95 °C [203 °F] (Figure 3-6) showed that the chromium concentration was depleted, while the nickel concentration was enriched in the bulk alloy below the passive film. The chromium concentration was also depleted in the bulk alloy in deaerated 1.14 M $NaHCO_3$ and 0.19 M NaCl, 1.14 M $NaHCO_3$, 0.19 M NaCl, and 1.14 M $NaNO_3$ solutions (Figures 3-10 through 3-14) at 95 °C [203 °F]. Interestingly, nickel was also depleted at the metal/oxide grain boundary in these environmental conditions, while the molybdenum concentration was enriched in the metal at the metal/oxide boundary.

4.2.3 Long-Term Implications of Chromium Depletion for Alloy 22

Chromium depletion may be a degradation process that occurs on Alloy 22 in the potential repository environment. The concentration of chromium has been shown to be directly related to the corrosion resistance of nickel-chromium-molybdenum alloys. The DOE and CNWRA data showed that chromium depletion at the metal/oxide interface is a real observation for Alloy 22 in simulated repository environments. However, chromium depletion was observed whenever a chromium oxide passive film was also observed. It is considered that the preferential oxidation

of chromium at the oxide/metal interface introduces a strong segregation of metallic elements. Once the chromium has segregated into the oxide, other elements that have a smaller affinity for oxygen can migrate to the interface and oxidize successively at the film surface (Halada, et al., 1996). The initial oxidation of the alloy in these solutions forms a chromium oxide, which leads to the chromium segregation along with the nickel or molybdenum enrichment. For this reason, it is not surprising that the chromium depletion was not observed in the DOE data where no chromium oxide seemed to have formed. Either there was no chromium passive film, or the film was so thin that it did not lead to noticeable chromium depletion in the base alloy. So while the chromium depletion may be present, it occurs when a chromium passive film that can reduce the general corrosion rate is formed.

One of the possible driving forces for nickel and molybdenum enrichment at the metal/oxide interface is the formation of molybdenum-nickel intermetallic phases such as $MoNi_4$. The Engel-Brewer model of intermetallic bonding would predict that bonding would be stronger between hyper d-electron metals, such as nickel, and hypo d-electron metals, such as molybdenum, in the second transition series as compared to chromium in the first transition series (Halada, et al., 1996). Rajeswari, et al. (2001) reported that the metallic nickel underneath the passive film may contribute to the passivation and improved pitting resistance through the formation of these intermetallic bonds with chromium and molybdenum that reduce the anodic dissolution. The intermetallic layer below the passive film may improve the corrosion resistance for the chromium-nickel-molybdenum alloys by providing an enriched source of oxide-forming metallic species.

Limited chromium depletion has been observed on Alloy 22 in certain tests. Without the chromium passive film on the surface, it would seem likely that the alloy would have a lower corrosion resistance to general or localized corrosion, even with the enriched nickel/molybdenum layer. However, the experimental testing including the long-term (5-year) tests did not show any increase in corrosion rates despite the presence of chromium depletion. This may be due to the fact that if chromium depletion is present in the base alloy, it must be the result of passive chromium oxide growth. There may also be some corrosion resistance due to the silica deposits on the material surface. The general assessment is that the chromium depletion below the passive film will in itself not affect the long-term stability of the material.

4.3 Film Spallation by Void Formation

Based on the Point Defect Model, Pensado, et al. (2002) extended the modeling to evaluate various transport mechanisms of passive oxide layers of nickel-chromium-molybdenum alloys at relatively low temperatures. Pensado, et al. (2002) postulate that the spallation of oxide film is caused by accumulation of vacancies with a neutral charge at the metal–oxide interface. According to the original Point Defect Model Macdonald (1992) developed, the injection of cation interstitials is accompanied by a creation of vacancies in the alloy. Recognizing the presence of the defects such as dislocations, high-angle misfit grain boundaries, preexisting voids in the alloy side, and any possible suitable regions at the interface as a vacancy sink, the created vacancies could be annihilated (or diluted) by incorporation into the noted defected regions. Furthermore, these vacancies can be diffused into the matrix alloy to balance the concentration gradient of vacancy in the alloy by a vacancy diffusion process. The transport of vacancies is also accompanied by the diffusion of metal atoms to the interface, which contributes to the oxide film formation.

In the original Point Defect Model, except for the neutrally charged vacancy generated at the metal–oxide interface to the alloy side, there are two different types of vacancies that also involve a passivation process: the cation interstitial vacancy and the anion oxygen vacancy. The cation vacancy is generated at the film-solution interface as a result of dissolution of substitutional and/or interstitial cations and diffusion through the barrier layers to the metal-barrier layer oxide interface, which is the reverse direction of the cation diffusion. The cation vacancy can be annihilated either by the formation of a cation–anion vacancy pair (i.e., Schottky-type vacancy defect) or by emission of cations from the metal into the oxide film. If the amount of annihilation of cation vacancies by both processes is less than the amount of the remaining cation vacancies arriving at the metal–oxide interface, the excess cation vacancies could be accumulated at the metal–oxide interface and/or within the film. This excess amount of cation vacancies could result in film rupture (e.g., pitting) if a critical concentration of accumulated cation vacancies is reached.

Macdonald (1992) postulated a mechanism for pitting corrosion by applying this type of film rupture to explain the pitting corrosion of stainless steel tested in NaCl-rich brines at 250 °C [482 °F]. This approach was partly adopted to explain the transpassive dissolution of Alloy 22 tested in deaerated chloride containing a pH 3 solution at 80 °C [176 °F] (Macdonald, et al., 2004).

From the view of a crystalline structure, the chromium oxide (Cr_2O_3) has an approximately hexagonal closed packed structure with a corundum-type crystal structure. In a corundum-type chromium oxide (Cr_2O_3), the oxygen anions are located at the hexagonal closed packed lattice sites, and the chromium cations occupy the octahedral interstitial sites. A corundum-type α-Cr_2O_3 is characterized by a p-type oxide because a deficiency of interstial chromium cations results in excess oxygen anions (Bloss, 1971; Kofstad, 1972; Kubaschewski and Hopkins, 1967; Smyth, et al., 2000).

If a chromium oxide formed on Alloy 22 in potential repository environments is a p-type semiconductor, the pitting or film spallation could occur due to an accumulation of cation vacancies at the metal–film interface according to the Point Defect Model. Figure 4-7 shows the cross-sectional views of oxides formed on the surface of Alloy 22 when Alloy 22 was polarized at three different anodic potentials in 1 M NaCl solution (pH 7.5). At 200mV versus saturated Ag/AgCl, a thin, smooth oxide was observed. Above the 300–350 mV versus saturated Ag/AgCl potential ranges, such as 400 mV versus saturated Ag/AgCl, thick, porous layers formed. The morphologies also exhibit rough features. At higher anodic potential, 650 mV_{SCE}, two layers were separated by an evident void formation between the outer porous layer and inner thin compact layer. This void formation could have resulted from the accumulation of cation vacancies within the passive film, but not at the metal–oxide interface. Based on the currently available long-term corrosion test data for Alloy 22 (such as DOE's 5-year long-term corrosion test facilities), however, there are no evidences or indications of the void formation at the metal-oxide interface.

By applying a energy band bending concept, Sato (2001) postulated that if a p-type of oxide is formed on Alloy 22, a passivity breakdown of Alloy 22 could occur due to a positive shift of the open circuit potential of the alloy by a p-type oxide, and if an n-type oxide formed, the film breakdown would be prevented. However, if a p-type oxide formed, the probability of hydrogen damage would be significantly higher through contact with the p-type oxide if a negative shift of the open circuit potential in the alloy occurred.

The repassivation of the alloy can also occur by the reformation of protective passive film onto the exposed alloy surface. If the exposed area contains enough chromium content and there are no significant negative factors to a film repair process, a protective passive oxide film may reform in a relatively short time period.

4.4 Anion-Selective Sorption

Another potential concern relating to the long-term persistence of passive film on Alloy 22 is the anion-selective sorption, identified originally by Sato (2001).

When a metal corrodes in aqueous solution, its surface is often covered by a porous outer hydrated oxide layer or other insoluble salts. This film may act as a solid membrane for cations and/or anions. Depending on the mobility and concentration of moving ions in the film, the hydrated metal oxides take on the role of either an anion-selective or cation-selective absorbing membrane. Most hydrated oxides of iron group metals are anion selective in acidic and neutral chloride solutions and cation-selective in alkaline solution (Sakashita and Sato, 1979; Sato, 1987). Table 4-3 summarizes the critical pH value where the ion selectivity is reversed (called point of iso-selectivity pH, pH_{pis}).

The ion-selective property of hydrated oxide membranes depends not only on the pH but also on the specific adsorption of foreign ions in the micropores of precipitates. Ferric hydroxide is anion selective in neutral chloride solutions as seen in Table 4-3, but it becomes cation selective in the same solution when molybdate anions (MoO_4^{2-}) are strongly adsorbed in their micropores due to forming the negative fixed charges within the hydrated membrane. The other anions such as CrO_4^{2-} or WO_4^{2-} were not effective and formed a weak bonding with the hydrated membrane (Sakashita and Sato, 1979).

If a porous outer layer has an anion-selective character, anions (e.g., chloride, fluoride, and the other possible detrimental anions) can selectively adsorb on the porous outer layer and then transport through the porous layers, which could be detrimental to passivation and/or repassivation of Alloy 22. If the anions reach the oxide or bare metal surface, the localized corrosion under the precipitates could be promoted due to a possible detrimental action of transported anions. Suleiman, et al. (1994) observed anion-selective sorption with an iron rust membrane to stabilize the pitting corrosion below the critical pitting potential in Type 304L stainless steel in 0.005 to 0.1 M NaCl at room temperature. The rust layer acted as a super crevice site combining the anion-selective action with a low ion resistance and prevented or greatly delayed the repassivation of metastable pits.

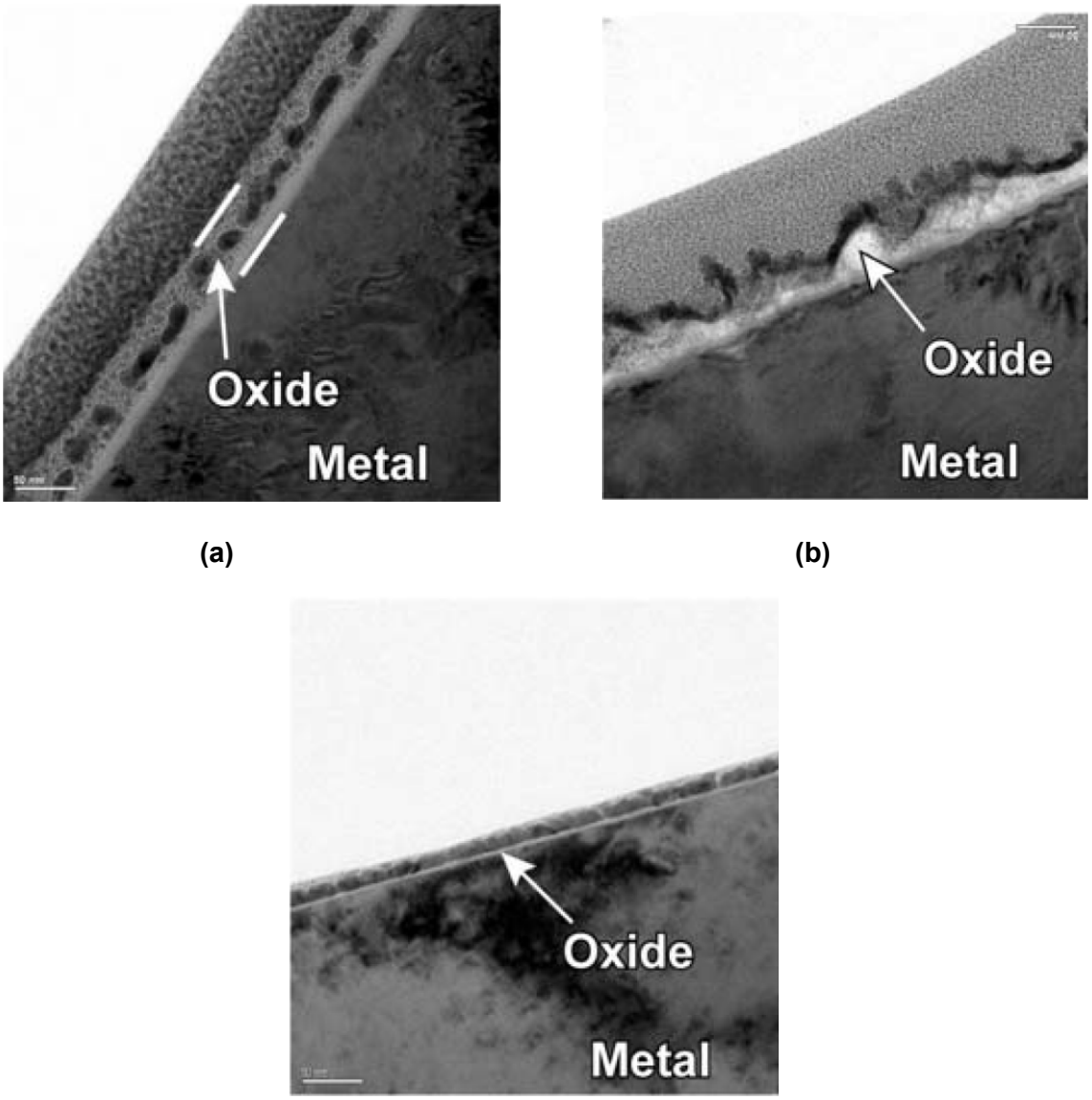

Figure 4-7. Cross-Sectional Views of Oxides Formed at (a) 650 mV Versus Saturated Ag/AgCl, (b) 400 mV Versus Saturated Ag/AgCl, and (c) 200 mV Versus Saturated Ag/AgCl in 1 M NaCl Solution Buffered to pH 7.5 (Orme, 2005)

Table 4-3. Point of Iso-Selectivity pH Value, pH_{pis}, of Hydroxide Membranes in KCl Solution*	
Membrane	pH_{pis}
Nickel(II) hydroxide	>13
Chromium(III) hydroxide	~11
Iron(II) hydroxide	>13
Iron(II, III) hydroxide	5.8
Iron(III) hydroxide	10.3
*Sato, N. "Some Concepts of Corrosion Fundamentals." *Corrosion Science*. Vol. 27, No. 5. pp. 421–433. 1987.	

If the films possess a bipolar character (i.e., a composite type of film consisting of an anion-selective inner layer on the metal side and a cation-selective outer layer on the solution side), the ion transport may take place in the cathodic direction, which does not allow anodic ion transport to occur (Sakashita and Sato, 1979). This ionic current rectification of a bipolar film is similar to the semiconductor p-n junction where the electric current can only flow forward. Therefore, a bipolar type of corrosion product will be the most corrosion resistant in terms of selective ion transport.

This ion selectivity of hydrated oxides might be also correlated to the semiconducting properties, [i.e., an n-type corrosion product on the metal side (most likely oxides) tends to be anion selective, and a p-type on the solution side (most likely hydroxides or other insoluble salts) tends to be cation selective]. If this bipolar type of the passive film (i.e., p-type of hydroxide in outer layer and n-type of oxide in inner layer) forms on Alloy 22 under potential repository conditions, the passive film could be protected by the intrusion of detrimental anions, such as chloride. Currently, there are no available data relating to the anion-selective sorption properties of the oxide layers formed on Alloy 22.

4.5 Large Cathodic Area Development and Increased Cathodic Kinetics

The potential nonpassive corrosion processes such as base metal chromium depletion and anion-selective sorption could be further accelerated by the availability of a large cathodic surface area of corrosion products by a possible non-stoichiometric corrosion front and/or more porous outer layer that develops with time. Thus, transient nonpassive corrosion rates could be increased simply by an increased surface area of accumulated cathodic corrosion products at a constant anodic surface area according to the mixed potential theory. In Pensado, et al. (2002), the evolution of a rough morphology and relevant experiment results showed that the variation of corrosion rate depending on the surface roughening was less than 10 percent. Recently, it was also recognized that the large cathodic surface may not serve as an effective cathode, especially in a limited water volume. The throwing power for cathodic reactions to balance with corresponding anodic reactions could be very limited (Kelly, et al., 2006). Therefore, it is expected that the development of large cathodic area with time will not appreciably affect the

long-term stability of passive film formed on Alloy 22; rather, an anion-selective sorption behavior of the cathodic corrosion products would be more important to the passivation of Alloy 22 if the base metal underneath the passive film is depleted of chromium.

The production of hydrogen peroxide (H_2O_2) and short-lived oxidizing radicals (e.g., HO, HO_2) by radiolysis from gamma radiation of nuclear waste and, if any, other oxidizing species (e.g., Fe^{3+} from the dissolution of stainless steel inner container) in aerated conditions may result in a degradation of the passive film formed on Alloy 22. These oxidizing species can increase the open circuit potential possibly above the critical potential of localized corrosion or even up to the transpassive potential.

A study on a Type 304 stainless steel showed an open circuit potential increase at 280 °C [536 °F] with a gamma radiation (Saito, et al., 1997). Another study on stainless steels also showed the anodic shift of the open circuit potential in the amount of 150–250 mV in J–13 well water at 25 °C [77 °F] (Glass, et al., 1986). At an H_2O_2 concentration of 72 ppm in simulated waters, the open circuit potentials of Alloy 22 were shifted about 225 and 300 mV in simulated acidic water and simulated concentrated water, respectively.

Observations and indications on the potential effects of gamma radiation on surrounding environments include (i) low yield of H_2O_2 by radiation in the moist-air gas system (Reed and Van Konynenburg, 1991), (ii) almost zero yield of H_2O_2 in water vapor (Spinks and Woods, 1990), (iii) a transition of unstable H_2O_2 to more stable benign species such as H_2O, OH^-, and O_2, (iv) the calculated low energy absorption rate on the environment in the proximity of the waste packages, and (v) significant decrease of dose amount with emplacement time in the potential repository environments.

Even if there is no evidence that radiation damage of the passive film on Alloy 22 will alter the film's protective properties, the final report of Waste Package Materials Performance Peer Review Panel (Beavers, et al., 2002) recommended some analysis work. This included an expected concentration of H_2O_2 in the potential repository water, a measurement of the open circuit potential of Alloy 22 at a relevant H_2O_2 concentration, and an assessment of stability of the open circuit potential of Alloy 22 as a function of time exposed to gamma radiation. In the current waste package design, the radiation will be shielded by the inner stainless steel container for an extended period of time until the radiation becomes weak.

Nevertheless, due to a lack of data from the currently available literature on radiation effects on the passive film stability of Alloy 22 in aqueous solution or thin water film, an evaluation of the effect of gamma radiation on the long-term passivity of Alloy 22 may be warranted.

4.6 Dry–Wet Cyclic Process

Over a long period, the waste package outer container will be exposed to elevated temperatures as high as 200 °C [392 °F]. Therefore, the oxide film formed on Alloy 22 in dry- and/or humid-air environments could be different than the passive film formed in the electrolytes or thin water films in terms of the structure and composition. Thus these oxides formed during the initial dry oxidation and humid-air corrosion periods may affect a long-term persistence of passive film on Alloy 22.

Orme (2005) conducted long-term oxidation tests for Alloy 22 at 400–750 °C [752–1,382 °F] in dry air. Some samples were solution annealed at 1,121 °C [2,050 °F] for 20 minutes in dry air to simulate the actual surface of the waste package outer container at the time of emplacement. The electrochemical testing results using potentiodynamic polarization techniques indicated that corrosion performance of the preoxidized sample was comparable to the mirror-polished control sample; however, it seems improved by the preoxidizing treatment as shown in Figure 4-5.

In Figure 4-8, the solution-annealed Alloy 22 disk specimens show that the currents at low anodic potentials are lower than the mirror-polished control samples and the anodic peak at the high anodic potentials does not occur in saturated concentrated water, which is observed in the mirror-polished control sample in the same solution. By examining the corroded surface of both samples using atomic force microscopy, transmission electron microscopy, and electron energy loss spectroscopy, Orme (2005) concluded that there are no appreciable morphological changes due to the electrochemical modification, and therefore, the studies on the annealed samples aged at lower repository temperatures {i.e., less than 200 °C [392 °F]} are unnecessary. The surface analyses results of Orme (2005) reveal that the oxide films formed on the solution-annealed samples both before and after corrosion tests are characterized approximately for 1-µm [3.937×10^{-2}-mils]-thick oxides. The oxides consist of about a 0.8-µm [1.181×10^{-2}-mils] thickness of chromium oxide near the metal substrate, a 0.1 to 0.5-µm [3.937×10^{-3} to 1.968×10^{-2}-mils] thickness of iron oxide onto chromium oxide, and a nickel oxide at the outmost oxide surface. The surface analyses results on the oxide films formed on Alloy 22 after aging at 25, 400, 550, and 750 °C [77, 752, 1,022 and 1,382 °F] for 8,000–10,000 hours in dry air provide additional evidence to support the arguments regarding potential effects of a dry–wet cyclic process. All aged Alloy 22 samples show a very similar oxide structure in terms of thickness and composition when they are oxidized at high temperatures up to 750 °C [1,382 °F].

Dunn, et al. (2003) measured the open circuit potential for a thermally oxidized Alloy 22 in NaCl solution at 95 °C [203 °F]. The samples were preoxidized at 200 °C [392 °F] for 30 days in the oven. The open circuit potential measurement results show that thermally oxidized Alloy 22 samples exhibit similar values of the open circuit potential compared to the mill-annealed control samples. The open circuit potentials for both samples stabilized near 250 mV_{SCE} in acidic NaCl solution. In neutral or weakly alkaline solutions at 95 °C [203 °F], the variation of the open circuit potentials of the preoxidized samples is greater than the mill-annealed samples; however, the open circuit potential seems independent of the surface conditions under the previously mentioned testing conditions.

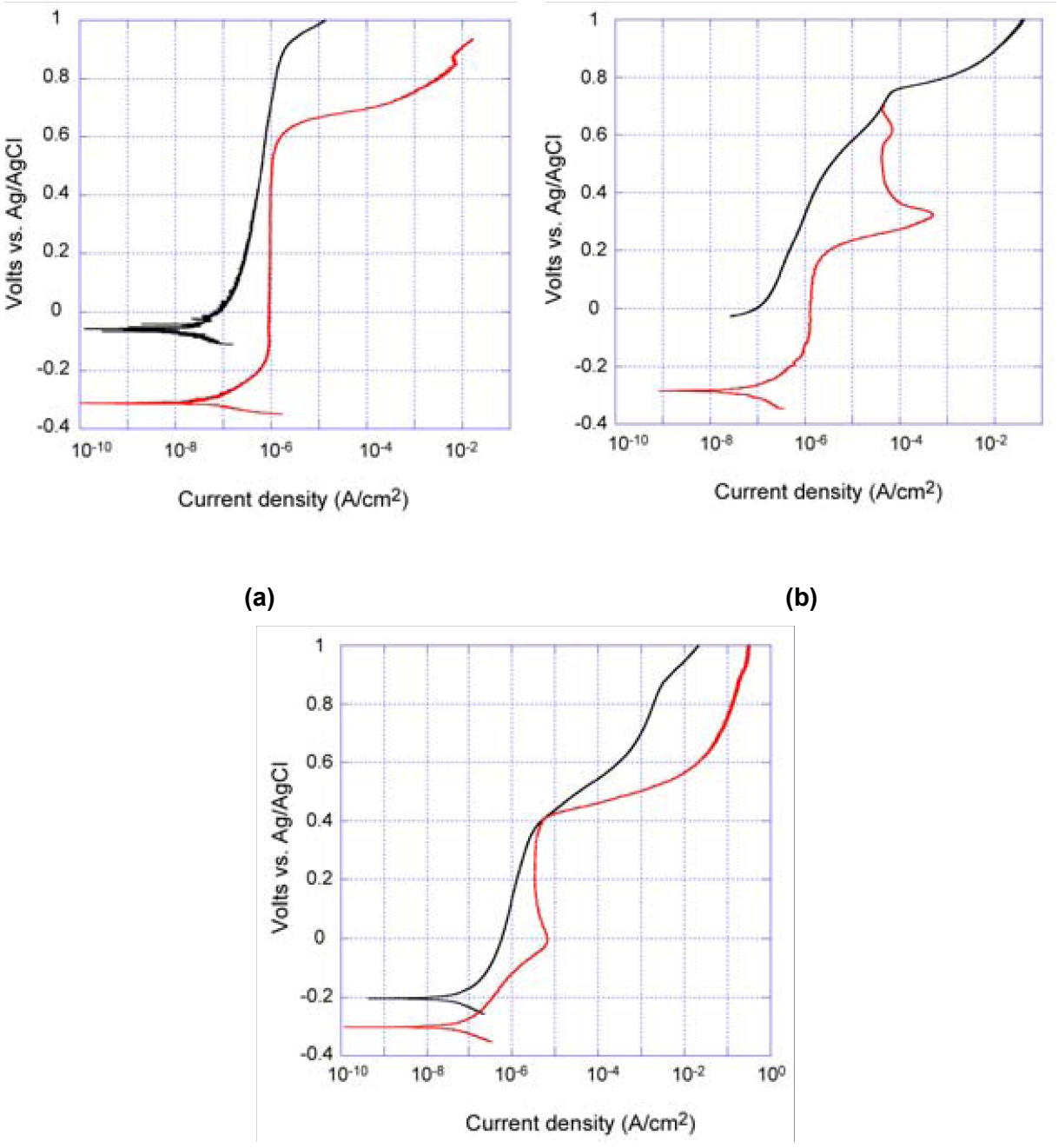

Figure 4-8. Electrochemical Responses of Solution-Annealed (Black-Colored) Versus Mirror-Polished (Red-Colored) Alloy 22 Disk Specimens in (a) Simulated Acidified Water; (b) Simulated Concentrated Water; and (c) Basic Saturated Water (Orme, 2005)

5 SUMMARY AND CONCLUSION

In this report, the long-term passive behavior of Alloy 22, a primary candidate for the waste package outer container, was evaluated by reviewing currently available literature data obtained from short-term tests on Alloy 22 and analog alloys. Results of this review, covering the general corrosion rate, passive film characterization data, and corrosion-related potential degradation processes, are summarized next.

5.1 General Corrosion Rate of Alloy 22

A number of studies are available in the literature that report values of the general corrosion rate from Alloy 22 under passive dissolution conditions. Corrosion rates have been found to decrease with time, although the mechanisms causing the decrease in time are not well understood. There is high scatter in the corrosion rates reported in the literature. For example, at 90 °C [194 °F], reported values of the corrosion rate range from 1 to 104 nm/yr [4×10^{-5} to 0.04 mpy]. The scatter is the result of the different times considered to perform the measurements (from hours to years) and the use of different techniques of varying resolution. Based on measurement of the passive current density for 100 days, the corrosion rate is estimated to be less than 100 nm/yr [0.004 mpy] at 100 °C [212 °F] (Dunn, et al., 2005). Pensado, et al. (2002) reported corrosion rates of less than 100 nm/yr [0.004 mpy], after 2 weeks in solutions at 95 °C [203 °F]. Data based on weight-loss measurements by the U.S. Department of Energy (DOE) indicate that corrosion rates at 90 °C [194 °F] fall below 100 nm/yr after one month, which is consistent with the data in Dunn, et al. (2005) and Pensado, et al. (2002). Corrosion rates exceeding 100 nm/yr [0.004 mpy] at 90 °C [194 °F] reported in the literature correspond to very short-term measurements, and such data must be used with caution.

Multiple studies have confirmed an Arrhenius dependence of the corrosion rate on the temperature. Effective activation energies reported by different authors range, approximately, from 25 to 45 kJ/mol [23.7 to 42.7 Btu/mol]. Corrosion rates extrapolated to 150 °C [302 °F] based on 5-year DOE data (median values) range from 29 to 91 nm/yr [1.2×10^{-3} to 3.6×10^{-3} mpy], which are below 600-day measurements by Rodríguez, et al. (2007) at 155 °C [311 °F]. From Figure 2-3 in Chapter 2, a decrease of the order of 63 percent, from 600 days to 5 years, is noted in the corrosion rates at 90 °C [194 °F]. Assuming a 63-percent decrease in the corrosion rate, the corrosion rates by Rodríguez, et al. (2007) might decrease to values of the order of 100 nm/yr [0.004 mpy] after 5 years, which is more consistent with the DOE extrapolations.

As noted in Chapter 2, it is important to understand the causes behind the decrease in time of the general corrosion rate of Alloy 22 under passive conditions. The decrease in time may correlate to (i) increase in thickness of the oxide film, (ii) compositional and structural changes of the oxide, (iii) formation of precipitated phases next to the passive film, and (iv) compositional and structural changes in the metal in the region next to the metal–film interface. If, for example, the decrease in time is a response to the formation of precipitated products on the oxide, making the transport of ions to a reactive region sluggish, then corrosion rates could be enhanced by removing of such precipitates. Corrosion rates measured in the absence of precipitated layers may be a reasonable bound of corrosion rates to use in performance assessments. It may be difficult to develop technical support for the use of lower corrosion rates, measured in the presence of precipitated layers, because that would require additional

assessment of the stability of the precipitated layers over time. If, on the other hand, the decrease in time of the current density is related to irreversible changes in the oxide film (structural or compositional), and further changes can be argued to occur as time elapses, then corrosion rates at the end of a measurement period would reasonably bound long-term corrosion rates. Therefore, designing experiments to track or estimate variables such as oxide composition and thickness as a function of time and investigating the existence of correlations between such variables and their time dependence and the anodic current density of Alloy 22 is recommended.

5.2 Significance and Stability of Passive Film on Alloy 22

Alloy 22 corrosion resistance is attributed to a chromium-rich passive film. Passive film features that can limit corrosion rates include: composition, thickness, and structure. These features have been examined for Alloy 22 and its industrial analogs in various environments.

In the passive region, it is sometimes assumed that the films grow by the logarithmic rate law, which would predict that the film would grow without bound as time elapses. However, this basic growth-rate equation has been mainly used to analyze short-term potentiostatic tests. The point defect model, on the other hand, postulates that the inner layer (the chromium-rich layer associated with the phenomenon of passivity) thickness is constant for a given set of environmental and electrochemical conditions. In this model, the thickness is a function of the pH, electrochemical potential, and rate constants for the reactions that occur at the interfaces between the alloy-film and the film-solution. However, certain experimental results (Orme, 2005) do not directly conform to the point defect model in some instances, which indicates that there may exist other aspects of the passive film affecting growth and corrosion resistance of Alloy 22.

Over time, dissolution will occur at local defects in the passive film. These sites will repassivate, leading to a restructuring of the passive film. The restructuring could affect both the inner layer, or possibly the outer layer. The role that the outer layer plays in corrosion resistance is in general considered less important than that of the inner compact layer.

Multiple studies have been conducted to evaluate the structure and composition of the passive film on Alloy 22. The results of these studies indicate that the main barrier for corrosion degradation processes is a chromium-rich oxide layer. The chromium is in the +3 oxidation state, which can take the form of Cr_2O_3 or $NiCr_2O_4$. Molybdenum may play a role in the passive behavior for Alloy 22 by reducing the anodic dissolution of the base material. Tungsten may lead to an increased film thickness, possibly decreasing the corrosion rate.

DOE accounts for the presence of a passive film and recognizes that the corrosion performance of the waste package outer barrier is dependent upon the film's integrity (Bechtel SAIC Company, LLC, 2004b). The low general corrosion rates depend upon the long-term stability of the passive film. In most of the experimental testing reviewed, the presence of a chromium-rich oxide film was identified. However, in long-term tests (greater than 2 years), there were environments where Alloy 22 was contaminated by silica or carbon due to the dissolution of the vessel material in which no chromium oxide layers were observed. It was assumed that the chromium oxide film was still present. However, the existence of a thin chromium oxide film or contamination layer controling Alloy 22 corrosion creates uncertainty. Future work in this area could help reconcile any uncertainties of the long-term stability of this passive film.

5.3 Effect of Corrosion-Related Potential Degradation Processes on the Long-Term Persistence of Passive Film on Alloy 22

5.3.1 Enhanced Dissolution Rate by Anodic Sulfur Segregation

Anodic sulfur segregation at the interface between the metal and the passive film and subsequent film breakdown may enhance the general corrosion of Alloy 22 and could lead to a localized corrosion. If the repassivation of Alloy 22 occurs during short time periods, the cyclic process of fast active corrosion upon sulfur segregation and subsequent formation of metal sulfides followed by slow passive corrosion upon repassivation is unlikely to significantly shorten the waste package lifetime. The beneficial effects of alloying elements (e.g., chromium and molybdenum), the presence of inhibitors (e.g., nitrates, sulfates and/or carbonates), and the presence of oxygen may overcome potential detrimental effects of anodic sulfur segregation on the passive film on Alloy 22 in aerated environments, for example, it is possible that sulfur may be significantly oxidized and removed by dissolution from the surface, thus ameliorating the possible long-term detrimental sulfur effects.

The complexity among these multiple factors warrants confirming whether the sulfur enrichment may actually occur and whether it may cause a breakdown in the passive film under potential repository conditions. Long-term studies using higher bulk sulfur concentrations in the alloy or sulfur-containing solutions (e.g., sulfides, thiosulfites, or thiosulfates) with oxyanions (e.g., nitrates, sulfates, or carbonates) may be warranted to better understand sulfur effects on the long-term persistence of Alloy 22 under potential repository conditions. A scratch polarization testing is an effective method to measure the repassivation capability of passive film formed on Alloy 22.

5.3.2 Base Metal Chromium Depletion on Passive Film Stability

Chromium depletion is believed to occur when the chromium concentration drops below the initial value in the base material. Based on stainless steels and nickel-based alloy observations, lower concentrations of chromium in the bulk alloy may cause the formation of a less passive film. Chromium depletion of the base metal under the passive film has been reported in the Alloy 22 literature. Chromium depletion is usually accompanied with either a nickel or molybdenum enrichment at the same location. This concentration distribution may be the result of the preferential oxidation of chromium at the oxide/alloy interface. Therefore, chromium depletion may occur whenever a chromium-rich passive film forms. There is no evidence in long-term (5-year) tests of enhanced corrosion rates due to limited chromium depletion in the base alloy. Therefore, there is no technical basis to assume that chromium depletion may affect the long-term stability of the passive film on Alloy 22.

5.3.3 Film Spallation by Void Formation

The breakdown and subsequent spallation of Alloy 22 passive film could occur by void formation due to an accumulation of cation vacancies at the metal–film interface or within the passive film. Alloy 22 showed film breakdown possibly due to void formation between the outer porous layer and the inner compact layer when polarized potentiostatically at 650 mV_{SCE} in NaCl solution (pH 7.5) (Orme, 2005). The transport of cation and anion vacancies with other ionic species within a passive film is closely related to the semiconducting properties of the passive film.

The passive film on Alloy 22 exhibits n-type semiconducting properties possibly indicating excess cation interstitials in deaerated NaCl solution (pH 3) at 80 °C [176 °F] (Carranza, et al., 2005; Macdonald, et al., 2004). Other studies suggest different semiconducting properties (i.e., p-type chromium oxide on pure chromium or chromium-containing iron- and nickel-based alloys). Differing semiconducting properties of chromium oxide could be ascribed to varying conditions such as chemical composition, microstructure, and or test conditions (e.g., solution chemistry, pH, temperature, surface roughness).

Under potential repository conditions, environmental conditions (e.g., water chemistry and temperature) could be very different from the testing conditions in the literature. Experimental measurements are usually carried out over very short times. Based on available long-term corrosion test data for Alloy 22, there is no evidence or indication of void formation at the metal–oxide interface.

Even if film breakdown were to occur in the repository, the passive oxide film may re-form in a relatively short time if the exposed area contains enough chromium content provided there are no factors impending the film repair process. Therefore, it would be warranted to confirm the repassivation in case of film breakdown under relevant repository conditions.

5.3.4 Anion-Selective Sorption

As discussed in Section 4.4, relevant nickel- and chromium-hydrated oxides tend to show ion-selectivity sorption behavior in chloride solutions. Based on characteristic pH criteria (i.e., point of iso-selectivity pH) to determine cation- or anion-selectivity of the hydrated oxides, most hydroxides such as Ni(II), Cr(III), Fe(II), or Fe(III) exhibit anion- rather than cation-selective sorption behavior in most solution pHs except in very strong alkaline pH (e.g., pH >11). Thus, it may be possible that anion-selective sorption could play a role in corrosion processes of Alloy 22 because the outer layer of passive film will be mostly nickel- and chromium oxi-hydroxides. Based on the currently available long-term corrosion test data for Alloy 22, there is no evidence or indication of the anion-selective sorption process on the passive oxide film.

5.3.5 Large Cathodic Area Development and Increased Cathodic Kinetics

A large cathodic area resulting from surface roughening may not be an effective factor for controlling corrosion of Alloy 22. In addition, the limited volume of water in thin liquid films on the waste package surface could limit the throwing power for the cathodic reactions.

Gamma radiation from nuclear waste may produce and increase the oxidizing power by radiolysis (e.g., generation of hydrogen peroxide and short-lived oxidizing radicals). A combination with other oxidizing species (e.g., dissolved oxygen and Fe^{3+}) may result in degradation of passive film formed on Alloy 22 by increasing the open circuit potential above a critical potential for localized corrosion or even beyond the transpassive dissolution potential. Some studies on stainless steel show an increase in the open circuit potential with gamma radiation in simulated groundwaters. Even if there is no clear evidence that radiation damage of the passive film on Alloy 22 could degrade its corrosion resistance, Beavers, et al. (2002) recommended analysis related to open circuit potential and film stability measurements for long terms under a range of gamma radiation doses. Considering that the inner stainless steel container offers shielding against gamma rays, confirmation of the relevance of this process may be needed.

5.3.6 Dry–Wet Cyclic Process

DOE concluded that the dry–wet cyclic process would not appreciably affect the long-term stability of the passive film formed on Alloy 22 in potential repository environments, considering lower expected repository temperatures than those in tests. Electrochemical test results (i.e., oxidation and aqueous corrosion tests) showed that the solution-annealed Alloy 22 samples, oxidized at 400–750 °C [752–1,382 °F] and then solution-annealed at 1,121 °C [2,050 °F] in dry air, exhibit very similar polarization behavior and surface morphologies after corrosion tests compared to the mirror-polished control Alloy 22 samples.

Dunn, et al. (2003) observed similar open circuit potential changes of thermally aged and mill-annealed Alloy 22 samples in neutral chloride solutions at 95 °C [203 °F]. Based on DOE, NRC, and CNWRA observations, it appears that dry–wet cyclic process may not be an important factor to the long-term stability of passive film on Alloy 22. However, further long-term confirmation for thermally aged Alloy 22 may be needed to assess time dependencies.

6 REFERENCES

Ahn, T., H. Jung, X. He, and O. Pensado. "Understanding Long-Term Corrosion of Alloy 22 Container in the Potential Yucca Mountain Repository for High-Level Nuclear Waste Disposal." Presentation at the Third International Workshop on Long Term Prediction of Corrosion Damage in Nuclear Waste Systems, May 14–18, 2007. ML071210587. State College, Pennsylvania. 2007. <www.nrc.gov/reading-rm/adams.html> (June 1, 2007)

Bechtel SAIC Company, LLC. "Transmittal of Appendices N and S, Technical Basis Document No. 6: Waste Package and Drip Shield Corrosion, Rev. 01, Addressing Key Technical Issue (KTI) Agreements Related to Container Life and Source Term (CLST) 1.08, 1.09, and 2.03 Additional Information Need (AIN)–1." Las Vegas, Nevada: Bechtel SAIC Company, LLC. 2004a.

———. "General Corrosion and Localized Corrosion of Waste Package Outer Barrier." ANL–EBS–MD–000003. Rev 02. Las Vegas, Nevada: Bechtel SAIC Company, LLC. 2004b.

Betts, A.J. and R.C. Newman. "The Effects of Alloyed Molybdenum on the Activation of Anodic Dissolution by Reduced Sulfur Compounds." *Corrosion Science*. Vol. 34. pp. 1,551–1,555. 1993.

Beavers, J.A., T.M. Devine, Jr., G.S. Frankel, R.H. Jones, R.G. Kelly, R.M. Latanision, and J.H. Payer. "Waste Package Materials Performance Peer Review Panel—Final Report." ML20020614.0035. Las Vegas, Nevada: U.S. Nuclear Waste Technical Review Board. 2002.

Birn, J., M. Janik-Czachor, A. Wolowik, and A. Summer. "Corrosion Behavior of High-Nickel and Chromium Alloys in Natural Baltic Seawater." *Corrosion*. Vol. 55. pp. 977–983. 1999.

Bloss, D. *Crystallography and Crystal Chemistry*. New York City, New York: Holt, Reinhart and Winston, Inc. pp. 252. 1971.

Boudin, S., J-L. Vignes, G. Lorang, M.D-C. Belo, G. Blondiaux, S.M. Mikhailov, J.P. Jacobs, and H.H. Brongersma. "Analytical and Electrochemical Study of Passive Films Formed on Nickel-Chromium Alloys: Influence of the Chromium Bulk Concentration." *Surface and Interface Analysis*. Vol. 22. pp. 462–466. 1994.

Brossia, C.S., L. Browning, D.S. Dunn, O.C. Moghissi, O. Pensado, and L. Yang. "Effect of Environment on the Corrosion of Waste Package and Drip Shield Materials." CNWRA 2001-03. San Antonio, Texas: CNWRA. 2001.

Brossia, C.S. and R.G. Kelly. "Influence of Alloy Sulfur Content and Bulk Electrolyte Composition on Crevice Corrosion Initiation of Austenitic Stainless Steel." *Corrosion*. Vol. 54, No. 2. pp.145–154. 1998.

Carranza, R.M., M.A. Rodriguez, and R.B. Rebak. "Passivity of Alloy 22 in Chloride and Fluoride Containing Solution." UCRL–PROC–212821. Livermore, California: Lawrence Livermore National Laboratory. 2005.

Chao, C.Y., L.F. Lin, and D.D. Macdonald. "A Point Defect Model for Anodic Passive Films: I. Film Growth Kinetics." *Journal of The Electrochemical Society*. Vol. 128. pp. 1,187–1,194. 1981.

Chiang, K.T., D.S. Dunn, Y.-M. Pan, O. Pensado, and P.K. Shukla. "Stress Corrosion Cracking of Waste Package Material—Modeling and Experiments." CNWRA 2007-01. San Antonio, Texas: CNWRA. 2007.

Closs, K.D. and K. Einfekd. "Overview of the FRG Activities on Spent Fuel Disposal." Proceedings Second International Conference on Radioactive Waste Management. Winnipeg, Canada: Canadian Nuclear Society. p. 26. 1986.

Combrade, P., P. Marcus, and A. Gelpi. "Effect of Sulfur on the Protective Layers on Alloys 600 and 690 in Low and High Temperature Environments." Proceedings of the Fourth International Symposium on Environmental Degradation of Materials in Nuclear Power Systems—Water Reactors." D. Cubicciotti, ed. Houston, Texas: NACE International. pp. 429–442. 1990.

Costa, D. and P. Marcus. "Modification of Passive Films formed on Ni-Cr-Fe Alloys With Chromium Content in the Alloy and Effects of Adsorbed or Segregated Sulphur." Proceedings of the European Symposium on Modifications of Passive Film, Paris, France, February 15–17, 1993. pp.17–25. 1993.

Cragnolino, G.A., D.S. Dunn, C.S. Brossia, V. Jain, and K.S. Chan. "Assessment of Performance Issues Related to Alternate Engineered Barrier System Materials and Design Options." CNWRA 1999-003. San Antonio, Texas: CNWRA. 1999.

CRWMS M&O. "Total System Performance Assessment for the Site Recommendation." TDR–WIS–PA–000001. Rev. 00 ICN 01. Las Vegas, Nevada: CRWMS M&O. 2000.

Da Cunha Belo, M., N.E. Hakiki, and M.G.S. Ferreira. "Semiconducting Properties of Passive Films Formed on Nickel-Base Alloy 600: Influence of the Alloying Elements." *Electrochimica Acta*. Vol. 44. pp. 2,473–2,481. 1999.

Day, S.D., M.T. Whalen, K.J. King, G.A. Hust, L.L. Wong, J.C. Estill, and R.B. Rebak. "Corrosion Behavior of Alloy 22 in Oxalic Acid and Sodium Chloride Solutions." *Corrosion*. Vol. 60, No. 9. pp. 804–814. 2004.

Devine, T.M. "The Mechanism of Sensitization of Austenitic Stainless Steel." *Corrosion Science*. Vol. 20. pp. 135–151. 1990.

DOE. DOE/RW–0539–1, "Yucca Mountain Science and Engineering Report: Technical Information Supporting Site Recommendation Consideration." Rev. 1. Las Vegas, Nevada: DOE, Office of Civilian Radioactive Waste Management. 2002.

Dunn, D.S., O. Pensado, Y.-M. Pan, R.T. Pabalan, L. Yang, X. He, and K.T. Chiang. "Passive and Localized Corrosion of Alloy 22–Modeling and Experiments." CNWRA 2005-02. Rev. 1. San Antonio, Texas: CNWRA. 2005.

Dunn, D.S., D. Daruwalla, and Y.-M. Pan. "Effect of Fabrication Processes on Materials Stability–Characterization and Corrosion." CNWRA 2004-01. San Antonio, Texas: CNWRA. 2003.

Elibiache, A. and P. Marcus. "The Role of Molybdenum in the Dissolution and the Passivation of Stainless Steels with Adsorbed Sulphur." *Corrosion Science*. Vol. 33, No. 2. pp. 261–269. 1992.

Evans, K.J., M.L. Stuart, R.A. Etien, G.A. Hust, J.C. Estill, and R.B. Rebak. "Long-Term Corrosion Potential and Corrosion Rate of Creviced Alloy 22 in Chloride Plus Nitrate Brines." UCRL–CONF–216910. Livermore, California: Lawrence Livermore National Laboratory. 2005.

Glass, R.S., G.E. Overturf, R.A. Van Konynenburg, and R.D. McCright. "Gamma Radiation Effects of Corrosion—I. Electrochemical Mechanisms for the Aqueous Corrosion Processes of Austenitic Stainless Steels Relevant to Nuclear Waste Disposal in Tuff." *Corrosion Science*. Vol. 26. pp. 577. 1986.

Gray, J.J., J.R. Hayes, G.E. Gdowski, B.E. Viani, and C.A. Orme. "Inhibiting Effects of Nitrates on the Passive Film Breakdown of Alloy 22 in Chloride Environments." *Journal of the Electrochemical Society*. Vol. 153, No. 5. pp. B156–B161. 2006a.

Gray, J.J., J.R. Hayes, G.E. Gdowski, B.E. Viani, and C.A. Orme. "Influence of Solution pH, Anion Concentration, and Temperature on the Corrosion Properties of Alloy 22." *Journal of the Electrochemical Society*. Vol. 153, No. 5. pp. B61–B67. 2006b.

Hakiki, N.E. and M. Da Cunha Belo. "Semiconducting Properties of Passive Films Formed on Stainless Steels." *Journal of the Electrochemical Society*. Vol. 145, No. 11. pp. 3,821–3,829. 1998.

Halada, G.P., D. Kim, and C.R. Clayton. "Influence of Nitrogen on Electrochemical Passivation of High-Nickel Stainless Steels and Thin Molybdenum-Nickel Films." *Corrosion Science*. Vol. 52. pp. 36–56. 1996.

Hua, F. and G. Gordon. "Corrosion Behavior of Alloy 22 and Ti Grade 7 in a Nuclear Waste Repository Environment." *Corrosion*. Vol. 60, No. 8. pp. 764–777. 2004.

Hur, D.H. and Y.S. Park. "Effect of Temperature on the Pitting Behavior and Passive Film Characteristics of Alloy 600 in Chloride Solution." *Corrosion*. Vol. 62. pp. 745–750. 2006.

Ilevbare, G.O. "Effect of Sulfate on the Passive and Crevice Corrosion Properties of Alloy 22 in 4 M Sodium Chloride." *Corrosion*. Vol. 62, No. 4. pp. 340–356. 2006.

Jones, D.A. *Principles and Prevention of Corrosion*. 2nd Edition. Upper Saddle River, New Jersey: Prentice-Hall, Inc. 1996.

Jones, R.H., D.R. Baer, C.F. Windisch, Jr., and R.B. Rebak. "Corrosion Enhanced Enrichment of Sulfur and Implications for Alloy 22." UCRL–CONF–217194. Livermore, California: Lawrence Livermore National Laboratory. 2005.

Kelly, R.G., A. Agrawal, F. Cui, X. Shan, U. Landau, and J. Payer. "Consideration of the Role of the Cathode Region in Localized Corrosion." Proceedings of the 11th International High-Level Radioactive Waste Management Conference, Las Vegas, Nevada, April 30–May 4, 2006. LaGrange Park, Illinois: American Nuclear Society. 2006.

Kofstad, P. *Nonstoichiometry, Diffusion, and Electrical Conductivity in Binary Metal Oxides*. New York City, New York: John Willey & Sons, Inc. pp. 203. 1972.

Kokajko, L. "Prelicensing Evaluation of Container Life and Source Term (CLST) Key Technical Issues Agreements 1.08 and 1.09." Letter to J. Ziegler, DOE. ML 043410098. Washington, DC: NRC. December 22, 2004.

Kubaschewski, O. and B.E. Hopkins. *Oxidation of Metals and Alloys*. 2nd edition. London, United Kingdom: Butterworths. pp. 24. 1967.

Kumai, C.S. and T.M. Devine. "Influence of Oxygen Concentration of 288 °C Water and Alloy Composition on the Films Formed on Fe-Ni-Cr Alloys." Proceedings of the CORROSION 2001 Conference. Paper No. 01150. Houston, Texas: NACE International. 2001.

Lian, T., J.C. Estill, G.A. Hust, and R.B. Rebak. "Passive and Transpassive Dissolution of Alloy 22 in Simulated Repository Environments." Proceedings of the CORROSION 2003 Conference. Paper 694. Houston Texas: NACE International. 2003.

Lloyd, A.C., D.W. Shoesmith, N.S. McIntyre, and J.J. Noël. "Effects of Temperature and Potential on the Passive Corrosion Properties of Alloys C22 and C276." *Journal of the Electrochemical Society*. Vol. 150. pp. B120–130. 2003.

Lloyd, A.C., J.J. Noël, S. McIntyre, and D.W. Shoesmith. "Cr, Mo and W alloying additions in Ni and Their Effect on Passivity." *Electrochimica Acta*. Vol. 49. pp. 3,015–3,027. 2004.

Lorang, G., N. Jallerat, K.V. Quang, and J.-P. Langeron. "AES Depth Profiling of Passive Overlayers Formed on Nickel Alloys." *Surface and Interface Analysis*. Vol. 16. pp. 325–330. 1990.

Macdonald, D.D. "The Point Defect Model for the Passive State." *Journal of the Electrochemical Society*. Vol. 139, No. 12. pp. 3,434–3,449. 1992.

Macdonald, D.D. and A. Sun. "Electrochemical Impedance Spectroscopic Study of the Passive State on Alloy-22." *Electrochimica Acta*. Vol. 51. pp. 1,767–1,779. 2006.

Macdonald, D.D., A. Sun, N. Priyantha, and P. Jayaweera. "An Electrochemical Study of Alloy 22 in NaCl Brine at Elevated Temperature: II. Reaction Mechanism Analysis." *Journal of Electroanalytical Chemistry*. Vol. 572. pp. 421–431. 2004.

Marcus, P. and J. Oudar. "Sulfur-Assisted Corrosion Mechanisms and the Role of Alloyed Elements." *Corrosion Mechanisms in Theory and Practice*. New York City, New York: Marcel Dekker, Inc. Publishers. pp. 239–263. 1995.

Marcus, P. and E. Protopopoff. "Potential pH Diagrams for Sulfur and Oxygen Adsorbed on Nickel in Water at 25 and 300 °C." *Journal of the Electrochemical Society*. Vol. 140, No. 6. pp.1,571–1,575. 1993.

Marcus, P. and J.M. Grimal. "The Anodic Dissolution and Passivation of Ni-Cr-Fe Alloys Studied by ESCA." *Corrosion Science*. Vol. 33. pp. 805–814. 1992.

———. "The Antagonistic Roles of Chromium and Sulfur in the Passivation of Ni-Cr-Fe Alloys Studies by XPS and Radiochemical Techniques." *Corrosion Science*. Vol. 31. pp. 377–382. 1990.

Marcus, P. and M. Moscatelli. "The Role of Alloyed Molybdenum in the Dissolution and the Passivation of Nickel-Molybdenum Alloys in the Presence of Adsorbed Sulfur." *Journal of the Electrochemical Society*. Vol. 136, No. 6. pp. 1,634–1,637. 1989.

Marcus, P. and H. Talah. "The Sulfur Induced Breakdown of the Passive Film and Pitting Studied on Nickel and Nickel Alloys." *Corrosion Science*. Vol. 29. pp. 455–463. 1989.

Marcus, P., H. Talah, and J. Oudar. "Breakdown of the Passive Film on Nickel and Nickel Alloys Induced by Sulfur." *Key Engineering Materials*. Vols. 20–28, Issue 4. pp. 3,947–3,952. 1988.

Marcus, P., A. Testier, and J. Oudar. "The Influence of Sulphur on the Dissolution and the Passivation of a Nickel-Iron Alloy—Electrochemical and Radiotracer Measurements." *Corrosion Science*. Vol. 24, No.4. pp. 259–268. 1984a.

Marcus, P., I. Olefjord, and J. Oudar. "The Influence of Sulfur on the Dissolution and the Passivation of a Nickel-Iron Alloy—Sulfur Analysis by ESCA." *Corrosion Science*. Vol. 24, No. 4. pp. 269–278. 1984b.

Marcus, P., J. Oudar, and I. Olefjord. "Studies of the Influence of Sulfur on the Passivation of Nickel by Auger Electron Spectroscopy and Electron Spectroscopy for Chemical Analysis." *Materials Science and Engineering*. Vol. 42. pp. 191–197. 1980.

Meck, N.S., P. Crook, S.D. Day, and R.B. Rebak. "Localized Corrosion Susceptibility of Nickel Alloys in Halide Containing Environments." Proceedings of the CORROSION 2003 Conference. Paper 682. Houston, Texas: NACE International. 2003.

Miyagusuku, M. and T.M. Devine. "In Situ Investigation of the Passivation of Alloy C22 and of the Passive Films Formed on Alloy C22 in Acidic Electrolytes at Room Temperature and at 90 °C." Proceedings of the CORROSION 2007 Conference. Paper No. 07586. Houston, Texas: NACE International. 2007.

Mohanty, S., T.J. McCartin, and D.W. Esh. "Total-system Performance Assessment (TPA) Version 4.0 Code: Module Description and User's Guide." San Antonio, Texas: CNWRA. 2002.

Newman, R.C. "The Dissolution and Passivation Kinetics of Stainless Alloys Containing Molybdenum—I. Coulometric Studies of Fe-Cr- and Fe-Cr-Mo Alloys." *Corrosion Science*. Vol. 25, No. 5. pp. 331–339. 1985.

NRC. NUREG-1762, "Integrated Issue Resolution Status Report." Rev. 1. Washington, DC: NRC. 2005.

———. "Risk Insights Baseline Report." ML040560162. Washington, DC: Division of High Level Waste Repository Safety, Office of Nuclear Material Safety and Safeguards. 2004. <http://www.nrc.gov/waste/hlw-disposal/reg-initiatives/resolve-key-tech-issues.html> (June 1, 2007)

———. NUREG–1804, "Yucca Mountain Review Plan—Final Report." Rev. 2. Washington, DC: NRC. July 2003.

Orme, C.A. "The Passive Film on Alloy 22." UCRL–TR–215277. Livermore, California: Lawrence Livermore National Laboratory. 2005.

Oudar, J. and P. Marcus. "Roles of Adsorbed Sulphur in the Dissolution and Passivation of Nickel and Nickel-Sulphur Alloys." *Application of Surface Science*. Vol. 3. pp. 48–67. 1979.

Pensado, O., D.S. Dunn, G.A. Cragnolino, and V. Jain. "Passive Dissolution of Container Materials—Modeling and Experiments." CNWRA 2003-01. San Antonio, Texas: CNWRA. 2002.

Rajeswari, S., K. Suresh Kumar Danadurai, T.M. Sridhar, and S.V. Narasimhan. "Surface Characterization and Pitting Behavior of High-Cr-Ni-Mo Alloys in Simulated White Water Environment." *Corrosion*. Vol. 57. pp. 465–477. 2001.

Rangel, C.M. and M. Da Cunha Belo. "Semiconductor Electrochemistry and Localized Corrosion." *Portugaliae Electrochimica Acta*. pp. 295–304. 2004.

Reed, D.T. and R.A. Van Konynenburg. "Effect of Ionizing Radiation on the Waste Package Environment." Proceedings of Second Annual International Conference on High-Level Radioactive Waste Management, Las Vegas, Nevada, April 28–May 3, 1991. pp. 1,396–1,403. LaGrange Park, Illinois: American Nuclear Society. 1991.

Rodríguez, M.A., M.L. Stuart, and R.B. Rebak. "Long Term Electrochemical Behavior of Creviced and Non-Creviced Alloy 22 in $CaCl_2$ + $Ca(NO_3)_2$ Brines at 155 °C." Proceedings of the CORROSION 2007 Conference. Paper No. 07577. Houston, Texas: NACE International. 2007.

Saito, N., E. Kikuchi, H. Sakamoto, J. Kuniya, and S. Suzuki. "Susceptibility of Sensitized Type 304 Stainless Steel to Intergranular Stress Corrosion Cracking in Simulated Boiling-Water Reactor Environments." *Corrosion*. Vol. 53, No. 7. pp. 537–545. 1997.

Sakashita, M. and N. Sato. "Ion Selectivity of Precipitate Films Affecting Passivation and Corrosion of Metals." *Corrosion*. Vol. 35, No. 8. pp. 351–355. 1979.

Sato, N. "On Long-Term Extrapolation of Passive Behavior." Proceedings From the International Workshop on Long-Term Extrapolation of Passive Behavior Conference. Arlington, Virginia, July 19–20, 2001. A.A. Sagues and C.A. Di Bella, eds. Arlington, Virginia: U.S. Nuclear Waste Technical Review Board. 2001.

———. "Some Concepts of Corrosion Fundamentals." *Corrosion Science*. Vol. 27, No. 5. pp. 421–433. 1987.

Sedriks, A.J. *Corrosion of Stainless Steels*. New York City, New York: Wiley-Interscience Publishers. 1996.

Smailos, E. "Corrosion of High-Level Waste Packaging Materials in Disposal Relevant Brines." *Nuclear Technology*. Vol. 104. pp. 343–350. 1993.

Smyth, J.R., S.D. Jacobsen, and R.M. Hazen. "Comparative Crystal Chemistry of the Dense Oxide Minerals." *Reviews in Mineralogy*. Vol. 41. pp. 157–186. 2000.

Spinks, J.W. and R.J. Woods. *Introduction to Radiation Chemistry*. 33rd Edition. Hoboken, New Jersey: John Wiley & Sons. 1990.

Sridhar, N. and G. Cragnolino. "Evaluation of Analogs for the Performance Assessment of High-Level Waste Container Materials." CNWRA 2002-02. San Antonio, Texas: CNWRA. 2002.

Suleiman, M.I., I. Ragault, and R.C. Newman. "The Pitting of Stainless Steel under a Rust Membrane at Very Low Potentials." *Corrosion Science*. Vol. 36. pp. 479–486. 1994.

Tsuchiya, H., S. Fujimoto, O. Chihara, and S. Toshio. "Semiconductive Behavior of Passive Films Formed on Pure Cr and Fe-Cr Alloys in Sulfuric Acid Solution." *Electrochimica Acta*. Vol. 47. pp. 4,357–4,366. 2002.

U.S. Nuclear Waste Technical Review Board. "Proceedings From the International Workshop on Long-Term Extrapolation of Passive Behavior Conference." Arlington, Virginia, July 19–20, 2001. A.A. Sagues and C.A. Di Bella, eds. Arlington, Virginia: U.S. Nuclear Waste Technical Review Board. 2001.

Urquidi-Macdonald, W. and D.D. Macdonald. "Transients in the Growth of Passive Film on High-Level Nuclear Waste Canisters." Proceedings of the International Workshop Prediction of Long-Term Corrosion Behavior Nuclear Waste Systems. Cadarache, France: Commissariat a l'Energie Atomique and Pennsylvania State University. 2002.

Windisch, Jr., C.F., D.R. Baer, R.H. Jones, and M.H. Engelhard. "Final Report for the Study on the S-Implanted Alloy 22 in 1 M NaCl Solutions." Report No. PNNL-15380. MOL.20051122.0363. Richland, Washington: Pacific Northwest National Laboratory. 2005. <http://www.osti.gov/bridge/servlets/purl/882573-fsJYio/> (July 16, 2007).